Mechanical and Thermo-Mechanical Properties of Particulate Reinforced Composites Made From Dry Powder-Powder Blends

by

Diane C. Raqué

Thesis submitted to the faculty of the
Virginia Polytechnic Institute and State University
in partial fulfillment of the requirements for the degree of

Master of Science

in

Materials Science and Engineering

APPROVED:

Ronald G. Kander, Chairman

Jesse J. Brown

Ronald S. Gordon

January, 1992

Blacksburg, Virginia

Abstract

A process for fabricating particulate reinforced composites from dry powder-powder blends was developed. The process was designed to exploit the nature of fine powder constituent materials, such that the energy input during the molding process could be reduced. Polymer and reinforcement materials were chosen, characterized, and molded into composite plaques. These composites were characterized in terms of mechanical and thermo-mechanical properties. Stiffness, coefficient of thermal expansion, and overall dimensional stability were found to improve; and strength, strain-to-failure, and toughness were found to decrease to varying degrees. The results of these predictions were compared with simple micromechanics models to gain a better understanding of their physical behavior.

Acknowledgements

I would like to extend heartfelt thanks to my advisor, Dr. Ronald G. Kander, for his constant support and encouragement over the course of this study. I would also like to thank Dr. Brown and Dr. Gordon for agreeing to serve as members of my committee. My work on this project would not have been possible without the funding I received from the Center for Advanced Ceramics and the Materials Science and Engineering Department, and I would like to extend my appreciation for their support.

In conducting the experimental work for this project, I received assistance from many knowledgeable and extremely helpful people. I would like to thank and recognize the assistance of: Charles Chandler, for his assistance in composite fabrication; Dr. Czarnek's research group, for conducting the laser interferometry measurements; Steve Liptak, for his help in epoxy molding; and Keith Lyon, for his preparation of PEEK powders.

I would like to thank my office mates, Shannon Namboodri and Karen Valentino, for their friendship, and understanding, which meant a great deal to me.

I would like to thank my parents, Raymond and Catherine Chervenak, and my entire family, for their continual love and support. And finally, the thanks felt most deeply in my heart are extended to my husband, Steven Raqué, for his support, love and infinite patience.

Table of Contents

List of Figures

List of Tables

1. Introduction

Although ceramics have been available in micron-sized powders for quite some time, high-temperature polymers and metals are only now being produced in large quantities with such small particle sizes[1,2]. Macroscopically, these particulates are powders, but microscopically they may be spheres, flakes, whiskers or irregularly shaped particles. The existence of these relatively new powders opens the possibility for new fabrication methods to form particulate reinforced composites. Because polymers (traditional matrix materials) as well as ceramics and metals (traditional reinforcement materials) are now available in fine powder form, these components can be dry mixed to a homogeneous state prior to molding or part formation. Since mixing occurs in the dry state and requires no heat or pressure, processing time and energy input are reduced, which is an economic advantage. With the judicious choice of matrix and reinforcement components, specialty particulate composite materials can be made.

Generally, composite materials are designed to take advantage of the desirable properties of two or more different types of materials. Unfortunately, improvements in some properties are

almost always accompanied by compromises in others. Each of the various classes of materials (e.g., polymers, ceramics, and metals) typically exhibits a unique range of properties. In other words, polymers typically have specific moduli which are in a certain range, while ceramics typically have specific moduli in a different range. These ranges of specific moduli are shown graphically in Figure 1[3]. Composite materials bridge the gaps in these ranges, and allow us to produce materials which behave differently than the individual components.

Particulate reinforced composites have typically received little attention because of their low impact strengths[4,5,6]. However, particulate reinforced polymers have many desirable properties such as high stiffness[4,5,6,7] and low density, and also exhibit isotropic[8] or planar isotropic[5,6] properties, thus making them useful in stiffness critical applications. Also, much of the impact strength of the original polymer may be maintained by the addition of short fiber reinforcements[4,5,6].

One specific application of interest is the use of polymer matrix composites in space structures which are exposed to atomic oxygen (AO) in low earth orbit (LEO). Polymer matrix composites are desirable for this application because of their light weight[9,10]; however, polymers are rapidly corroded when exposed to AO[11,12], and studies have shown that unprotected polymers degrade at an unacceptable rate in LEO[9]. The search for an AO-resistant material that is also lightweight and can withstand the necessary stresses has been the subject of much research. One of the materials most resistant to attack by AO is mica[13,14]. Mica filled polymer composites have been found to corrode less severely in AO than similar unfilled composites[14]. This improved resistance is due in part to mica's natural resistance to AO; mica flakes exposed at the surface of the composite will protect the underlying polymer. Another factor in this protection mechanism is the tendency for mica flakes to align themselves with the mold wall during composite formation. This

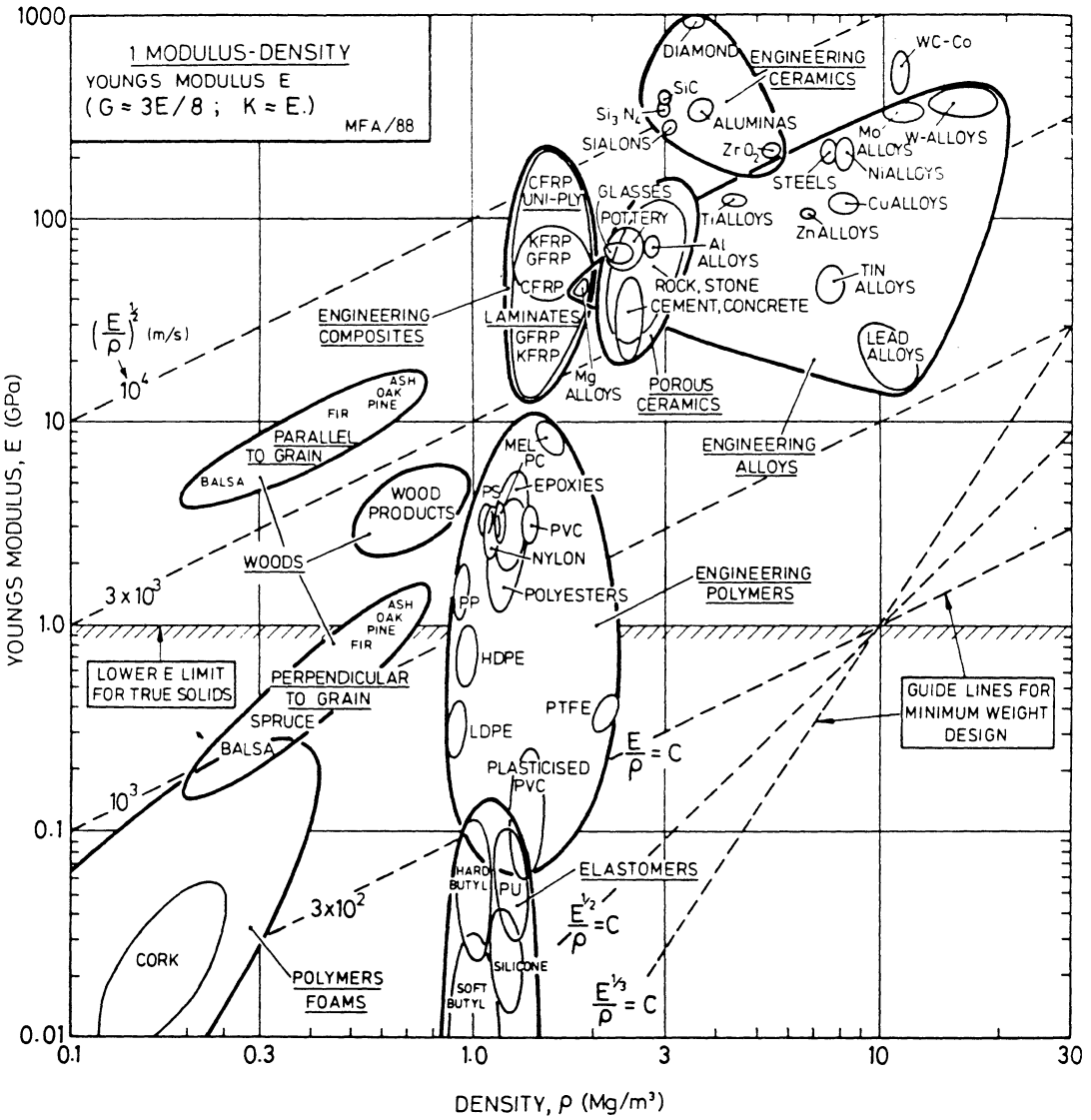

Figure 1. Comparison of specific moduli ranges for different classes of materials. (Taken from ref. 3)

results in several overlapping layers of parallel mica flakes near the surface of the material which will provide complete protection of the part within a few microns of the surface. This phenomenon is illustrated in Figure 2.

Another material of interest is polymer/metal composites, which offer extremely high stiffnesses combined with the strength of the polymer matrix, and can be made into complex shapes quickly and easily. Parts made from these materials could be used in many of the same stiffness-critical applications as powder metallurgy parts, such as gears, bushings or various types of connectors. A primary advantage of these composites over powder metallurgy parts would be lower processing temperatures. Powder metallurgy parts are sintered at temperatures ranging from 600-1300°C, depending on the metal, and may also require complex heating cycles of several steps[15]. Since powder-powder composites are processed at temperatures designed for polymer flow rather than metal sintering, part consolidation is achieved in shorter times as well as at lower temperatures. Sintering of powder metallurgy parts also requires special atmospheres for composition control, burnout of lubricants, and efficient heat transfer[15]. This added expense is not necessary in the fabrication of polymer/metal composites. In addition to the ease of processing powder-powder metal/polymer composites, these materials represent a large potential weight savings over powder metallurgy parts. One disadvantage to using metal reinforcements in polymer matrix composites is the potential for metal catalyzed degradation of the polymer. This can be avoided by choosing polymer/metal pairs which are inert with respect to each other. Another disadvantage to using metal reinforced polymers rather than powder metallurgy parts, would be a lower maximum use temperature.

In this thesis, a dry powder-powder blend compression molding process for the fabrication of particulate reinforced composites is developed. These materials are characterized, compared with similar composites fabricated by more traditional

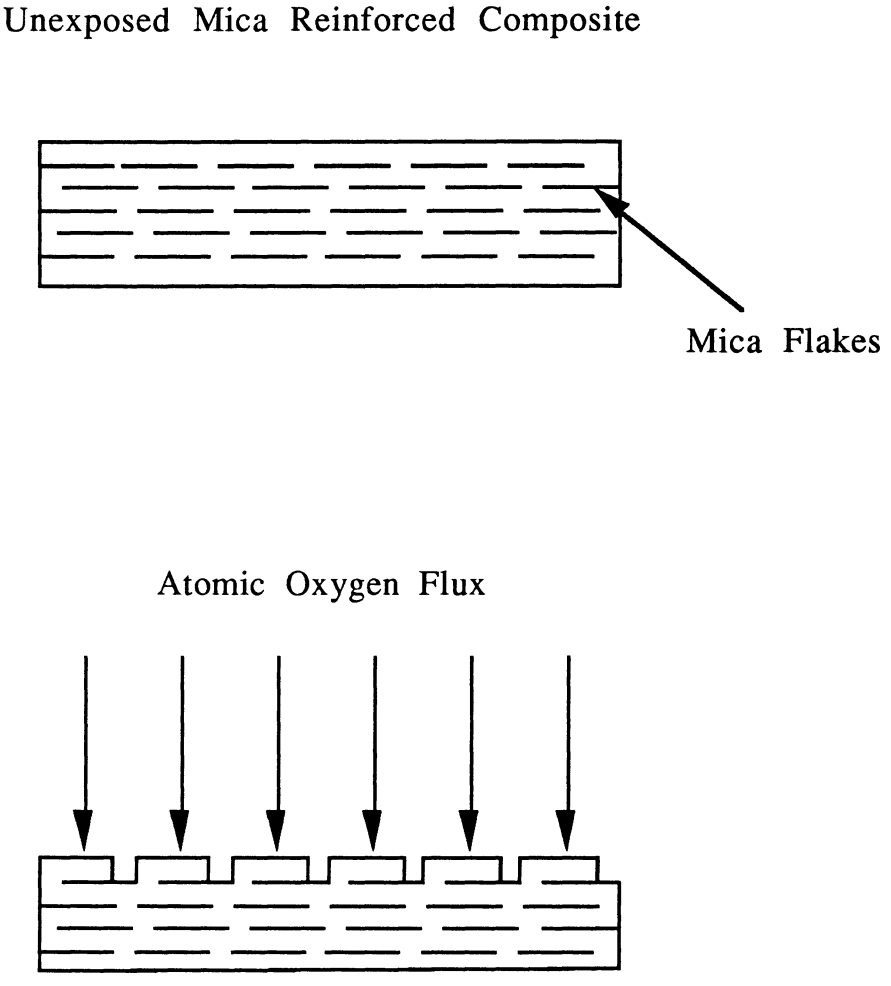

Figure 2. Schematic of atomic oxygen protection by means of reinforcement with mica flakes. (sketched after ref. 13)

methods, and compared with theoretical models of particulate composites. In Chapter 2, the materials used in this work are described. In Chapter 3, details of the fabrication processes used in making the composites, and techniques used to characterize these materials are described. In Chapter 4, some features of the dry powder-powder blend compression molding technique, as well as the mechanical and thermal behavior of the composite materials included in this study are discussed. In Chapter 5, the behavior of the materials made in this study are compared to predictions made through simple micromechanics modeling of the material systems. In Chapter 6, the work of this thesis is summarized, potential applications are addressed, and future work in this area is proposed.

2. Materials

2.1 Polymer matrix materials

2.1.1 LaRC-TPI

LaRC-TPI is a thermoplastic polyimide powder developed by and named for NASA *La*ngley *R*esearch *C*enter[16]. LaRC-TPI is currently manufactured by Mitsui Toatsu Chemical Co., which is the source of the polymer used in this study. The LaRC-TPI polymer used here is lot #58-704, #1500 series, and is supplied as a molding powder. The chemical structure of LaRC-TPI is shown in Figure 3.

LaRC-TPI was developed for use in many forms. It has been made as an adhesive, a molding powder, a high-temperature film, and fibers[16]. The form used in this study is a molding powder with an average particle size of 10μm as determined by centrifugal particle size analysis. A micrograph of the powders, illustrating the particle sizes and shapes, is shown in Figure 4.

LaRC-TPI is formed from its monomers by solution polymerization to form polyamic acid. It is precipitated as a solid powder by pouring into a rapidly stirred liquid (water or methanol),

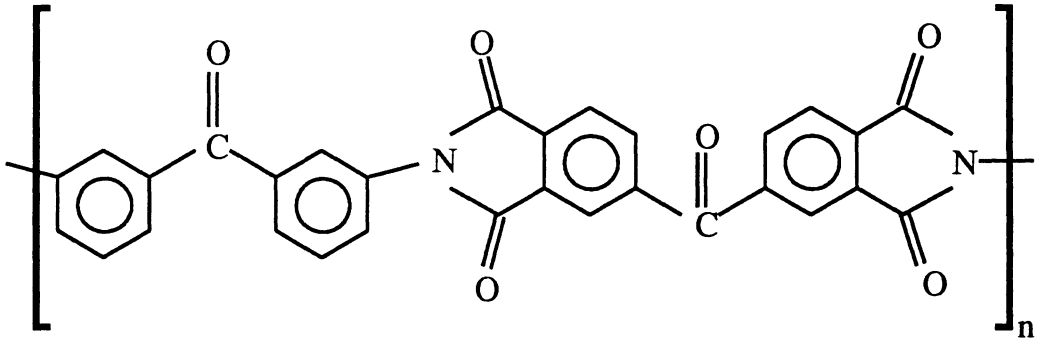

Figure 3. Chemical structure of LaRC-TPI. (after ref. 16)

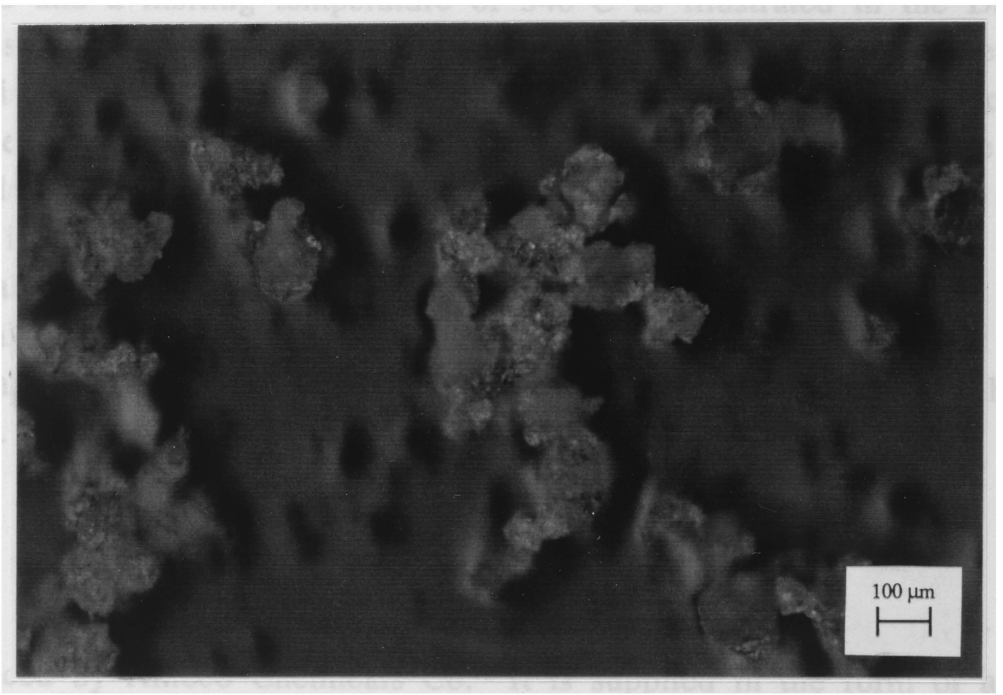

Figure 4. Optical micrograph of LaRC-TPI powder.

followed by drying and heating to achieve full imidization. It is because of this imidization step that LaRC-TPI can be processed as a thermoplastic, without the evolution of volatiles[16].

LaRC-TPI is stable to relatively high temperatures. It is a semicrystalline polymer with a glass transition temperature (T_g) of 240°C and a melting temperature of 340°C as illustrated in the DSC curves of Figure 5. In this and all subsequent DSC curves presented in this chapter, the solid curve is the initial heating of the as received powder, and the dashed curve is the second heating of the same sample. Note that the melting peak is absent in the second DSC run. This indicates that cooling has proceeded too quickly for crystallization to occur, leaving an amorphous (glassy) polymer. An annealing step below the melting temperature would induce crystallization and return the polymer to its original semicrystalline state.

2.1.2 Torlon

Torlon is the trade name for a poly(amide-imide) polymer produced by Amoco Chemicals Co. It is supplied in the form of a molding powder used primarily for injection molding. Two different Torlon powders, with widely different particle sizes, were used in this study. The coarse powder (lot #91208) has particle sizes ranging from millimeters to microns. The fine powder (lot # JLLR-076-LF) has a mean particle size of 6.6μm as determined by centrifugal particle size analysis. Micrographs of the two powders are shown in Figure 6, illustrating the difference in particle size. These powders are used in compression molding to demonstrate the effect of particle size on the integrity of the molded composite. The general chemical structure of poly(amide-imide) is shown in Figure 7. The grade of polymer used in this study is Torlon 4000T, which designates that no additives have been included in the polymer, and that the polymer is 96% fully imidized.

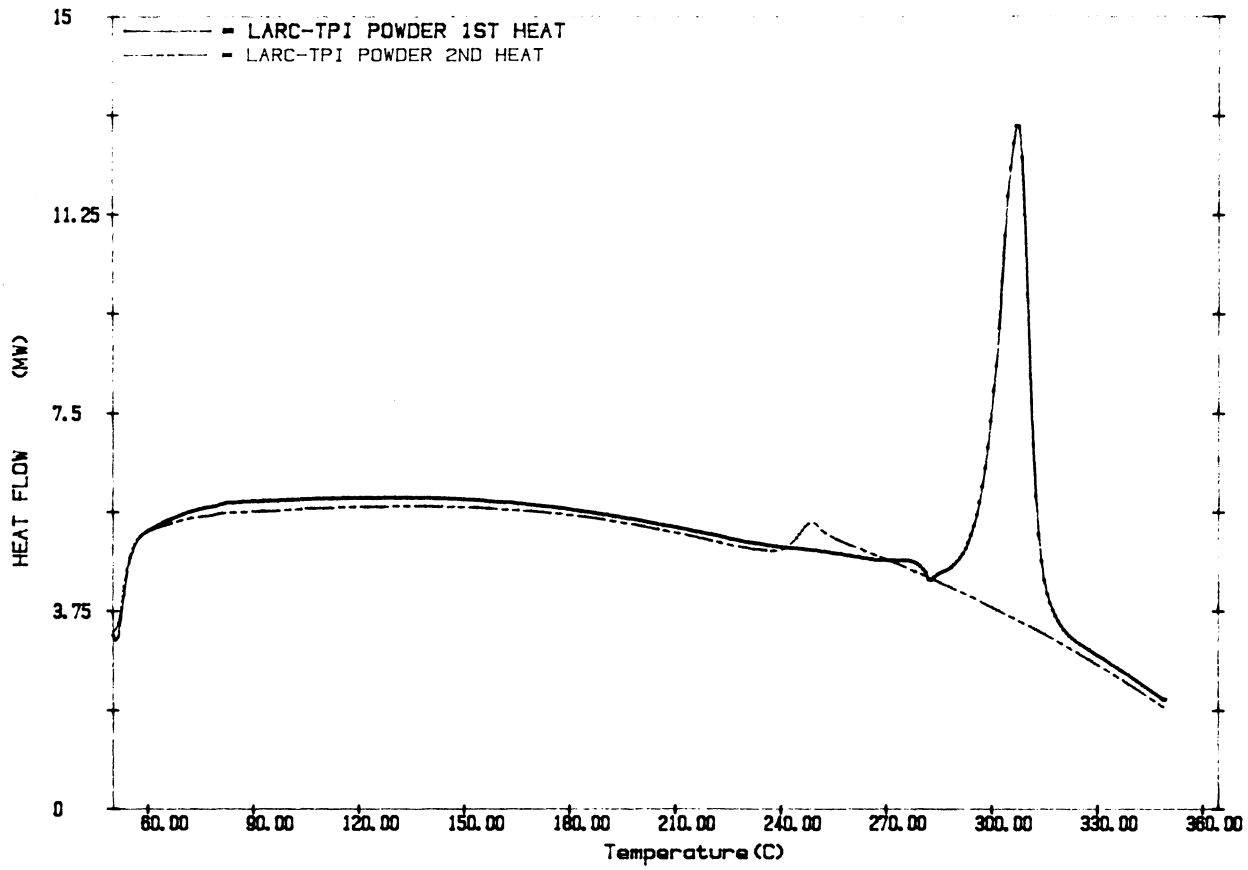

Figure 5. Differential scanning calorimetry traces of first and second heatings of LaRC-TPI powder.

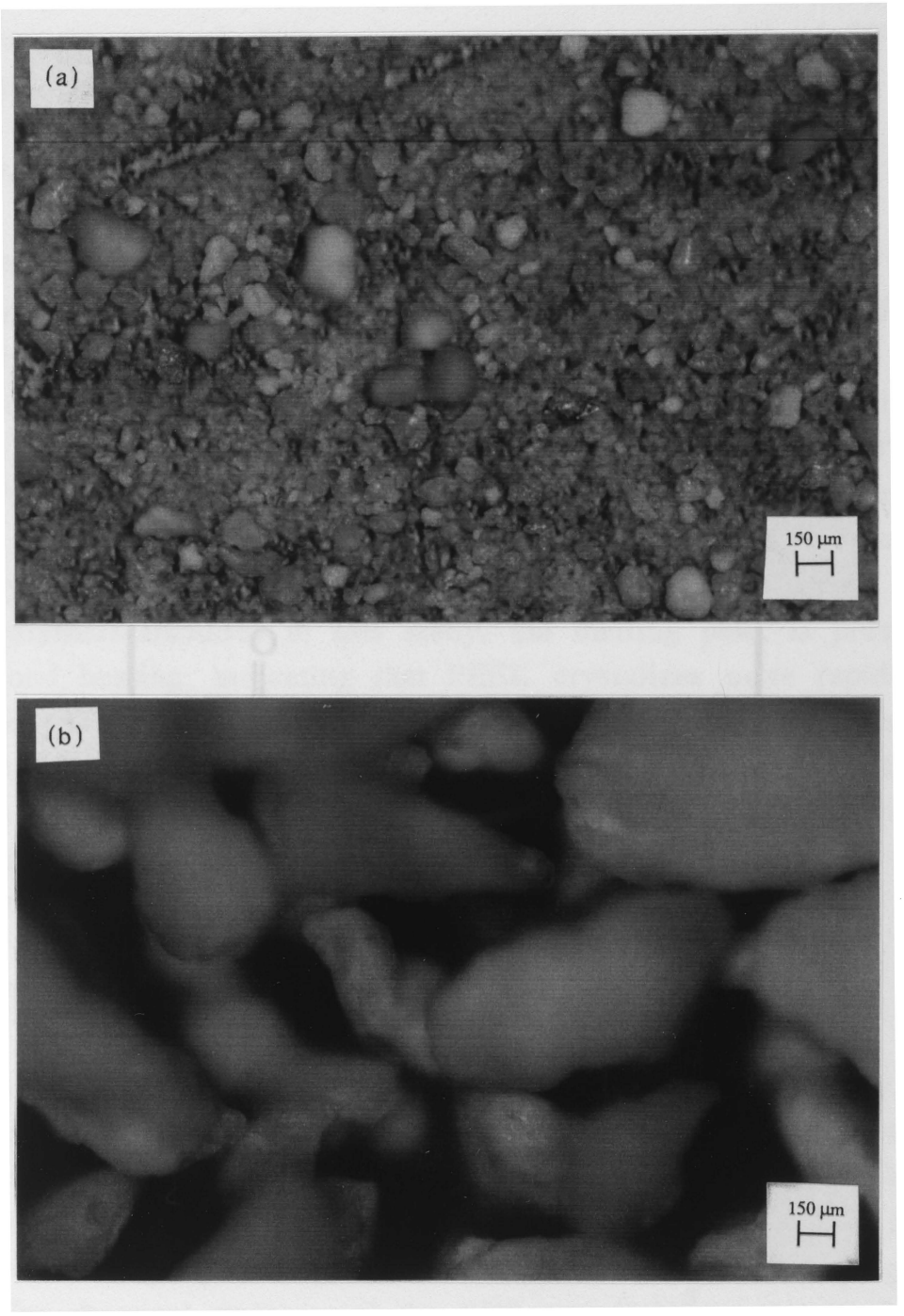

Figure 6. Optical micrographs of (a) fine and (b) coarse Torlon powders.

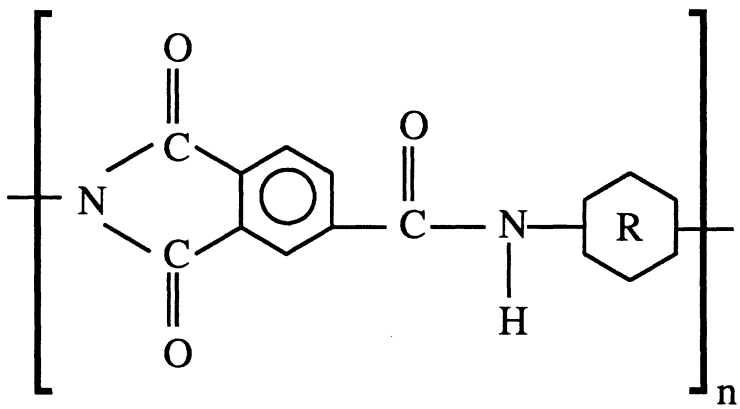

Figure 7. Chemical structure of poly(amide-imide). (after ref. 17)

Torlon is an amorphous polymer which is stable at relatively high temperatures. It has a glass transition temperature of 290°C, which can be observed in the DSC scan shown in Figure 8.

2.1.3 Poly(aryl Ether Ether Ketone) "PEEK"

PEEK is a high temperature thermoplastic polymer manufactured commercially by ICI. The chemical structure of PEEK is shown in Figure 9. The PEEK powder used in this study was prepared by Keith Lyon, a chemistry graduate student at Virginia Tech. The powder has an average particle size of less than 5μm.

Figure 10 shows DSC scans of the PEEK powder. PEEK melts at 315°C, and undergoes a glass transition at 150°C. PEEK's unusually high crystallinity is evident in the curves of Figure 10. Unlike the other polymers included in this study, the melting peak is present on the second heating, indicating that PEEK crystalizes more rapidly than the LaRC-TPI powder, and that composites made with this polymer are likely to be semicrystalline even after rapid cooling.

An indication of the size and shape of the PEEK particles is shown in Figure 11. This micrograph also shows the tendency of the PEEK to agglomerate into large groups of particles.

2.1.4 TGDDM/DDS epoxy

An epoxy resin system of MY721, supplied by Ciba Geigy, cured with diaminodiphenylsulfone (DDS), from Aldrich, was examined as a representative thermosetting composite matrix resin. MY721 is more than 95% tetraglycidyl diaminodiphenylmethane (TGDDM), a tetrafunctional epoxy whose chemical structure is shown in Figure 12a. The chemical structure of the DDS crosslinking agent is shown in Figure 12b.

MY721 is a thermally stable epoxy. When cured with DDS it is reported to have a T_g of 265°C[18].

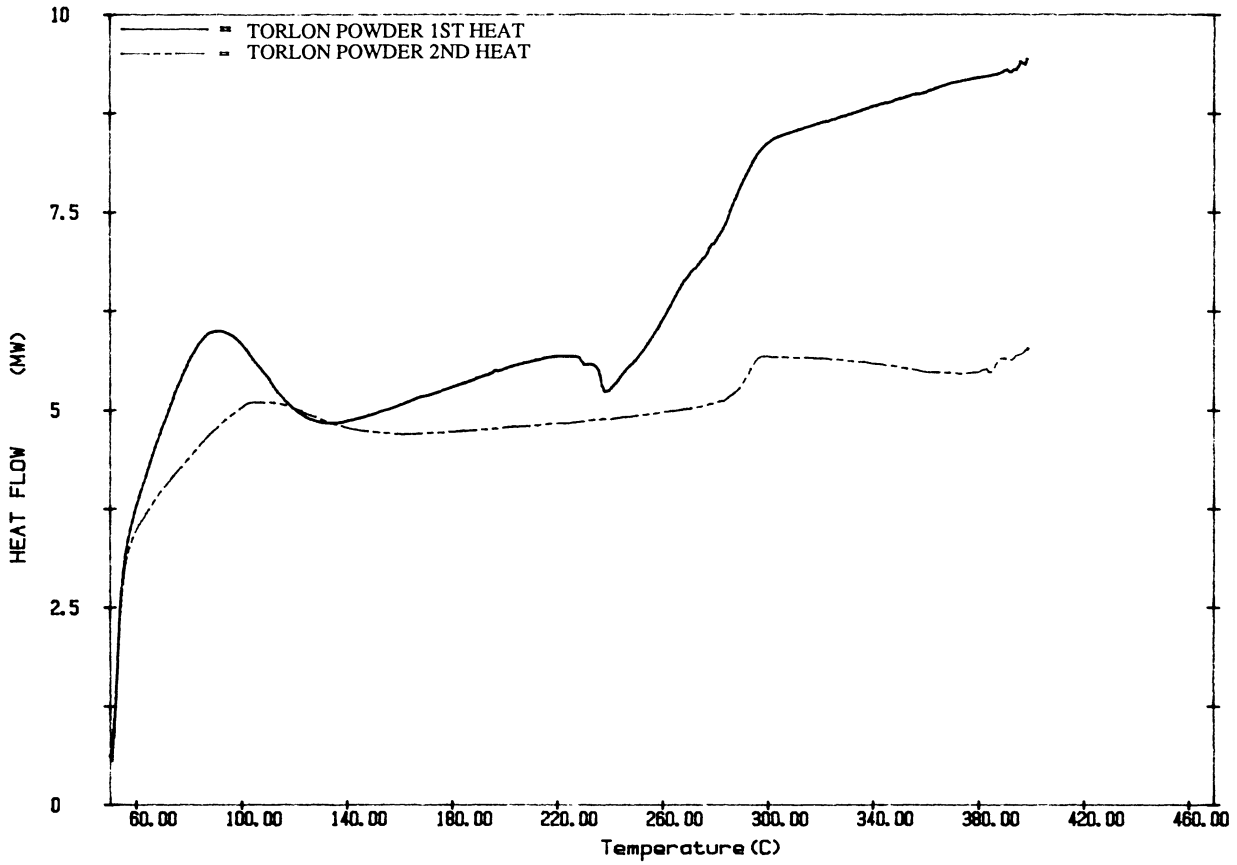

Figure 8. Differential scanning calorimetry traces of first and second heatings of Torlon powder.

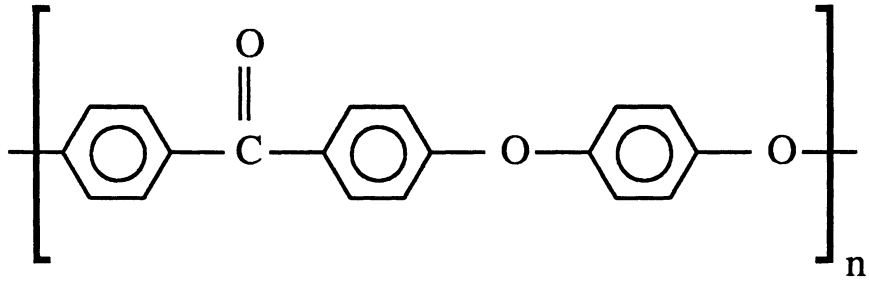

Figure 9. Chemical structure of Poly(aryl Ether Ether Ketone).

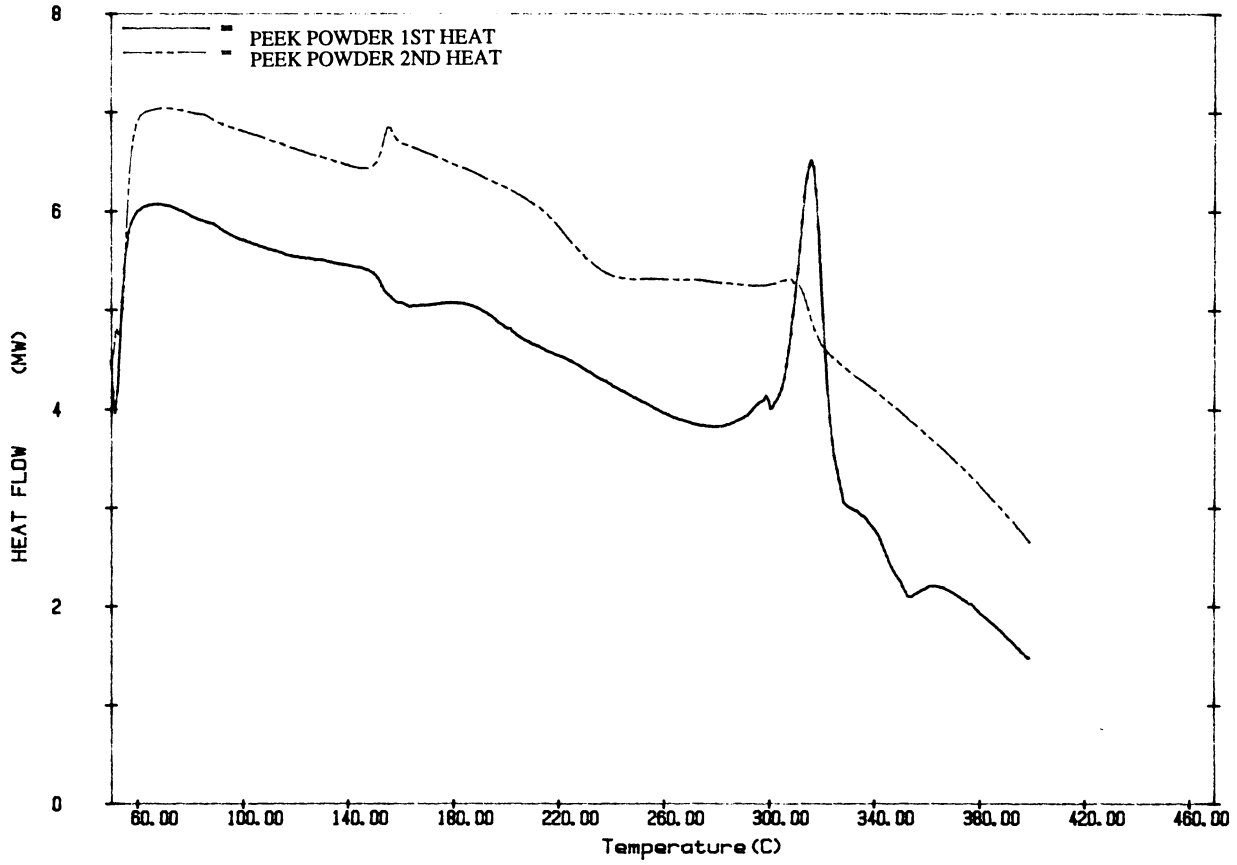

Figure 10. Differential scanning calorimetry traces of first and second heatings of PEEK powder.

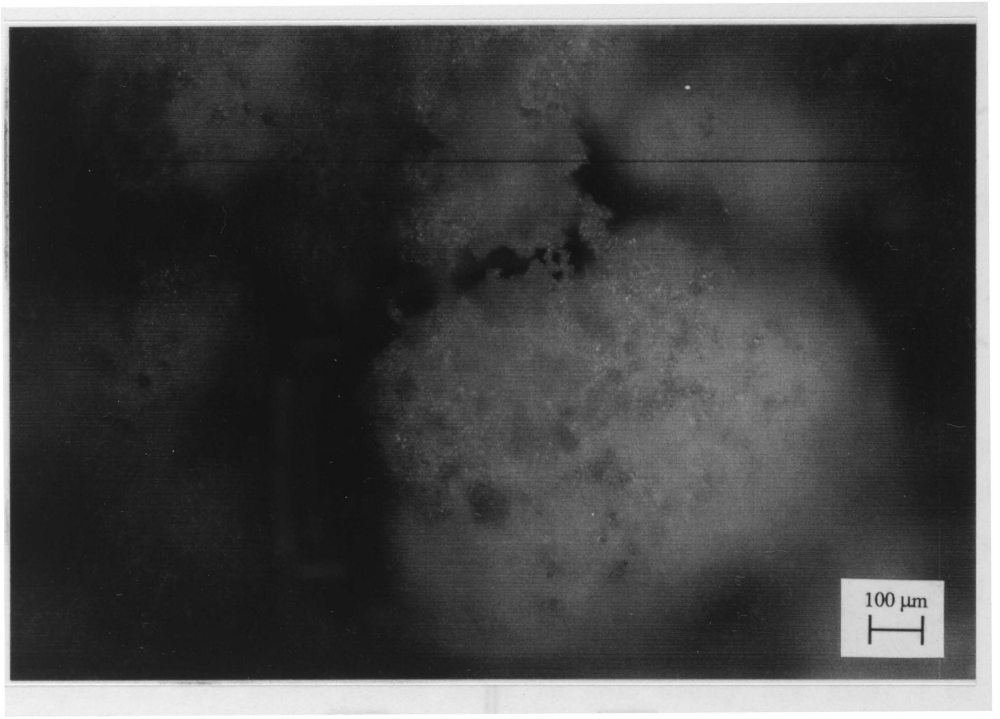

Figure 11. Optical micrograph of PEEK powder.

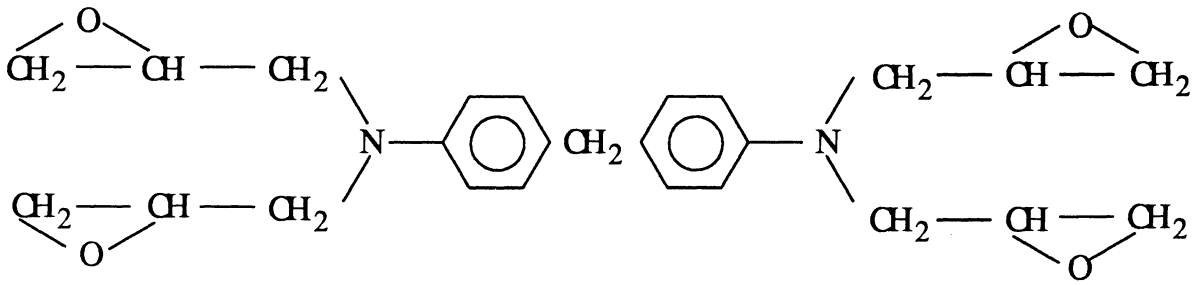

(a)

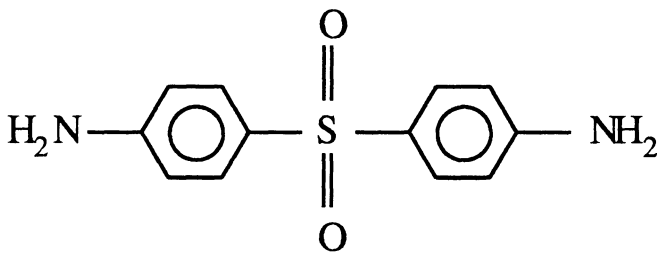

(b)

Figure 12. Chemical structures of (a) TGDDM and (b) DDS.

Samples were fabricated using standard techniques for epoxy resins which will be described in the following chapter.

2.2 Reinforcement Materials

Flake, acicular and spherical particulates were used as reinforcements. The primary gain expected from these reinforcements is increased stiffness. The primary drawback expected of the flake and spherical reinforcements is lower impact strength.

2.2.1 Mica

Mica is an abundant, naturally occurring mineral, which can also be produced synthetically. It is available in many different forms which are characterized by compositional variances. Three forms of mica are examined in this study: suzorite (a variety of natural phlogopite), muscovite and synthetic fluorophlogopite. Micrographs of the three micas used in this study are shown in Figure 13, illustrating the sizes of the particles, and the irregular shapes of the mica flakes. The types of sizings (surface coating intended to improve adhesion) and aspect ratios for these three forms of mica are given in Table 1. Sizings in this study were applied by the supplier of the mica. The aspect ratio of the particle is defined as the ratio of average diameter to thickness. An average diameter must be used since the flakes are irregularly shaped and not circular.

Suzorite is unique among natural micas in that it contains less than 1% water in its structure that is retained upon heating up to 440°C, whereas other micas can have up to 10% water which is lost at temperatures near 200°C[19,20]. Because of this, composites made with suzorite are expected to be more thermally stable than those reinforced with other types of natural mica.

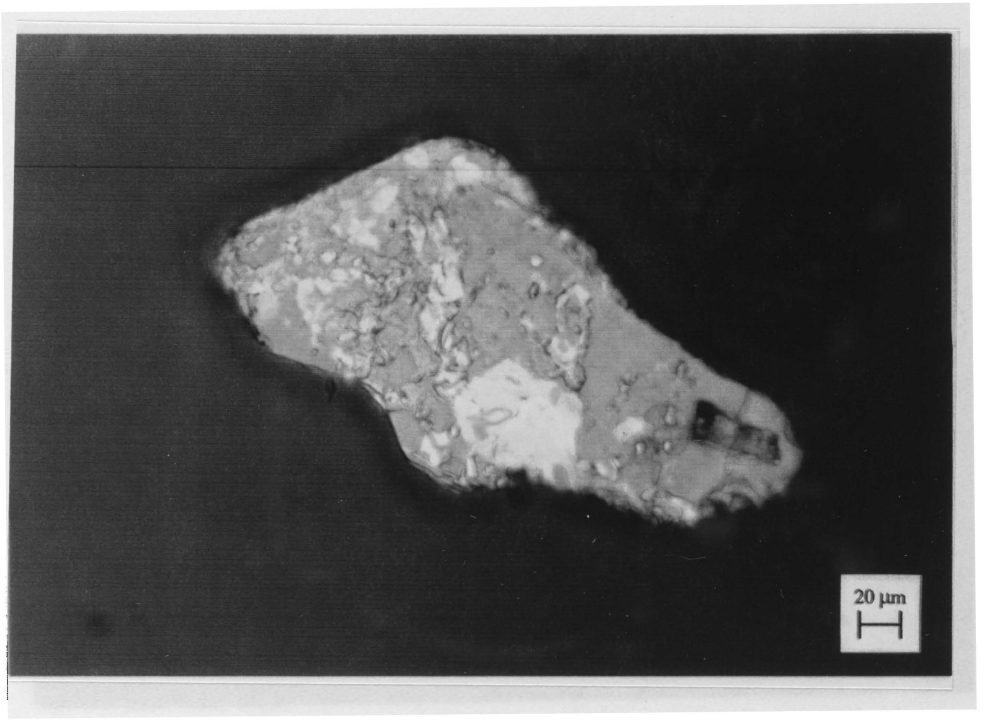

Figure 13. (a) Optical micrograph of a suzorite particle.

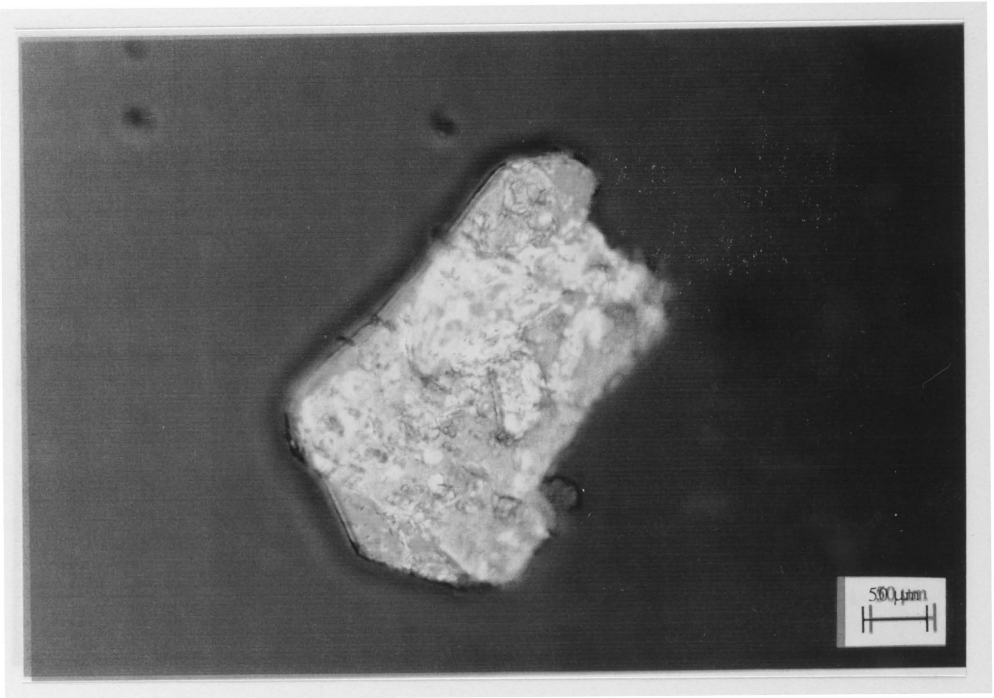

Figure 13. (b) Optical micrograph of a muscovite particle.

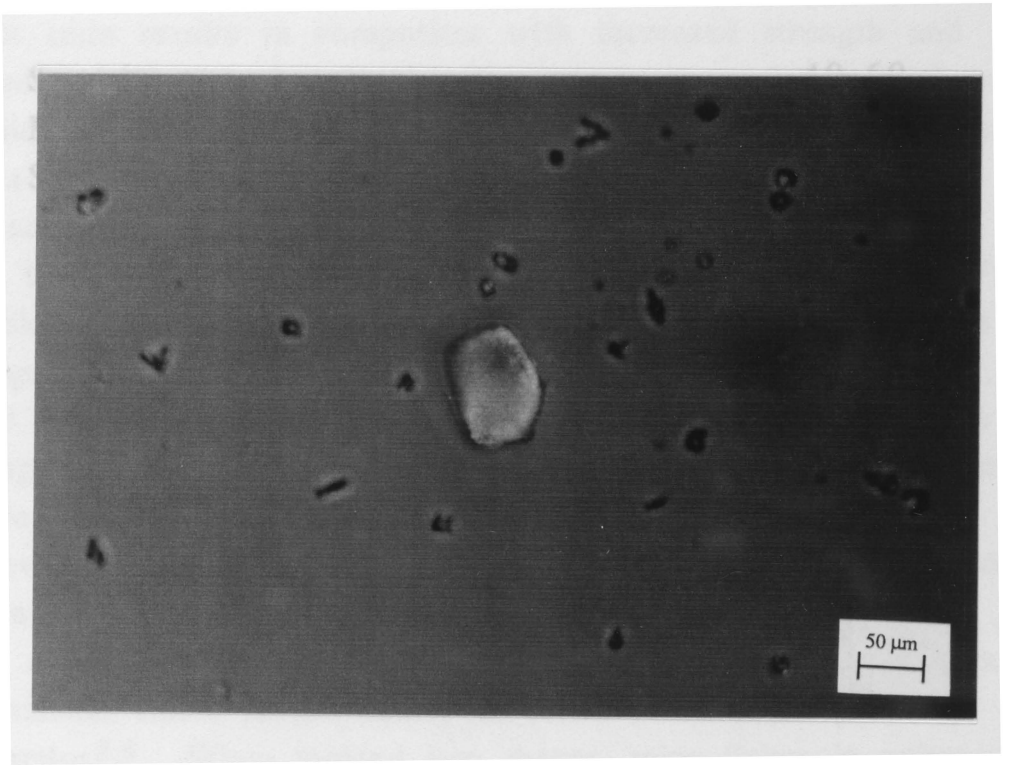

Figure 13. (c) Optical micrograph of a synthetic fluorophlogopite particle.

Table 1. Mica Systems Used in This Study

Specific Type	Sizing	Aspect Ratio
Suzorite	none	40-60
Muscovite	amino type	43-53
Synthetic Fluorophlogopite	none	<10

While the micas considered in this study are in the form of powders, the individual particles have distinct flake or platelet shapes. It is the flat shape of the mica particles which allow them to carry load in a composite[5,7,20]. It has been shown that increased aspect ratio results in composites with increased strength and stiffness[4,5,6,7]. Aspect ratio influences many mechanical properties of mica reinforced composites, and it has been demonstrated that an aspect ratio of at least 100 is necessary for optimum property enhancement[5,6,7,20].

Once mica is processed into flakes with high aspect ratios[20,21], a suitable composite processing method must be found which will not damage the flakes and break them down into smaller diameter, lower aspect ratio particles. Compression molding, preceded by mixing in a rotating drum is considered the most attractive method of preserving aspect ratio during composite processing[4,6,7]. However, mica reinforced polymers have been successfully injection-molded[5].

An advantage of using two-dimensional flakes rather than one-dimensional fibers is the ability to attain planar isotropic properties[5,6]. When molded into shapes, mica flakes in polymer matrix composites tend to align with the mold walls[5,6,7]. This alignment of the flakes defines the plane in which planar isotropic properties are observed. Figure 14 illustrates the difference in modulus with respect to test angle in flake reinforced composites as compared to fiber reinforced composites. In this figure, the modulus of the flake reinforced composite is seen to remain constant with test angle. Even when fibers are arranged quasi-isotropically, such as the Boron 0°-45°-90° curve in Figure 14, property variation with test angle is still observed. It is interesting to note the difference between the unidirectional (0°) and quasi-isotropic (0°-45°-90°) curves for Boron fiber reinforced composites, and also their relationship to the flake reinforced composite curve. The modulus of the unidirectional Boron fiber reinforced composite drops to nearly one quarter of its value when the composite is made quasi-isotropic.

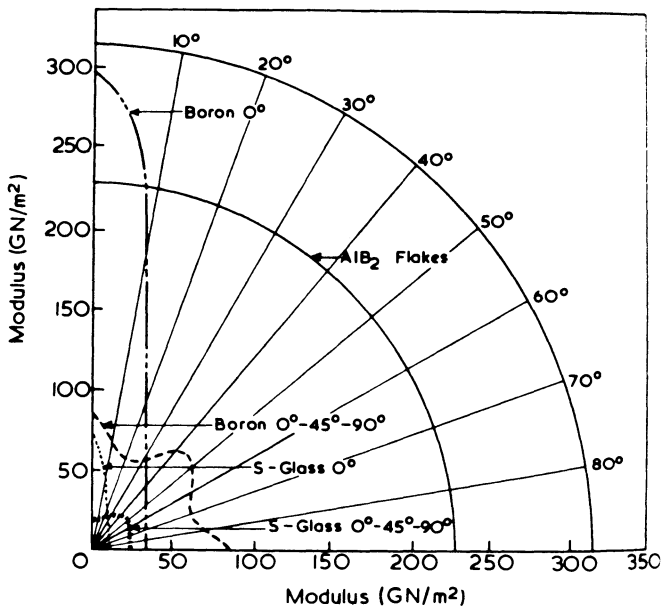

Figure 14. Illustration of planar isotropic nature of flake reinforced composites compared to anisotropy of fiber reinforced composites. (from ref. 6)

It should also be noted that although the Boron 0° curve indicates a higher modulus than the AlB_2 Flakes curve, the Boron 0°-45°-90° curve lies substantially below the AlB_2 Flakes curve. We can conclude from this figure that flake reinforcements are much more effective at producing composites with isotropic properties than any type of fiber.

2.2.2 Metal

The metal used in this study was supplied as a fine powder. Fine powder metallurgy is a relatively new field in which ever smaller particle sizes are being achieved[1]. The descriptive term "fine" is entirely relative, and although nanometer sized metal powders have been produced[1], the "fine" powders used in this study range from approximately 5-50 μm in size.

Several metals are currently available as fine powders with particles less than 10 μm in size[22]. Powders with particles less than 1 μm in size include tungsten, silver, nickel, iron, cobalt, and palladium as well as an aluminum-copper alloy and a silver-palladium alloy[22,23]. Fine powders of several other alloys have also been produced[1].

The specific metal used in this study is a copper-aluminum-nickel alloy. Metal powders of two different particle sizes were available; powders with average particle sizes of 12 and 45 microns were used. A micrograph of the 45μm Cu-Al-Ni powders is shown in Figure 15, which shows the spherical shape of the particles as well as the typical particle size. The 12 mm powder was molded with LaRC-TPI at 40 volume percent of reinforcement. All other metal reinforced samples contain the 45μm powder.

The Cu-Al-Ni alloy used here belongs to a class of metals known as shape memory alloys. Shape memory alloys are unique in that once they are quenched into a martensitic phase, they can be deformed and then returned to their previous shape by heating to a certain temperature. Shape memory alloys of the Cu-Al-Ni system

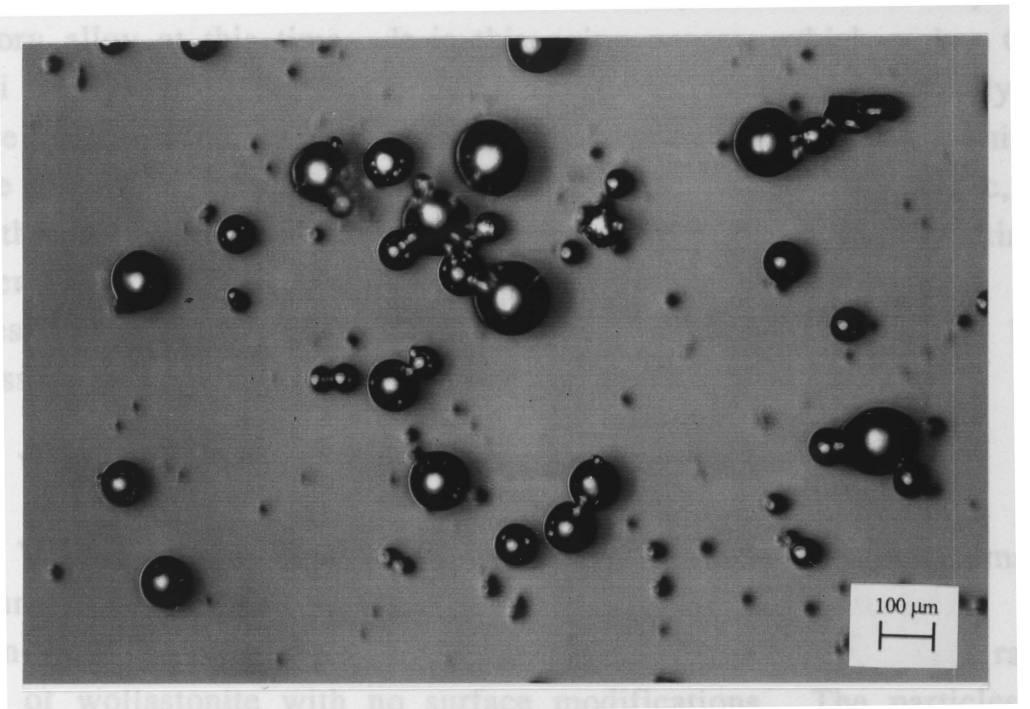

Figure 15. Optical micrograph of Cu-Al-Ni powder.

undergo aging at relatively low temperatures. During aging, phase separation occurs through diffusion, thus destroying the shape memory effect in the metal. In Cu-Al-Ni, aging occurs between 200 and 400°C[24], since this is a lower temperature range than other shape memory alloys, Cu-Al-Ni is a relatively unattractive shape memory alloy at this time. It is this aging process which makes Cu-Al-Ni an interesting reinforcement for the polymers in this study. Figure 16 is a DSC curve of the alloy powder before molding. This figure shows that this phase transformation is highly exothermic, and that the temperature of transformation is very close to the melting temperatures of both LaRC-TPI and PEEK. This situation has interesting ramifications for future work in this area, which will be discussed in detail in the final chapter.

2.2.3 Wollastonite "whiskers"

Wollastonite is a naturally occurring mineral which is primarily calcium metasilicate, $CaSiO_3$. The material used in this study is known as NYAD G® wollastonite powder, which is a high aspect ratio grade of wollastonite with no surface modifications. The particles are acicular, or whisker-like, in shape and have an aspect ratio of about 20, as shown in the micrograph of Figure 17. Wollastonite melts at 1540°C, and is therefore thermally stable in the temperature range required to mold the composites in this study.

Because of its high aspect ratio, wollastonite has potential as a substitute for short fiber reinforcements. Wollastonite has been examined as a reinforcement in a variety of polymeric resins[25], and also as a replacement for glass fiber in bulk molding compound[26] with positive results. Wollastonite is available with sizings that enhance bonding to a polymer matrix, and these sizings have been shown to dramatically improve the effectiveness of wollastonite as a reinforcement, particularly in the area of impact resistance[25]. Unsized wollastonite was used in this study due to its availability at the present time.

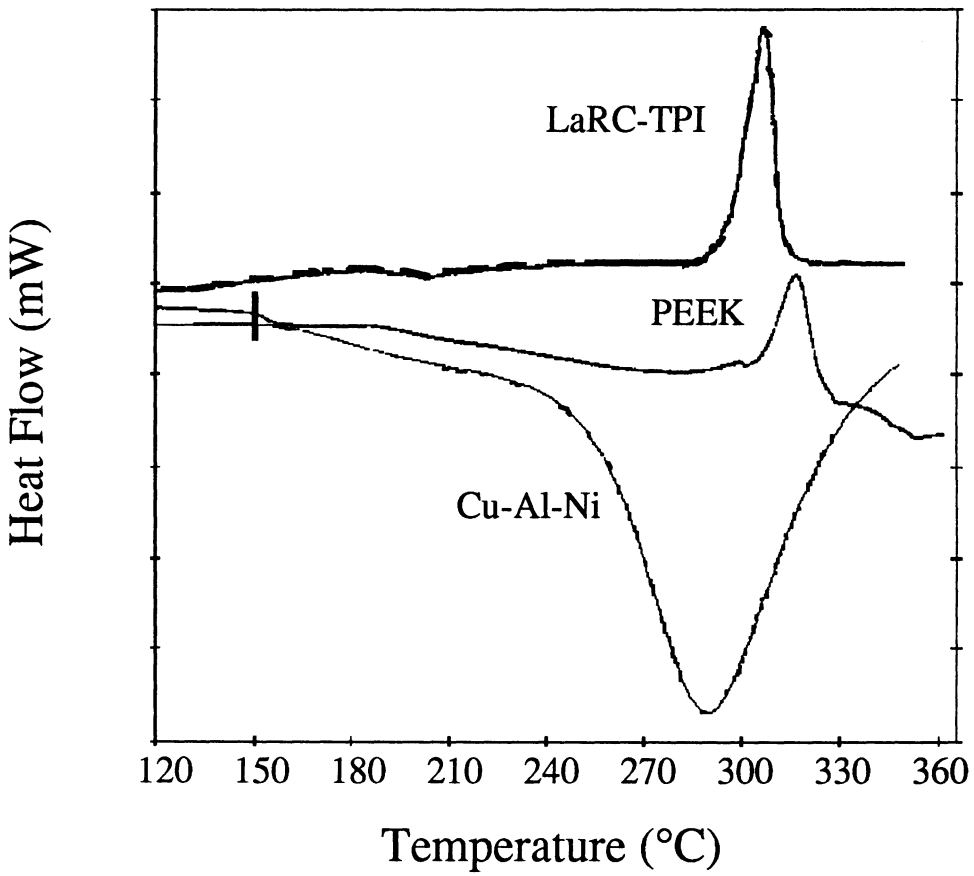

Figure 16. Differential scanning calorimetry trace of Cu-Al-Ni powder. Also shown are initial DSC scans of LaRC-TPI and PEEK powders.

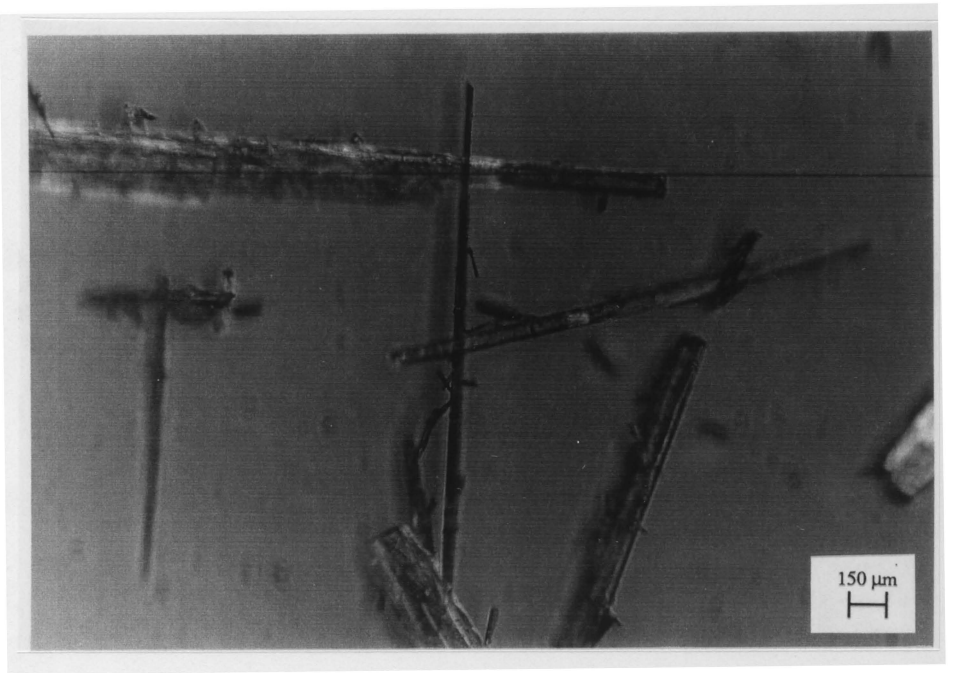

Figure 17. Optical micrograph of wollastonite powder.

Wollastonite was chosen as a reinforcement material because of its fiber-shaped particles. With such small, acicular particles, a fiber-like reinforcement can be incorporated into these particulate composites without altering the powder blending and compression molding fabrication method.

3. Experimental

3.1 Fabrication

3.1.1 Compression Molding of Dry Powder-Powder Blends

This technique is possible only when all of the components of the composite system are available as fine powders. With particles on the order of microns in size, intimate mixing in the dry state becomes possible. A schematic diagram of the fabrication process is shown in Figure 18. Mixing of the polymers and reinforcements in this study was achieved by placing proportional amounts of the constituent materials into a container and agitating by hand until a homogeneous mixture is obtained. Although homogeneity was determined by visual observation, and was somewhat subjective, the properties of the resulting composites show no evidence of spatial inhomogeneity. Interferometry was also performed on the molded samples to confirm that homogeneous mixtures have been achieved. On a larger scale, mixing could be achieved by use of a conventional mixer, or a rotating drum if the reinforcement particles are fragile[4].

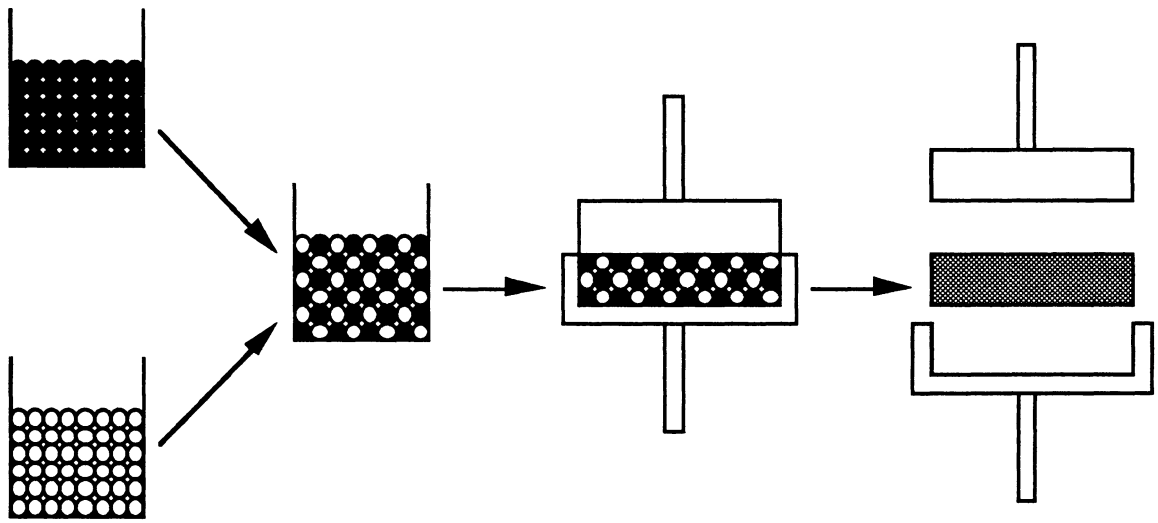

Figure 18. Schematic of dry-blending and compression molding fabrication process.

Once the powders are mixed, consolidation is a simple process. The powder mixture was placed into a 7.62 cm square steel mold. The mold was placed into a hot press and minimal contact pressure was applied. The temperature was raised to allow the polymer to flow, and then full pressure was applied, followed by cooling of the assembly (at approximately 3-4°C/min.) to below T_g of the polymer, and removal of the specimen. Specific temperatures and pressures used for each system are shown in Table 2.

Although the mold was not preheated in this study, the powder mixture could be placed into a mold that was preheated to just below the T_g of the polymer. This would decrease molding time, and therefore improve the economics of the molding process.

3.1.2 Molding of TGDDM/DDS Epoxy Composites

The MY721 resin is in the form of a viscous liquid, and the DDS is in the form of a powder. First, the resin is placed into a 2-neck round bottomed flask, and is vacuum degassed in a vent hood, while being stirred and heated in a silicon oil bath at 135°C to reduce viscosity. The curing agent is then added, and the mixture is again vacuum degassed. The reinforcement is then added, and degassing is completed. The mixture is reheated to 135°C to allow the curing reaction to begin. This mixture is then poured into a preheated 7.62x12.7 cm steel mold, with Teflon spacers to obtain a controlled specimen thickness. For the neat resin specimen, the mold is preheated to 190°C. The entire mold assembly is then placed into a hot press under contact pressure. The neat resin specimen is cured at 190°C for 120 minutes, and post-cured at 240°C for 120 minutes[27]. When reinforcements are added, the mold is preheated to 120°C and an initial step of 120°C for 120 minutes is added to the hot press cycle to minimize the viscosity drop which would allow the reinforcement to fall out of suspension. Although this process modification does not completely eliminate this problem, it does

Table 2. Processing Conditions for Compression Molded Powder Blend Composites.

Polymer	T_{mold}	T_g	Full pressure	Reinforcements
LaRC-TPI	340°C	250°C	345 kPa	Cu-Al-Ni suzorite muscovite fluorophlogopite
Torlon	315°C	290°C	690 kPa	Cu-Al-Ni suzorite muscovite fluorophlogopite
	325°C			wollastonite suzorite/wollastonite
PEEK	330°C	150°C	690 kPa	Cu-Al-Ni suzorite

reduce it enough so as not to affect the properties of the mica reinforced composite

The only reinforcement added to the epoxy system is suzorite mica. Due to processing limitations, the epoxy/suzorite composite contains only 20 volume percent of reinforcement. Upon removal from the mold, the Epoxy/suzorite samples were slightly warped, indicating that some degree of sedimentation of the mica had occurred. However, this did not affect the flexural properties of the specimens. The density of the Cu-Al-Ni powder caused it to fall out of suspension despite the lower temperature cure step, and therefore no usable epoxy/Cu-Al-Ni composite samples were made.

3.1.3 Sample Dimensions

Molded plaques are machined into 76x12x3 mm three-point-bend, impact fracture, and interferometry specimens; 25x3x3 mm dilatometry specimens; and various sizes of microscopy samples.

3.2 Characterization

3.2.1 Mechanical Properties

Mechanical properties were measured in order to determine the ability of the materials to withstand stress. Flexure and impact tests were performed, and fracture surfaces were examined to determine failure modes.

Three-point-bend flexural tests were performed on an MTS 810 hydraulic test frame. Tests were run using either a 100N or 1000N load cell. A span to depth ratio of 16 was used for all samples. Crosshead speed was either 5 or 10 mm/min. Load and displacement were explicitly measured and converted to flexural stresses and strains using linear beam theory. These tests provide information on modulus, strength, ductility/brittleness, as well as giving a qualitative measure of toughness.

A more quantitative measure of toughness was obtained by instrumented impact testing. Impact testing was performed on a Tinius-Olsen Charpy Impact Machine instrumented with a Dynatup load cell. In these tests, toughness was defined as the energy absorbed during fracture, and was determined by measuring the integrated area under the load vs. time curve during impact.

Scanning electron microscopy (SEM) was performed on a Jeol Scanning Microscope (model JSM 35C). This technique was used to examine the fracture surfaces of failed specimens to learn more about the mode of failure. In addition, information about the degree of particle/matrix bonding was obtained.

Optical microscopy was performed on an Olympus photo-microscope (model BHSM). Samples were examined in transmitted and reflected light, in both bright and dark field, using polarized and non-polarized light.

3.2.2 Thermal Properties

Thermal properties were examined because many potential applications of these materials call for exposure to elevated temperatures. Differential scanning calorimetry (DSC), dilatometry and laser interferometry were the techniques used to examine the high temperature behavior of the materials in this study.

DSC was performed on a Perkin Elmer Differential Scanning Calorimeter (model DSC7). Samples were scanned from 50 to 300°C, and powders were scanned to 400°C, at a rate of 20°C/min. This test provided information on melting points and glass transition temperatures, as well as any reactions that may occur upon heating.

Dilatometry and laser interferometry are two techniques which measure thermal expansion. Dilatometry was performed on a Netzsch Dual-push-rod Dilatometer (model 402 ED). Samples were heated from 30 to 200°C at rates of 5 or 10°C/min. Dilatometry is used to measure the coefficient of thermal expansion (CTE), as well as the thermal expansion behavior as a function of temperature or time.

Laser interferometry is a "full field" thermal expansion technique by which laser interference patterns, generated by reflection from a grid etched onto the sample surface, indicate changes in local strain fields as temperature is increased. These tests provide an explicit measure of expansion anisotropy as well as a qualitative indication of sample homogeneity.

4. Results and Discussion

4.1 Observations on the Fabrication Process

A strong interfacial bond between the matrix and reinforcement is critical to the transfer of load in a composite, and thus is also central to the overall quality of the composite. Several methods were used to gain information on the quality of the interfaces in the materials under study. In some cases, visual appearance of the composite was informative. Laser interferometry and micrographs of the powder blends both yielded useful information on the quality of the matrix/reinforcement interfaces. SEM examination of the fracture surfaces also yielded information on the matrix/reinforcement bond. The examination of the powder blend micrographs is unique in that information about the interaction between a pair of particulate materials can be obtained before any samples are molded.

Some of the combinations of polymer and reinforcement did not mix well, and therefore produced inhomogeneous composites. The most severe of these were visibly segregated on a macroscopic scale. For example, LaRC-TPI/fluorophlogopite,

Torlon/fluorophlogopite, and PEEK/suzorite all appear macroscopically inhomogeneous.

Laser interferometry, which was performed to gain information on thermal expansion coefficient and anisotropy, also proved useful in determining homogeneity of the composites. Laser interferometry results, in the form of fringe patterns for the LaRC-TPI series of composites, is shown in Figure 19. These experiments were carried out by Dr. Czarnek's research group, in the Engineering Science and Mechanics Department. The photos for the unreinforced polymer (19a) and the Cu-Al-Ni reinforced composite (19b) show straight, evenly spaced fringes, characteristic of a homogeneous material. The presence of dark spots on the photos is usually an indication of porosity in the specimen. The LaRC-TPI/fluorophlogopite photo (19c) contains many dark areas, while the LaRC-TPI/suzorite (19d) photo shows a few small spots. Interferometry photos were also taken of the LaRC-TPI/muscovite sample, which behaved much like the LaRC-TPI/suzorite sample in this respect. In the case of these materials, the "porosity" indicated by the photos is probably caused by agglomerations of reinforcement particles which are not well bonded to the matrix. These results indicated that the metal reinforced composite is a macroscopically homogeneous material, while the suzorite and muscovite reinforced composites posses nearly perfect macroscopic homogeneity, and the fluorophlogopite reinforced composite is not a macroscopically homogeneous material. Since these materials do contain agglomerations, there are many reinforcement particles which are not in contact with polymer. Therefore, the amount of interfacial surface area is reduced, and the quality of the composite is correspondingly lowered.

Micrographs of the powder blends were taken prior to molding to examine the interactions between particles. These micrographs are shown in Appendix A. In the mixes containing metal reinforcement, Figures A1 through A3, the two component powders appear well dispersed, and the polymer and metal particles appear to be attracted to one another. This attraction appears to be more

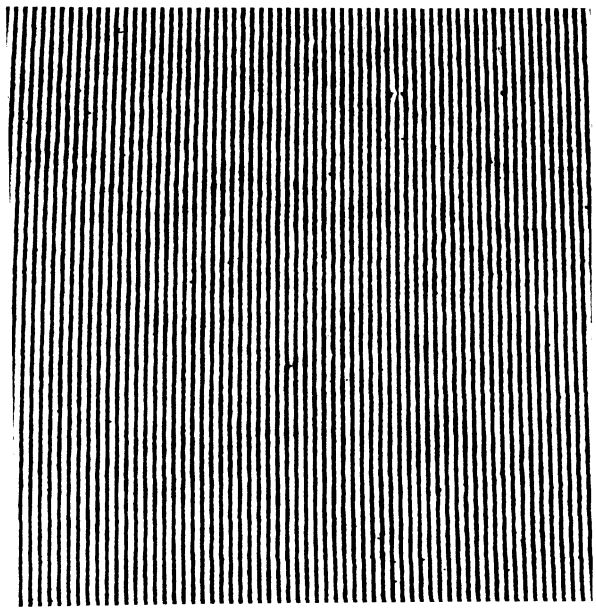

(a)

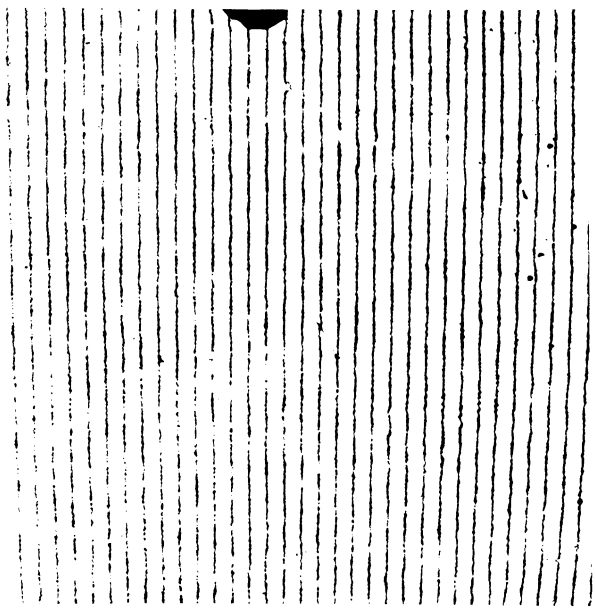

(b)

Figure 19. Laser interferometry photographs of (a) LaRC-TPI and (b) LaRC-TPI/Cu-Al-Ni. (Data courtesy of Dr. Czarnek's research group.)

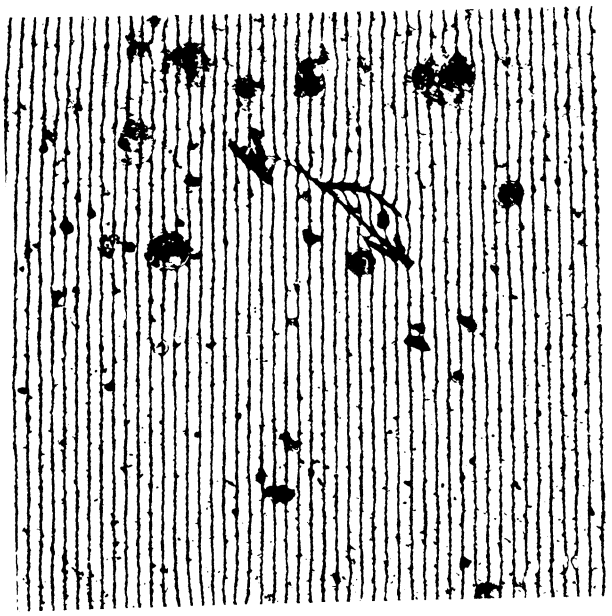

(c)

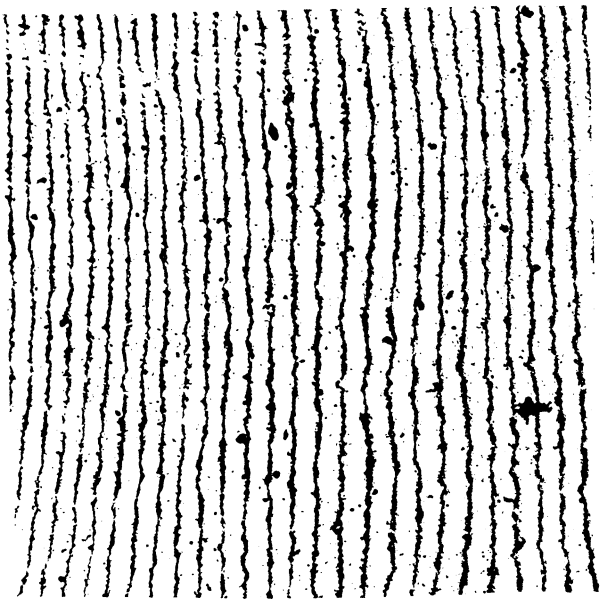

(d)

Figure 19. Laser interferometry photographs of (c) LaRC-TPI/fluorophlogopite and (d) LaRC-TPI/suzorite.

pronounced in the polyimide systems, where no metal particles could be found which were not in contact with at least one polymer particle. This is in contrast to the PEEK system, in which some isolated metal particles are seen, and agglomerations of PEEK particles persist to some degree. It is possible that the polymer particles are statically charged, and are attracted to the metal particles in an attempt to dissipate this charge. The attraction between the metal and Torlon powders appears to be unique due to the presence of some extremely fine polymer particles, which are strongly attracted to the metal. As shown in Figure A2, these very fine Torlon particles have entirely coated some of the larger metal particles. Since the particle size of the PEEK powder is less than 5μm, we might expect to see a similar phenomenon in the PEEK/metal system, but no such observations were made. It does appear that the presence of metal particles in the PEEK powder has reduced, but not eliminated, the agglomeration present in the PEEK alone.

The mixes containing mica reinforcement exhibit a distinctly different powder "morphology", as seen in Figures A4 through A6. In combination with the polyimide polymers, the suzorite mica is well mixed, but there is no interparticle attraction evident. Several isolated particles of both mica and polymer are visible in the micrographs. The mixture of PEEK and suzorite mica reveals a lesser degree of mixing and, again, no indication that any attraction exists between the two powders. The mixing appears to be less complete in this system as evidenced by large agglomerations of polymer still present.

Figure A7 is a micrograph of the Torlon/wollastonite mix. This micrograph shows the attraction of small Torlon particles to the wollastonite, as well as the particle size compatibility between these two materials.

The microscopically observed quality of particulate mixing appears to correlate well with quality of the molded plaques. Therefore, powder mixing quality may prove to be an inexpensive preliminary test for moldability.

One conclusion that can be drawn from these observations is that the metal reinforced systems are expected to show good wetting, while the mica reinforced systems should exhibit less perfect wetting. However, firm conclusions on the wetting of the polymer onto the reinforcement particles could be substantiated through the use of hot stage microscopy. In such an examination, the particulate mixtures could be observed at the molding temperature, and contact angles between the reinforcement particles and the molten polymer could actually be measured. Interferometry measurements on and visual inspection of the molded mica reinforced composites indicates that the quality of the interface is dependent on the type of mica being used. Another conclusion is that the PEEK powder tends to prefer polymer/polymer contacts over polymer/reinforcement contacts. However, this may not be a problem because of the particle size of this PEEK powder. If the polymer agglomerations are of approximately the same size as the reinforcement particles, the composite should still be homogeneous upon molding. These conclusions are supported by the mechanical and thermal data to be presented in the remainder of this chapter.

4.2 Mechanical Properties

The primary mechanical properties, such as strength, stiffness, and strain to failure, were determined by three-point-bend flexure tests (described in the previous chapter). Graphs showing the mechanical behavior of the polymers and composites tested in this study are shown in Appendix B. As expected, the addition of particulate reinforcements improves the stiffness of the polymer, with either a reduction or slight increase in strength. Figures B1 through B4 show how the flexural behavior of the metal and mica reinforced composites compare with the unreinforced polymer for each of the four matrix resins studied. In each case, the metal reinforced composite has a higher strength than the mica reinforced composite. This suggests a more effective transfer of load to the

reinforcement in the metal composite, and hence concurs with the idea that the polymer/metal interface is superior to the polymer/mica interface. The mica is a more effective stiffening reinforcement than the metal powder. This is not unexpected since mica is stiffer than the copper alloy, and the mica flakes posses aspect ratio while the metal particles are equiaxed.

Composites made from the three types of mica also exhibit a wide range of mechanical properties. Figures B5 and B6 show flexural stress-strain curves for LaRC-TPI and Torlon reinforced with each of the three types of mica. Suzorite is consistently the best mica reinforcement, exhibiting both higher stiffness and strength than either muscovite or synthetic fluorophlogopite. This difference in mechanical behavior is most probably due to the higher aspect ratio of the suzorite mica, since aspect ratio has been shown to have a strong effect on the reinforcement quality of mica[5,7]. However, there are also compositional and surface coating differences among the three types of mica which will most probably influence interface quality. Suzorite's high temperature retention of water may also help to improve its performance in these composites. For these reasons, suzorite was chosen as the preferred mica, and is used exclusively in the other two resin systems.

The effect of reinforcement volume fraction on mechanical properties was studied using LaRC-TPI reinforced with the Cu-Al-Ni alloy. Figure B7 shows stress-strain curves for this material with 40, 50, and 60 volume percent reinforcement. As the amount of metal reinforcement is increased, the stiffness also increases with an apparent diminishing return, while the strength of the material remains essentially unchanged. The relatively small increase in stiffness upon increasing the metal volume fraction from 50 to 60 percent is probably due to approaching the packing limit of the reinforcement spheres. The theoretical packing limit of spheres of equal size is 74 volume percent. The presence of a viscous polymer during consolidation makes it unlikely that this theoretical limit can be achieved in practice. It appears that a practical packing limit in

this case lies near 60 volume percent of metal reinforcement. Other volume fractions of copper alloy reinforcement could not be made in this study due to a very limited supply of the metal powder. At even higher reinforcement volume fractions, a point will eventually be reached at which there will be insufficient polymer to bind together the reinforcement particles. For example, suzorite mica reinforced Torlon plaques were molded with up to 80 volume percent mica. These plaques were extremely weak, and could not even be machined into test bars without crumbling due to lack of polymer binder.

To illustrate the importance of polymer/reinforcement particle size matching, synthetic fluorophlogopite mica was molded with both a coarse and a fine Torlon powder. The stress-strain curves of these two samples are shown in Figure B8. The modulus and ultimate strength of the coarse polymer composite are significantly lower than that of the fine polymer composite. In fact, the mechanical behavior of the coarse polymer composite indicates that it lacks structural integrity, and can bear essentially no load. In the samples made with the coarse polymer, the two constituent powders are not able to mix well. Since there is a significant amount of large polymer particles, there will be large resin-rich regions in the molded material corresponding in size to these large particles. Since the mica does not mix into these regions, it forms agglomerations of its own, resulting in a poorly mixed powder blend and therefore a poor composite. On the other hand, the fine Torlon powder is nearly the same size as the mica powder, and they are able to mix well in the dry powder state, resulting in a composite in which each mica particle is surrounded by polymer after molding. These results support the idea that particle size matching is critical to the successful fabrication of a composite by this method.

Figure B9 shows the flexural behavior of the Torlon/wollastonite and Torlon/suzorite/wollastonite samples in comparison to the Torlon/suzorite sample. Wollastonite used alone as a reinforcement increases the stiffness of the Torlon without

affecting its strength. Wollastonite used as a reinforcement with suzorite yields a composite with relatively low stiffness and strength. It is important to recall that the use of sized wollastonite will substantially improve the properties of both of these composites. The use of wollastonite was originally intended to improve the strength of the mica reinforced composites. Since the use of the unsized wollastonite resulted in properties which are so far below expectations, we must conclude that unsized wollastonite is unsuitable for this purpose. However, the use of sized wollastonite may still be worth investigating since the acicular nature of wollastonite particles is so unique.

Although the area under the stress-strain curve can be used as a general indication of toughness, a more quantitative measure of impact toughness is desired. The energy absorbed during impact was measured as described in the previous chapter in order to quantify toughness. The results of these impact tests are given in Table 3. As expected, the impact resistance was reduced upon reinforcement with particulates, with the exception of LaRC-TPI/Cu-Al-Ni reinforced at 40 volume percent. It seems that this particular combination of matrix and reinforcement resulted in a stronger interface than any other combination of materials considered in this study. In any given polymer system, the metal reinforced composite has a higher impact resistance than the mica reinforced composite, thus indicating again that the metal has a superior interfacial bond to the polymer as compared with the mica composite. While it was hoped that reinforcement with wollastonite would have produced higher values of impact resistance, it should again be noted that the wollastonite used here is unsized, and that sizings have been demonstrated to dramatically improve the mechanical properties of wollastonite reinforced polymers. Unfortunately, sized wollastonite samples were not available for testing in this study.

Failure mode was studied using SEM as described in the previous chapter. Fracture surface micrographs for several of the specimens are in Appendix C. Figures C1 through C5 show fracture

Table 3. Toughness Defined as Energy Absorbed During Impact.

Material	Energy (J)
LaRC-TPI	0.34
LaRC-TPI/Cu-Al-Ni	0.46
LaRC-TPI/Cu-Al-Ni(50)	0.29
LaRC-TPI/Cu-Al-Ni(60)	0.29
LaRC-TPI/suzorite	0.085
LaRC-TPI/muscovite	0.10
LaRC-TPI/fluorophlogopite	0.087
Torlon	1.44
Torlon/Cu-Al-Ni	0.59
Torlon/suzorite	0.03
Torlon/muscovite	0.02
Torlon/fluorophlogopite	0.10
Torlon/wollastonite(10)	0.37
Torlon/suzorite(30)/wollastonite(10)	0.04
PEEK	>>3*
PEEK/Cu-Al-Ni	0.29
PEEK/suzorite	0.035
Epoxy	0.31
Epoxy/suzorite(20)	0.05

* Samples did not fracture, but deformed so as to pass through the fixture unbroken.

Note: All composites are 40% reinforcement by volume unless otherwise indicated.

surface micrographs for LaRC-TPI and its composites. Unreinforced LaRC-TPI failed brittlely, and its fracture surface is shown in Figure C1. Figure C2 shows two micrographs of the fracture surface of LaRC-TPI/Cu-Al-Ni at different reinforcement volume fractions. In Figure C2(a), the 40 volume percent sample is shown, and matrix cracking is clearly evident as the predominant failure mode. Figure C2(b) shows the 60 volume percent sample. This micrograph shows an increase in fracture surface area due to the larger reinforcement surface area. In this sample the fracture surface is forced to move around the reinforcement particles in a convoluted path, rather than forming the relatively flat fracture surface of Figure C2(a). The lack of any exposed metal particles demonstrates the excellent adhesion in this system. Figure C3 is a fracture surface micrograph of LaRC-TPI/suzorite, showing clean mica flakes protruding from the plane of the photo, lacking any residually adhered resin. This would indicate that the failure mode in this case is flake pullout. Figure C4 shows a fracture surface of LaRC-TPI/muscovite, showing pulled out mica flakes that appear to have resin still attached. While this would seem to indicate an improved interface and therefore improved properties, we must also consider the importance of aspect ratio. Although the suzorite and muscovite composite fracture surfaces may appear to be very similar, the photo of the LaRC-TPI/muscovite surface is taken at more than twice the magnification. This confirms that the aspect ratio of the suzorite is significantly higher than that of the muscovite, and will therefore have a higher fracture surface area due to the pulled out flakes. This explains the superior strength and stiffness of the suzorite composite. Figure C5 is a micrograph of the fracture surface of LaRC-TPI/fluorophlogopite. The lack of mica visible on the surface, as well as the texture of the surface, indicates that the very small mica particles have completely debonded from the polymer. This indicates that the fluorophlogopite mica has the poorest interface of any of the reinforcement materials considered in this study.

Figures C6 and C7 are fracture surface micrographs of Torlon/Cu-Al-Ni and Torlon/suzorite composite. The interface in the Torlon/Cu-Al-Ni sample appears to be good, as evidenced by the resin which is attached to the metal particles. However, there are a few areas in which parts of exposed metal particles can be seen. This interface is probably not as strong as the LaRC-TPI/Cu-Al-Ni interface, but is still strong enough to make this material an attractive composite. The Torlon/suzorite fracture surface shows protruding mica flakes similar to the LaRC-TPI/suzorite sample. The mica flakes in this photo appear to protrude less than the other suzorite reinforced materials. Since the mechanical behavior of this sample is poor, both strength and stiffness are lower than expected, this effect is probably due to breakage of the mica during fracture rather than reduced pullout (which might indicate a stronger interface).

Figures C8 and C9 are fracture surface micrographs of PEEK/Cu-Al-Ni and PEEK/suzorite. The interface of Cu-Al-Ni with PEEK is much poorer than that of Cu-Al-Ni with the other two polymers, as indicated by the exposed Cu-Al-Ni particles on the fracture surface. The apparent interface strength as determined from the fracture surfaces, is directly proportional to the density of functional groups in the polymer structure (see structures in Figures 3, 7, and 9.). This may explain the variation in interface quality, and would explain the lowered failure strength of the PEEK/Cu-Al-Ni sample. Figure C8 gives the appearance that the PEEK and metal are not in good contact. This would normally be an indication of a weak interface, because in general, a weak interface allows a crack to propagate easily through a material. However, the stiffness and CTE reduction of this material are both good, indicating that load is indeed being transferred to the reinforcement at low strains. These results indicate that the interface is the weakest link in the composite during failure, but that the quality of the interface is good at low strains. The PEEK/suzorite fracture surface shows the characteristic protrusion of mica flakes, as well as the tough PEEK matrix deformed between the flakes. This

material exhibits good strength for a mica reinforced composite, but its stiffness is only slightly higher than the PEEK/Cu-Al-Ni sample. The lower than expected stiffness of PEEK/suzorite indicates that this sample has a less than ideal interface. The PEEK/suzorite composite is one of the samples which appears visually inhomogeneous, leading us to conclude that some agglomeration or segregation of the reinforcement exists. This would result in a lower effective interface area. A reasonable conclusion is that the interface that does exist in this sample is good, but that the interface area is reduced causing a deterioration of properties. Unlike the other composites in this study, the PEEK/suzorite composite appears to have failed by a combination of flake pullout and matrix deformation. This matrix deformation may explain the high relative failure strength of this sample as compared to the other suzorite reinforced composites.

Figure C10 is a fracture surface micrograph of epoxy/suzorite. Unlike the other suzorite reinforced composites, the mica in this composite is randomly oriented. The mica flakes appear to be broken at the fracture surface, rather than pulled out as in the other suzorite reinforced samples. Since this would indicate that the interface is strong, we expect this composite to have a high stiffness, which it does. epoxy/suzorite also has a lowered strength, which is easily explained by the features present in the micrograph of Figure C10. First, since the suzorite flakes are randomly arranged in the matrix, only a fraction of them are reinforcing effectively in the direction of the applied load. Secondly, the failure process involves breaking the flakes in a bending mode. The suzorite flakes are brittle, and will break easily in bending. In a sense, the bonding in this composite is too good. The debonding process is one which absorbs energy, and since the reinforcements in this composite are fracturing instead of debonding, it will require less energy in order to fail. Energy absorption is maximized at a certain optimal adhesion level, and in most composite systems, this optimal level is not the case of maximum adhesion.

Figures C11 and C12 are fracture surface micrographs of Torlon/wollastonite and Torlon/suzorite/wollastonite. Figure C11 shows how the wollastonite particles have pulled out from the matrix. There is no resin attached to the particles, indicating a relatively weak interface. Figure C12 shows that the Torlon/suzorite/wollastonite sample looks much like the Torlon/suzorite sample, with the exception of the presence of voids out of which the wollastonite particles have been pulled. The lowered strength of this composite in comparison to the Torlon/wollastonite composite may be due to the reduced amount of polymer (60 volume percent as opposed to 90 volume percent). A reduced amount of polymer will result in a lower strain-to-failure (this phenomenon will be described in detail in the next chapter). If the strain-to-failure is decreased, but the modulus is unaffected, the strength must correspondingly decrease.

4.3 Thermal Properties

The thermal expansion coefficient of a material is a direct measure of its dimensional stability upon heating. The lower the coefficient of thermal expansion (CTE), the less the size and shape will change with temperature. For dimensional stability, a low CTE is desired. However, when parts made of many different materials are joined together, they must have similar CTEs. If there is a large CTE mismatch, failure of the joints may occur. Therefore, the possibility of a CTE mismatch must also be considered when determining which CTE is most desirable.

In general, thermal expansion coefficients of ceramics are lower than those of metals, which are in turn lower than those of polymers. When these materials are combined as they are in these composites, intermediate CTE values are obtained. Upon heating, the reinforcement particles expand a small amount. The polymer surrounding each particle wants to expand to a greater degree, but is restricted from doing so by its bond with the reinforcement particle.

Therefore, we expect the CTE of a polymer to be reduced upon reinforcement with particulates. The smaller the CTE of the reinforcement material, the larger the reduction in the composite CTE should be. If, however, the interfacial bond is so weak that it fails at low thermal strains, the CTE will increase, and the composite will no longer be useful due to the failed interface. Since the mechanism by which the thermal expansion coefficient is decreased involves a transfer of load across the interface, one would expect lowering of the CTE in these composites to follow the same trends as the increase in elastic modulus. This is, in fact, the trend observed in the data of this study.

Appendix D contains the graphs showing thermal behavior. Figures D1 through D4 show the effect of reinforcement on the thermal expansion behavior of the four resin systems under consideration. The thermal expansion behavior upon cooling to room temperature was also measured, but is not shown in these figures for the sake of clarity. The thermal expansion coefficient is determined by the slope of these expansion versus temperature curves. Also, the CTE values of all composites in this study are listed in Table 4. As expected, the composites have lower CTEs than the unreinforced polymer, with the mica having a more pronounced effect than the metal. Again, mica has a larger effect not only because of its low CTE, but also because of its aspect ratio.

The thermal expansion behavior of the PEEK composites (Figure D3) is unique in that the temperature range studied includes the glass transition temperature (T_g) of the polymer. When a polymer is heated through its T_g, the CTE of the polymer increases; a positive $\Delta\alpha$ exists, where $\Delta\alpha$ is the difference between the CTE of the rubbery, high temperature state and the CTE of the glassy, low

Table 4. Coefficients of Thermal Expansion. ($x10^{-6}/°C$)

Material	Measurement Technique: Interferometry	Dilatometry: 10°C/min.	Dilatometry: 5°C/min.
LaRC-TPI	46.3	41.9	47.7
LaRC-TPI/Cu-Al-Ni	30.9	29.5	29.5
LaRC-TPI/Cu-Al-Ni(50)			27.8
LaRC-TPI/Cu-Al-Ni(60)			25.1
LaRC-TPI/suzorite			14.7
LaRC-TPI/muscovite			14.4
LaRC-TPI/fluorophlogopite	28.3	25.5	27.1
Torlon			44.5
Torlon/Cu-Al-Ni			30.9
Torlon/suzorite			14.0
Torlon/suzorite(50)			13.7
Torlon/suzorite(60)			12.4
Torlon/suzorite(70)			12.3
Torlon/suzorite(80)			12.2
Torlon/muscovite			12.8
Torlon/fluorophlogopite			12.0
Torlon(coarse)/fluorophlogopite			25.9
Torlon/wollastonite(10)			10.4
Torlon/suzorite(30)/wollastonite(10)			7.3
PEEK			14.9
PEEK/Cu-Al-Ni			11.8
PEEK/suzorite			8.4
Epoxy			53.4
Epoxy/suzorite(20)			39.6

Note: All composites are 40% reinforcement by volume unless otherwise indicated.

temperature state.[1] This phenomenon is clearly evident in Figure D3. The T_g of PEEK as indicated by these expansion measurements is 145°C, and is only slightly less than the DSC value of 156°C. This effect is seen best in the second and subsequent tests on a given sample, because the first time a sample is heated through its T_g in a dual-push-rod dilatometer, the sample deforms at T_g to relieve the stress applied by the push-rod. It is interesting to note that not only is the overall CTE decreased upon reinforcement, but $\Delta\alpha$ is also reduced.

Different types of mica reinforcement have different effects on the composite thermal expansion coefficient. For example, Figure D5 shows the thermal expansion behavior of LaRC-TPI/mica composites. The CTE of LaRC-TPI/fluorophlogopite is nearly twice that of LaRC-TPI/suzorite and LaRC-TPI/muscovite. Since we already have evidence that the LaRC-TPI/fluorophlogopite composites have agglomerations of mica particles, there may be a substantial reduction in effective interface area. This would mean that there was less restraining force on the polymer as it attempted to expand, resulting in the higher CTE.

Figure D6 shows the thermal expansion behavior of the Torlon/mica composites. Although the CTE values of the suzorite and muscovite reinforced composites are not as close as in the LaRC-TPI system, they do exhibit similar behavior. The change in slope of these two expansion curves may be due to weak interfacial bonding in these materials. If the interface is very weak, the stress resulting from the CTE mismatch between the polymer and the mica may be enough to fail the interface. If a significant portion of the particles are debonded from the matrix at a certain temperature, the CTE

---

[1] $\Delta\alpha$ is an important quantity to measure in thermodynamic modeling of the glass transition of polymers. The thermal expansion coefficient and the other second derivatives of Gibb's free energy, heat capacity and compressibility, are discontinuous at T_g. These discontinuities are related by the Ehrenfest equation[28,29]. When attempting to prove the validity of a thermodynamic model, it is essential to measure each of these discontinuities independently.

would undergo a discontinuous increase. This appears to happen in the Torlon/suzorite sample at about 100°C, and in the Torlon/muscovite sample at about 70°C, as indicated by the changes in slope at these temperatures in Figure D6.

The Torlon/fluorophlogopite sample exhibits entirely different behavior in Figure D6. I believe the extreme structural weakness of this material allows the sample to compress in the push-rod dilatometer during the first third of the heating cycle. Above 100°C, the CTE of this material is only slightly less than the CTE of the unreinforced polymer, indicating that there is almost no coupling of the reinforcement to the polymer at this point.

In an attempt to determine the effect of particle size mismatch on thermal expansion behavior, Torlon/fluorophlogopite samples fabricated with both fine and coarse Torlon powder were tested. The resulting curves are shown in Figure D7. Both of these samples are extremely weak, and apparently undergo compression during the test as described above. It is not surprizing that the curve for the composite made from coarse powder lies above that for the composite made from fine powder. The large particles of resin provide less of a chance for interfaces to form, thus allowing the large thermal expansion of the polymer to dominate.

As the reinforcement volume fraction is increased, the CTE is expected to decrease. Two sample series with varying reinforcement content were studied: LaRC-TPI/Cu-Al-Ni and Torlon/suzorite. Their thermal expansion curves are shown in Figures D8 and D9, respectively. Figure D8 shows the expected drop in CTE with reinforcement volume fraction, and the average values for the LaRC-TPI/Cu-Al-Ni series in Table 4 show a considerable decrease in CTE with increasing volume fraction. On the other hand, Figure D9 reveals some puzzling results for the Torlon/suzorite system, with an initial decrease in CTE and then an increase in CTE as the reinforcement volume fraction is increased from 40 to 80 percent. This is inconsistent with the values listed in Table 4 for this series. This inconsistency is due to the fact that the graph of Figure D9

shows the initial heating runs of the samples, while the table lists the average CTE values of three runs. The average values for both of these series follow the expected trend of decreasing CTE upon higher volume fraction reinforcement. However, although the trends are as expected, the CTE drop diminishes as higher volume fractions are reached. This is a sign that the practical packing limit of the composites has been reached. At such high reinforcement volume fractions, the amount of polymer in the composite becomes insufficient to form an interface with all of the reinforcement particles. If the reinforcement particles do not form an interface, they do not contribute to the modification of properties. This also gives us some insight as to why the behavior of the suzorite reinforced composites breaks down at a lower reinforcement fraction than in the Cu-Al-Ni reinforced composites. The surface-to-volume ratio is higher for flakes than for spheres. Therefore, increasing flake reinforcement from 40 to 50 volume percent represents a larger increase in reinforcement surface area than increasing sphere reinforcement from 40 to 50 volume percent. Since the polymer forms an interface with the surface area of the reinforcement particles, a composite would be expected to tolerate a larger amount of spherical reinforcements before properties begin to suffer.

Figure D10 is a graph showing the thermal expansion behavior of the wollastonite reinforced composites in comparison to Torlon and Torlon/suzorite. Wollastonite appears to be more effective at reducing the CTE than suzorite. Torlon/wollastonite has a lower CTE at a much lower volume fraction of reinforcement. Also, Torlon/suzorite/wollastonite has the lowest CTE of all composites considered in this study. The CTE of wollastonite is lower than any of the other reinforcements used, in fact it is only about half of the value of suzorite. This low CTE combined with the aspect ratio of wollastonite's particles may be responsible for the extremely low CTE of these composites. It is unusual that the wollastonite reinforcement appears to be ineffective in improving the elastic modulus of the composite, and at the same time, very effective in

improving the CTE, since both of these processes rely on a good interface. However, the difference between these two properties is the strain level at which they are measured. Apparently, the Torlon/wollastonite interface is efficient at transferring load at the low strains involved in the thermal expansion measurement, but begins to fail at the higher strain levels experienced during a flexure test. The strains experienced during modulus determination are two orders of magnitude higher than those experienced during CTE testing.

The glass transition temperature, T_g, of all of the composite materials in this study were measured by DSC, as described in the preceding chapter. The results are listed in Table 5. These results show that no significant change in T_g has occurred as a result of reinforcement. However, the heat distortion temperature of a material depends not only on T_g, but also on modulus. Since the modulus is increased and the T_g is unaffected, heat distortion temperature must also increase. Since heat distortion temperature is a thermo-mechanical property rather than a strictly thermal property, it is a more appropriate measure of the high temperature behavior of these materials under stress. Therefore, although the heat distortion temperature was not explicitly measured, we expect that the heat distortion temperature of these composites will be higher than that of the unreinforced resins.

Table 5. Glass Transition Temperature as Determined by DSC.

Material	T_g (°C)
LaRC-TPI	246
LaRC-TPI/Cu-Al-Ni	250
LaRC-TPI/Cu-Al-Ni(50)	253
LaRC-TPI/Cu-Al-Ni(60)	247
LaRC-TPI/suzorite	247
LaRC-TPI/muscovite	248
LaRC-TPI/fluorophlogopite	247
Torlon	281
Torlon/Cu-Al-Ni	281
Torlon/suzorite	285
Torlon/muscovite	282
Torlon/fluorophlogopite	283
Torlon/wollastonite(10)	288
Torlon/suzorite(30)/wollastonite(10)	288
PEEK	156
PEEK/Cu-Al-Ni	151
PEEK/suzorite	155
Epoxy	190
Epoxy/suzorite(20)	188

Note: All composites are 40% reinforcement by volume unless otherwise indicated.

5. Mathematical Models

Many mathematical models have been proposed to predict the behavior of composite materials. These models typically take into account several of the following factors which affect the properties of a composite: the properties of the constituent components, the shape of the reinforcement phase, the morphology of the system, and the nature of the interface[30]. These models have resulted in equations which can be used to calculate certain properties of a composite material. In this chapter, the calculations of some of these models will be examined as approximations to the experimental data gathered in this study.

Rigorous models specific to the materials made here simply do not exist. This being the case, simple general models will be examined as upper and lower bounds, or used as approximations of the measured material properties. This will lead to a general understanding of the experimental results, rather than a quantitative prediction.

The rule-of-mixtures (ROM) and the inverse rule-of-mixtures provide good first order approximations of composite properties in a wide variety of cases. Therefore, these models will be used to

calculate upper and lower bounds for the elastic modulus and coefficient of thermal expansion in our systems. It should be noted, however, that these models assume a brittle matrix and reinforcement. Since two of the matrix materials (Torlon and PEEK) are ductile, these models may not be completely accurate. However, they should still provide a reasonable first approximation. Strain-to-failure, strength and toughness will be predicted by a simple model proposed by Nielsen[31].

5.1 Rule-of-Mixtures and Inverse Rule-of-Mixtures

The rule-of-mixtures assumes that load is applied to a composite under isostrain conditions. This means that the composite undergoes spatially uniform strain, with the matrix and reinforcement experiencing the same strain level. Since the matrix and reinforcement will typically have different moduli, they will therefore be under different amounts of stress that can be summed to give the total stress level. These conditions may be written:

$$\varepsilon_c = \varepsilon_m = \varepsilon_r$$

$$\sigma_c = \sigma_m + \sigma_r$$

where ε is strain, σ is stress, and the subscripts indicate "composite", "matrix", and "reinforcement", respectively. These subscripts will remain consistent throughout this chapter. While the rule-of-mixtures is most commonly used to predict elastic modulus, it is also valid for properties such as thermal conductivity, diffusivity, and electrical conductivity[32]. Substituting the linear elastic expression $\sigma=\varepsilon E$ into the sum of stresses equation above yields the traditional ROM expression for modulus:

$$E_c = E_m v_m + E_r v_r$$

where E is elastic modulus and v is volume fraction. The corresponding ROM equation for predicting coefficient of thermal expansion under isostrain conditions is as follows:

$$\alpha_c = (\alpha_m E_m v_m + \alpha_r E_r v_r)/(E_m v_m + E_r v_r)$$

where α is coefficient of thermal expansion, E is elastic modulus, and v is volume fraction[32].

The inverse rule-of-mixtures assumes isostress conditions. In other words, the matrix and reinforcement experience the same amount of stress, but undergo different amounts of strain that can be summed to give the total strain level. These conditions are written as:

$$\sigma_c = \sigma_m = \sigma_r$$

$$\varepsilon_c = \varepsilon_m + \varepsilon_r$$

This model is generally more accurate for predicting particulate reinforced composite properties than the rule-of-mixtures. This is due to the strain magnification which occurs in the matrix, much like the illustration in Figure 20 Substituting the linear elastic expression $\varepsilon=\sigma/E$ into the sum of strains equation above yields the following harmonic mean expression for modulus:

$$1/E_c = v_m/E_m + v_r/E_r$$

The corresponding harmonic mean equation for predicting coefficient of thermal expansion under isostress conditions is:

$$\alpha_c = (1+\nu_m)\alpha_m v_m + \alpha_r v_r$$

where ν is Poisson's ratio[32]. This equation is valid when the reinforcement volume fraction is greater than 0.3, a condition which

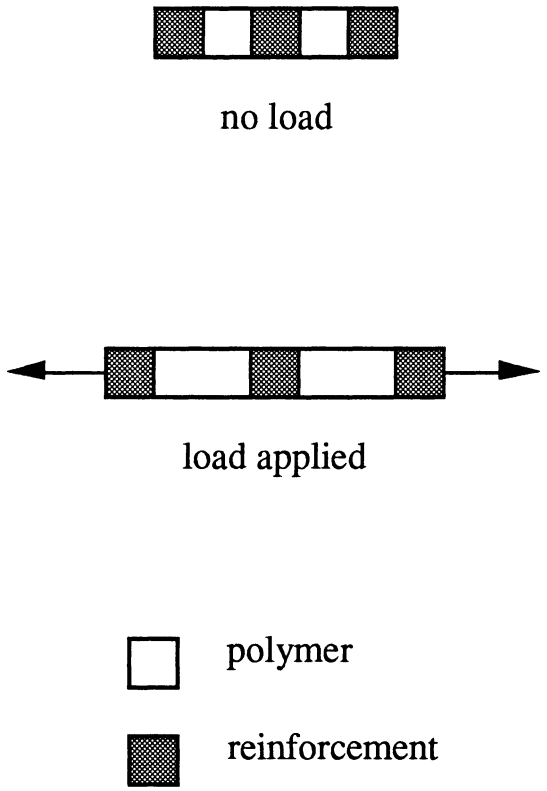

Figure 20. Illustration of preferential elongation of polymer when a composite is loaded under isostress conditions. (after ref. 31)

is met by all of the composites in this study. The value of Poisson's ratio is taken to be the homogeneous material value, 0.3, for all of the matrix materials considered here.

5.2 Predictive Equations for Strain-to-Failure, Strength and Toughness

The strain-to-failure of a composite must be different from its component materials as long as the matrix and reinforcement have different moduli. In the case of a reinforcement which is much stiffer than its matrix, the elongation of the reinforcement phase can be neglected, and the strain-to-failure of the composite should be much less than that of the unreinforced resin. This phenomenon is illustrated in Figure 20. In order for a composite to undergo a certain amount of overall strain, the polymer matrix must elongate to a higher local strain to compensate for the reinforcement particles, which contribute essentially no elongation. Therefore, the polymer phase may reach its failure strain locally, while the composite as a whole experiences a relatively low overall strain. The strain-to-failure in particulate reinforced composites has been shown to be well represented by the expression[31]:

$$\varepsilon_c = \varepsilon_m(1 - v_r^{1/3})$$

It should be noted that this relationship was derived for the case of perfect particulate/matrix adhesion. The case of no adhesion will result in strains-to-failure much closer to that of the polymer matrix[31]. Therefore, large positive deviations from these predictions may indicate a lack of good matrix/reinforcement bonding.

If the stress-strain curve of the composite is assumed to be a straight line (i.e. a linear elastic material with a brittle failure mode) the prediction of strength and toughness is a simple matter. For the composites in this study, the above assumption is fairly accurate.

Once the elastic modulus and strain-to-failure are known, one can calculate failure strength from the simple linear elastic relationship:

$$\sigma_f = E\varepsilon_f$$

Toughness may be estimated by the area under the stress-strain curve. In the case of a linear elastic stress-strain curve, toughness is simply the triangular area:

$$\text{Toughness} = \sigma_f\varepsilon_f/2 = E\varepsilon_f^2/2$$

5.3 Relationship between Tensile and Flexural Properties

Most models propose equations based on tensile loading rather than flexural loading. Because these conditions are not equivalent, and the data in this study includes strictly flexural data, I will discuss some of the discrepancies between tensile and flexural properties. The only significant discrepancy is likely to occur in fracture strength.

Determinations of the strength of a material by tensile test and by flexural test often result in different values. This is due to the different states of stress that are induced by the two different loading situations. In a tensile test, the entire specimen is in pure tension. In a three-point-bend flexural test, tensile, compressive and shear stresses are present in the sample, and the point on the lower surface of the bar directly under the nose of the test fixture is the point of maximum tensile stress. The relative magnitudes of these different types of stresses depend on the geometry of the test specimen, specifically the "span-to-depth ratio". The "span" is the distance between the outer supports of the test fixture, and may be limited by the length of the sample. The "depth" is the thickness of the sample in the direction of the applied load. A span-to-depth ratio of 16:1 is commonly accepted as sufficient to ensure that the

sample fails due to the tensile stress. However, it is possible for shear stresses to affect the failure of the specimen even at a ratio of 16:1. The three-point-bend flexural tests in this study were conducted at a span-to-depth ratio of 16:1 due to the size and shape of the specimens. If shear stresses are affecting the strength results, they would tend to cause a lower measured strength to be obtained, as compared to a tensile test.

Materials which fail brittlely behave differently in tension and in flexure for an additional reason. Failure in brittle materials tends to initiate at the largest flaw in the region under stress. This is because flaws act as stress concentrators, raising the local level of stress and initiating a crack. In a tensile test, the entire specimen experiences the same amount of stress, and the largest flaw will initiate failure regardless of its location. In a flexural test, a small region under the loading nose of the test fixture experiences the largest amount of stress. Therefore, failure should initiate at the largest flaw in that small region. Statistically, specimens tested in flexure should initiate failure at smaller flaws, and therefore should fail at higher stresses. Since all of the composite materials considered in this study failed brittlely, this effect may play a role in any discrepancy between measured and calculated strength values.

Both effects presented above have the potential of affecting the comparison of measured flexure properties with predicted tensile properties. Since the two effects act in opposition to each other, it is difficult to predict how the measured values will be affected.

5.4 Comparison of Measured Data with Predictive Models

The isostrain and isostress models are expected to be upper and lower bounds for the experimental data. We can use some combination of these two models to achieve a better approximation of the data. One common intermediate prediction was developed for the case of short fibers randomly distributed and randomly oriented

in a matrix. In this prediction, the two models are combined in the following way:

$$\text{mixed mode} = (3/8)\text{isostrain} + (5/8)\text{isostress}.$$

Although this mixed mode model is most probably not quantitatively accurate for the materials studied here, it does give a better first order approximation than the isostrain or isostress model alone.

The component properties used in the calculations are listed in Table 6, along with referenced sources. The resulting predictions for modulus and coefficient of thermal expansion are listed in Tables 7 and 8, respectively. The modulus data are bounded by the isostress and isostrain models, whereas the CTE data do not fall entirely within those bounds.

In order to gain a better understanding of how the measured data compare with the models, the elastic modulus and CTE data for the LaRC-TPI/Cu-Al-Ni compositional series is plotted together with the various model calculations. This comparison for elastic modulus is shown in Figure 21, and this comparison for coefficient of thermal expansion is shown in Figure 22. One important note about Figure 22 is that the three models predict different values at zero reinforcement volume fraction. This is because this version of the isostress model breaks down below 0.3 reinforcement volume fraction. As was expected, the mixed mode model using 3/8 and 5/8 of the isostrain and isostress values is inadequate in describing the behavior of the data. However, by choosing different coefficients for the isostrain and isostress terms, a new mixed mode model can be created which will more adequately describe the data. This new model is represented in Figures 21 and 22 by the dashed curves. The new mixed mode model coefficients for all of the Cu-Al-Ni and suzorite reinforced composites are listed in Table 9. All of the polymer/Cu-Al-Ni moduli are heavily dominated by isostress behavior, as indicated by the isostress coefficients near 1.0. This is not unexpected because, in the case of particulate reinforcement,

Table 6 Material Property Values for Individual Components.

Material	E (GPa)	σ_f (MPa)	ε_f	CTE ($x10^{-6}$/°C)
LaRC-TPI	4.2[a]	153[a]	.037[a]	47.7[a]
Torlon	3.3[a]	170[a]	.15[b]	44.5[a]
PEEK	3.1[a]	158[a]	1.5[c]	14.9[a]
Cu-Al-Ni	125[d]	-	-	17.6[e]
suzorite	172[f]	-	-	13.7[f]

[a] measured value
[b] from ref. 17
[c] from ref. 33
[d] modulus of Cu-Al alloy of similar composition, from ref. 34
[e] CTE of copper, from ref. 35
[f] from ref. 20

Table 7 Comparison of Measured Elastic Moduli to Predicted Values. (GPa)

	Isostrain	Isostress	Mixed Mode	Measured
LaRC-TPI/Cu-Al-Ni	52.5	6.9	24.0	13.7
LaRC-TPI/Cu-Al-Ni(50)	64.6	8.2	29.3	20.4
LaRC-TPI/Cu-Al-Ni(60)	76.7	10.0	35.0	24.1
Torlon/Cu-Al-Ni	52.0	5.4	22.9	8.5
PEEK/Cu-Al-Ni	51.9	5.1	22.6	7.4
LaRC-TPI/suzorite	71.3	6.9	31.1	27.2
Torlon/suzorite	70.8	5.4	29.9	12.4
PEEK/suzorite	70.6	5.12	29.7	11.0

Table 8 Comparison of Measured Coefficients of Thermal Expansion to Predicted Values. ($x10^{-6}/°C$)

	Isostrain	Isostress	Mixed Mode	Measured
LaRC-TPI/Cu-Al-Ni	19.1	44.3	34.8	29.5
LaRC-TPI/Cu-Al-Ni(50)	18.6	39.8	31.9	27.8
LaRC-TPI/Cu-Al-Ni(60)	18.3	35.4	29.0	25.1
Torlon/Cu-Al-Ni	18.6	41.8	33.1	30.9
PEEK/Cu-Al-Ni	17.5	18.7	18.2	11.8
LaRC-TPI/suzorite	15.0	42.7	32.3	14.7
Torlon/suzorite	14.6	40.2	30.6	14.0
PEEK/suzorite	13.8	17.1	15.9	8.4

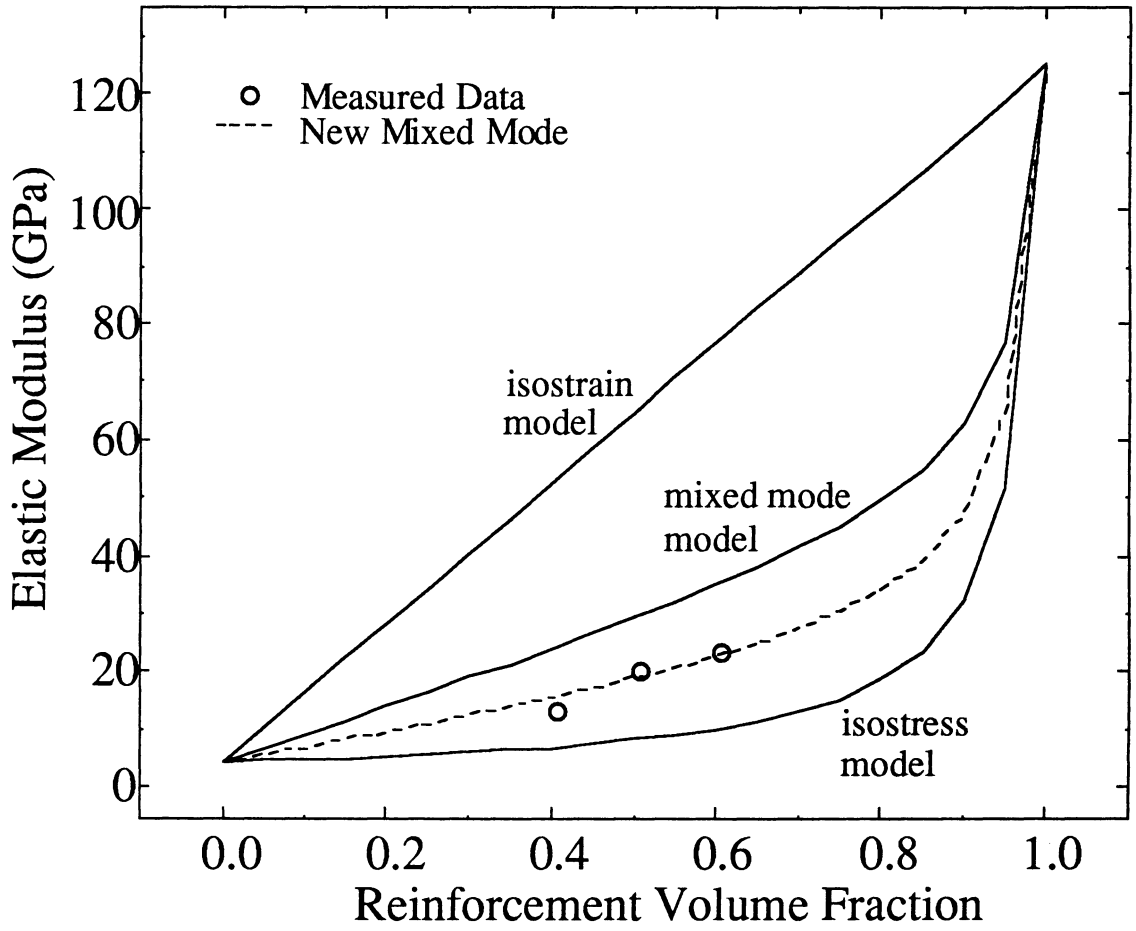

Figure 59. Modulus data for LaRC-TPI/Cu-Al-Ni in relation to predictive models.

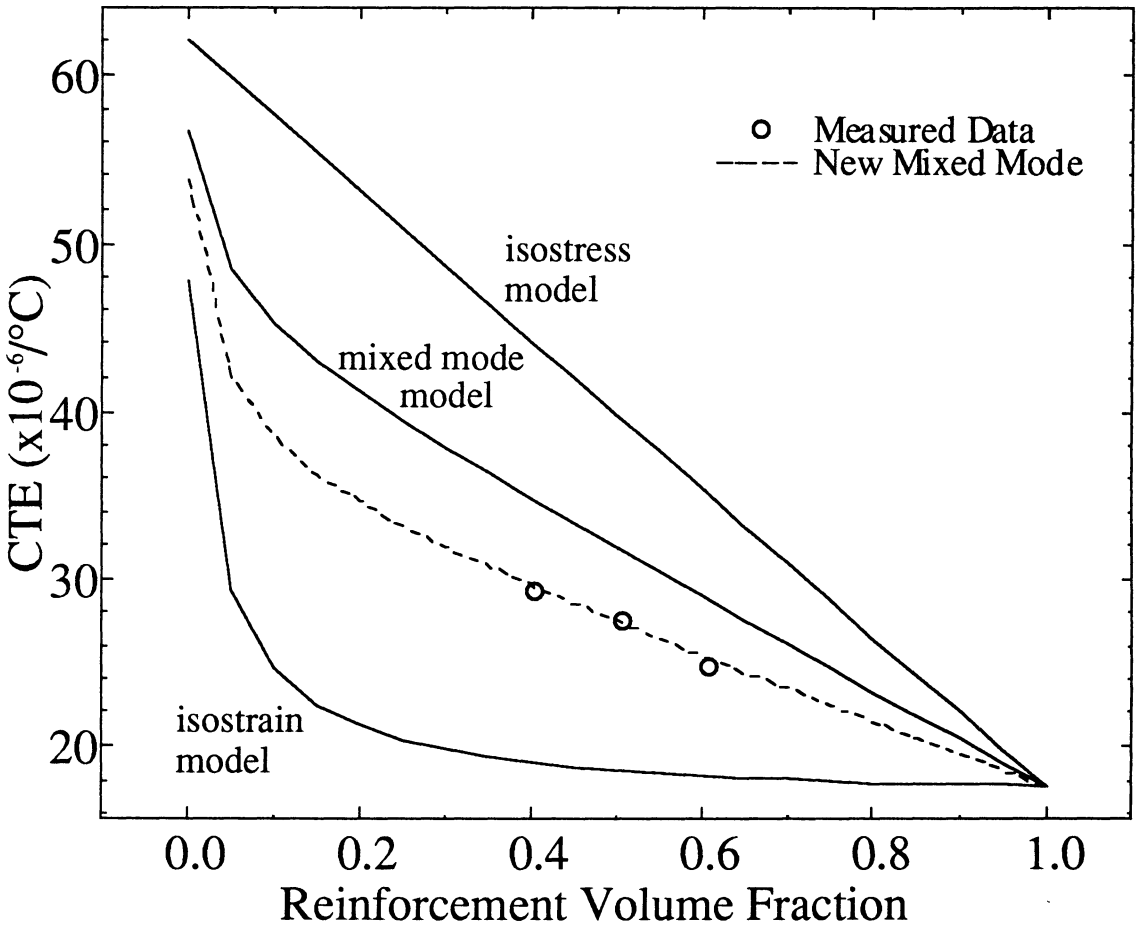

Figure 60. CTE data for LaRC-TPI/Cu-Al-Ni composites in relation to predictive models.

Table 9 Coefficients for Modified Mixed Mode Models.

Elastic Modulus

	Isostrain Coefficient	Isostress Coefficient
LaRC-TPI/Cu-Al-Ni	.19	.81
Torlon/Cu-Al-Ni	.07	.93
PEEK/Cu-Al-Ni	.05	.95
LaRC-TPI/suzorite	.32	.68
Torlon/suzorite	.11	.89
PEEK/suzorite	.09	.91

Coefficient of Thermal Expansion

	Isostrain Coefficient	Isostress Coefficient
LaRC-TPI/Cu-Al-Ni	.58	.42
Torlon/Cu-Al-Ni	.47	.53
PEEK/Cu-Al-Ni	*	*
LaRC-TPI/suzorite	1.0	0
Torlon/suzorite	1.0	0
PEEK/suzorite	*	*

* Composite value lies outside the isostrain-isostress bounds.

there are no constraints on the reinforcement requiring it to strain to the same degree as the matrix, and therefore, a largely isostress condition exists. Also, the stiffness of Cu-Al-Ni is more than twenty times that of LaRC-TPI, which means that the contribution of Cu-Al-Ni to the elongation of the composite will be essentially negligible. On the other hand, the polymer/Cu-Al-Ni coefficients of thermal expansion behave as a nearly equal combination of the isostrain and isostress models, as indicated by the coefficients in Table 9. This would indicate that the polymer phase of the composite is no longer providing nearly all of the overall elongation. This suggests that the reinforcement particles are straining to a greater degree, relative to the polymer, than they were in the mechanical loading situation. The CTE of Cu-Al-Ni is about one third that of LaRC-TPI, which means that, under a thermal load, Cu-Al-Ni will provide a significant amount of the composite elongation. This can be contrasted to the elastic moduli of the polymers and Cu-Al-Ni, which varied by a factor of twenty, and exhibited much more isostress behavior.

The moduli of the polymer/suzorite composites also exhibit mostly isostress behavior, but to a consistently lesser degree than the corresponding polymer/Cu-Al-Ni composites. This is to be expected since the suzorite flakes have aspect ratio in the direction of the applied stress. Because of the flake shape of the particles, the elongation, at a given strain level, in the plane of the flake will be higher than if the particle were a sphere. Therefore, a flake reinforced composite will tend to resemble an isostrain condition more so than a sphere reinforced composite. The suzorite reinforced materials appear to behave entirely in an isostrain manner under a thermal load. This may be due to the morphology of the composite. Because of the shape of the mica flakes, and their tendency to align, the interparticle spacing will be very small. This means that the polymer, at any point in the composite, will be sandwiched between suzorite particles. In this situation, the mica will be able to prevent the polymer from expanding very effectively.

Table 10 Comparison of Predicted and Measured Strains-to-Failure.

	Predicted	Measured
LaRC-TPI/Cu-Al-Ni	.0097	.014
LaRC-TPI/Cu-Al-Ni(50)	.0076	.0080
LaRC-TPI/Cu-Al-Ni(60)	.0058	.0080
Torlon/Cu-Al-Ni	.039	.016
PEEK/Cu-Al-Ni	.39	.021
LaRC-TPI/suzorite	.0097	.0043
Torlon/suzorite	.039	.005
PEEK/suzorite	.39	.0093

The thermal expansion of the PEEK composites is very unusual and warrants attention. For these composites, the isostrain and isostress models do not bound the data. This may be due in part to the fact that PEEK is an extremely ductile polymer, and these models assume a brittle matrix. The CTE values measured for these two composites are actually lower than the CTE of either of the components. This is highly unusual and would make an interesting topic for further study.

The strain-to-failure calculations are compared with the measured values in Table 10. The LaRC-TPI/Cu-Al-Ni data agree fairly well with the predictions. The 60 volume percent reinforced specimen exceeds the prediction, but this is easily understood since this specimen has already shown signs of approaching the practical packing limit. This would decrease the effective interface area, making the composite behave as a poorly bonded system, which would have a higher strain-to-failure. The Torlon/Cu-Al-Ni and PEEK/Cu-Al-Ni composites fail at lower than the predicted strains. In examination of the fracture surfaces of these two composites, some exposed reinforcement was observed (Figures C6 and C8). This would indicate that failure of the interface is playing a role in the failure of the sample. This would explain why the full failure strain of the polymer is not being reached. Additionally, the amount of exposed reinforcement on the fracture surface seems to correspond to the degree to which the measured and predicted failure strains disagree. In the Torlon/Cu-Al-Ni fracture surface, only small portions of some particles are exposed, and the measured strain-to-failure is about half of the predicted value. In the PEEK/Cu-Al-Ni fracture surface, nearly every particle on the surface is entirely exposed, and the measured strain-to-failure is less than one tenth of the predicted value.

The strains-to-failure of the suzorite composites are greatly overpredicted by this model. This is due in part to the high aspect ratio of the suzorite particles. With respect to the illustration of Figure 20, the areas of reinforcement would be even larger in

relation to the areas of the polymer, making the strain magnification in the polymer even higher than the equiaxed particulate reinforcement case. Therefore, we would expect the strain-to-failure to be even lower in the suzorite reinforced samples. In addition, interface failure is most probably affecting the results similarly to the Cu-Al-Ni reinforced Torlon and PEEK samples.

At this point, the strength and toughness of the composites could be calculated by assuming a linear stress-strain curve, as shown earlier in this chapter. This would require the use of predicted moduli and strains-to-failure. Since none of the moduli were quantitatively predicted, experimental values could be used along with predicted values for strain-to-failure. This would be possible for the LaRC-TPI/Cu-Al-Ni 40 and 50 volume percent reinforced, samples. But, since the other strains-to-failure are not well predicted, the results of these calculations would not be very informative.

Overall, the combination of isostrain and isostress models provides a method of understanding the trends in the data using a micromechanics approach. By using these simple models, the numerical results can be explained in terms of the structure of the composite material.

6. Conclusion

6.1 Summary

The objectives of this thesis are to develop a fabrication process for particulate reinforced composites which exploits the nature of fine powder matrix and reinforcement materials, and to characterize the properties of composites molded by this process. These objectives have been realized through the following accomplishments:

- The component materials were thoroughly characterized. DSC was used to identify all phase transitions in the component materials during the molding cycle. Optical microscopy was used to study particle shape and to give an estimate of particle size and its distribution. Optical microscopy also yielded information about particle interactions.

- A fabrication process tailored to the use of fine powders was developed. A dry powder blending step which provided for intimate mixing of the polymer and reinforcement was employed. A suitable combination of molding temperature and pressure were determined for each system studied.

- This process was used in the fabrication of eleven different composite specimens. LaRC-TPI, Torlon and PEEK polymer powders were each molded with Cu-Al-Ni metal powders and suzorite mica powders. Wollastonite and other types of mica powders were also used as reinforcements in some of the polymers.

- The composites were characterized in terms of mechanical and thermo-mechanical properties. Three-point-bend flexure tests were performed to determine strength, stiffness and strain-to-failure. Instrumented impact tests were performed to determine toughness. SEM was conducted on the fracture surfaces to determine failure mode. Dilatometry and laser interferometry were performed to determine coefficient of thermal expansion. Glass transition temperatures, determined from DSC scans, were combined with elastic modulus data to draw conclusions about heat distortion temperature.

- Simple isostrain and isostress models were used as upper and lower limits in estimating the behavior of these materials. Mixed mode models were used to more closely estimate the observed behavior.

These accomplishments lead to the following conclusions:

- Homogeneous, structurally sound, particulate reinforced composites can be made without the necessity of melt-mixing the components.

- The fabrication method is one requiring little energy input, giving it the potential to be a very economic process.

- The composites made in this study have mechanical and thermomechanical properties equivalent to, and in most cases superior to the properties of the unreinforced polymer. Elastic modulus was increased as much as 5.6 times over the unreinforced polymer. Coefficient of thermal expansion was decreased to as low as 16% of the unreinforced polymer value.

- Particle size matching was found to be an important factor in producing high quality composites by this method.

- The importance of reinforcement particle aspect ratio on the improvement of stiffness and thermal expansion was reconfirmed.

- These composites have been shown to behave in a reasonable manner when compared with simple micromechanics model calculations.

6.2 Possible Extensions of this Research

The two most obvious extensions of this research are the study of other material systems and other mechanical and physical properties.

One interesting variation on the materials theme would be the use of metal flake reinforcements. This would allow a direct comparison of metal and mica reinforcements without the added factor of particle shape differences. If the same metal could be obtained in both a spherical and a flake particle shape, the effect of particle shape could also be isolated. Currently, gold and silver are available in both spherical and flake powders of similar, fine particle sizes[23]. Although the cost of these powders would prohibit their use in practical applications, they are available for experimental study of particle shape effects.

The examination of sized wollastonite powders would also be of interest, specifically in relation to the information presented here. In addition, the use of other mineral reinforcement powders could be studied. Many minerals, including calcium carbonate, kaolin and silica[20], have been used as polymer fillers for years and are easily attainable. Minerals would be attractive because of their low density in relation to metals, and their extremely low cost (usually on the order of pennies per pound)[20].

The powder molding method described in this thesis can be used to aid in the forming of superconductors into useful parts. The recently developed high temperature superconductors are very brittle, making them of limited practical use. In current research at Virginia Tech, superconducting powder has been molded with polyimide powder to form a composite plaque which exhibits the superconducting property known as the Meissner effect[36].

Reinforcement of polymers with particulates has been shown to affect properties such as creep and stress relaxation, dynamic mechanical properties, hardness and wear[30]. It would be of interest to study composites made by this method in terms of these or other properties. Combinations of matrix and reinforcement which yield exceptional properties may be found. Also, composites may be made with properties similar to existing materials, but which may be fabricated more simply and less expensively.

In addition to a widened scope of materials and properties, variations on the fabrication process itself may also be interesting topics for further study. In this work, molding pressure was kept at a minimum, while temperature was used as the primary factor driving part consolidation. Thus, temperatures sufficient to melt the polymer matrix material were required. If higher pressures are used, lower temperatures may be sufficient to achieve the same degree of consolidation. This would reduce not only the amount of heat-energy required for fabrication, but also the heating and cooling time of the molding cycle. Also, in characterizing the powder blends, the use of hot stage microscopy would provide much valuable information.

One particularly interesting idea raised by this work involves the presence of an exothermal martensitic phase transformation in the metal reinforcement in the temperature range of the molding cycle. It may be possible to use the heat released during this phase transformation to aid in the consolidation of the plaque. If the amount of heat given off by the metal is great enough, the mold containing the powder mixture could be heated to the transformation

temperature of the metal, and consolidation of the composite could be completed by the heat of transformation. The excess heat could be used to raise the temperature of the polymer to its melting point, and then supply enough heat to complete the melting process. This may be possible in the LaRC-TPI/Cu-Al-Ni system, since the heat of fusion of LaRC-TPI is only about 9.7 J/g and the heat of transformation of Cu-Al-Ni was measured to be about 15.3 J/g. The success of this type of process would also depend on the relative amounts of polymer and Cu-Al-Ni. If the heat of transformation were sufficiently large to heat a neighboring reinforcement particle to the transformation temperature, another processing modification could be explored. One small region of the powder mixture could be heated to the transformation temperature, which would then supply enough heat to melt the surrounding polymer and heat nearby reinforcement particles to the transformation temperature, at which point more heat would be generated, and the process would continue until the entire part was consolidated. This would require an extremely large exotherm, since the heat of transformation would be required to supply sensible heat and heat of transformation both to the matrix and to other reinforcement particles. It would be possible to calculate the heat required for these processes from heat capacity and heat of fusion data. An ideal situation would be a reinforcement with a large exotherm at a low temperature combined with a polymer with a small heat of fusion and a low melting temperature. Experimental and theoretical work in this area is underway in our group.

Although fine powdered polymers and metals are currently quite expensive, I want to emphasize that this type of fabrication should become more attractive with time because of the growing technology related to fine powders. Currently at Virginia Tech, research efforts to produce sub-micron polymer powders via aqueous suspension polymerization techniques is underway[2]. One alternative source of fine powders is from industrial waste streams. Many processes produce dust as a byproduct. In some cases, this

dust may be useful as one of the components in a composite material. For example, current work in our group involves a feasibility study for the use of a waste stream from brake pad manufacture as particulate reinforcements[37]. This would be an extremely economical source of fine powders, as well as an attractive use for these materials which would otherwise be waste.

Appendix A Optical Micrographs of Powder Mixes

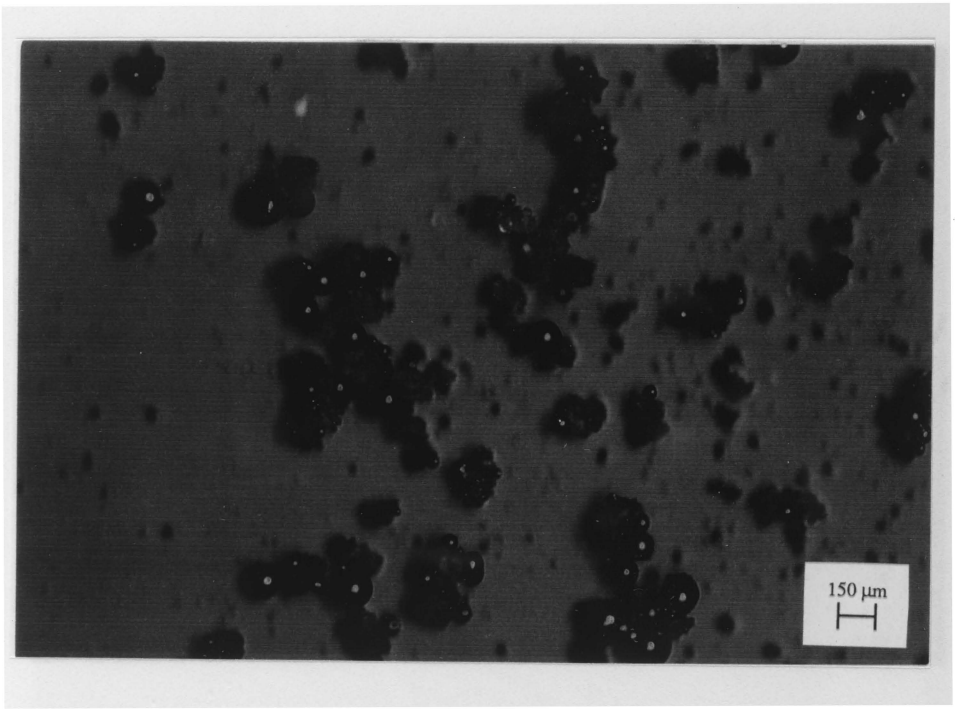

Figure A1. Micrograph of LaRC-TPI/Cu-Al-Ni powder mix.

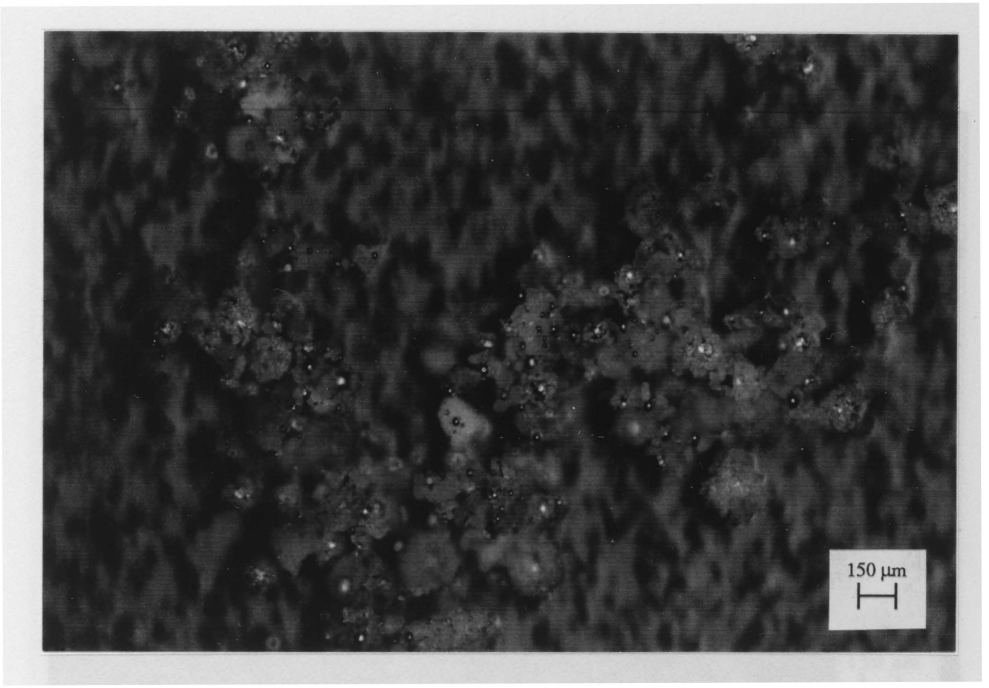

Figure A2. Micrograph of Torlon/Cu-Al-Ni powder mix.

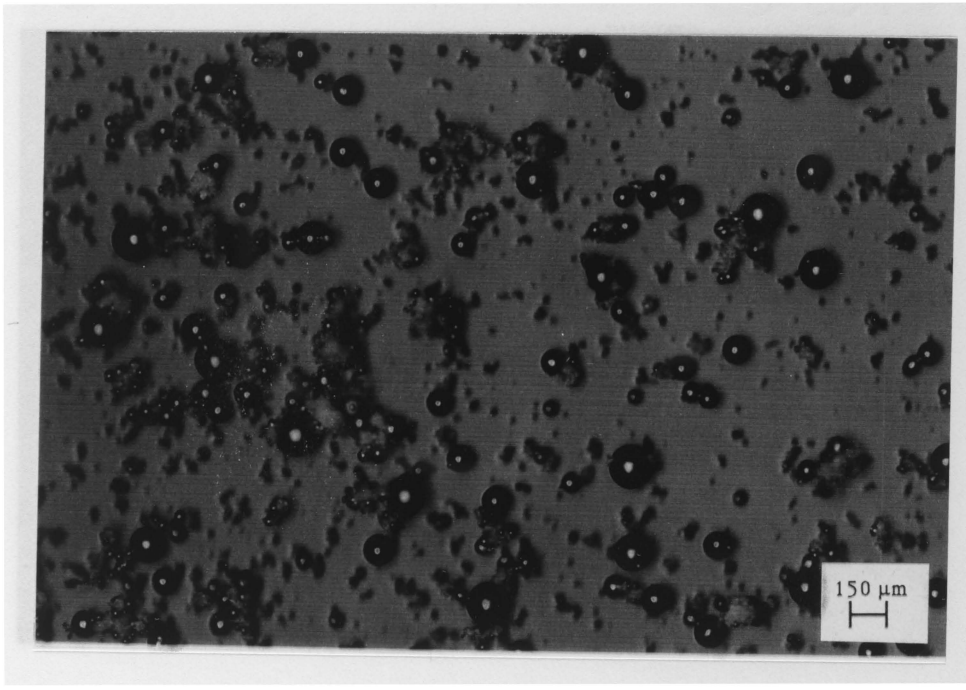

Figure A3. Micrograph of PEEK/Cu-Al-Ni powder mix.

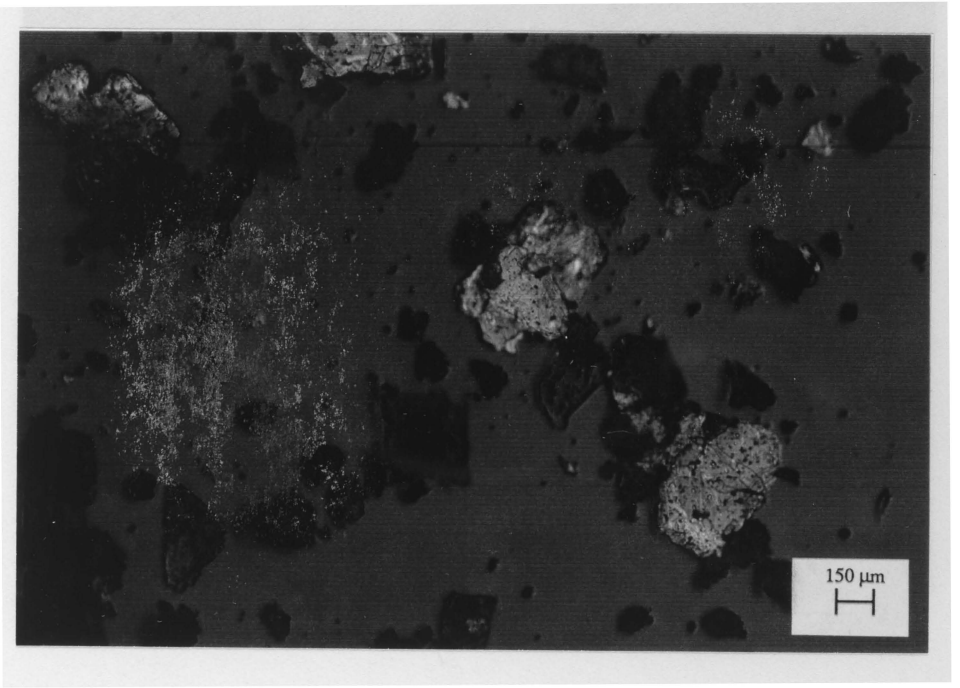

Figure A4. Micrograph of LaRC-TPI/suzorite powder mix.

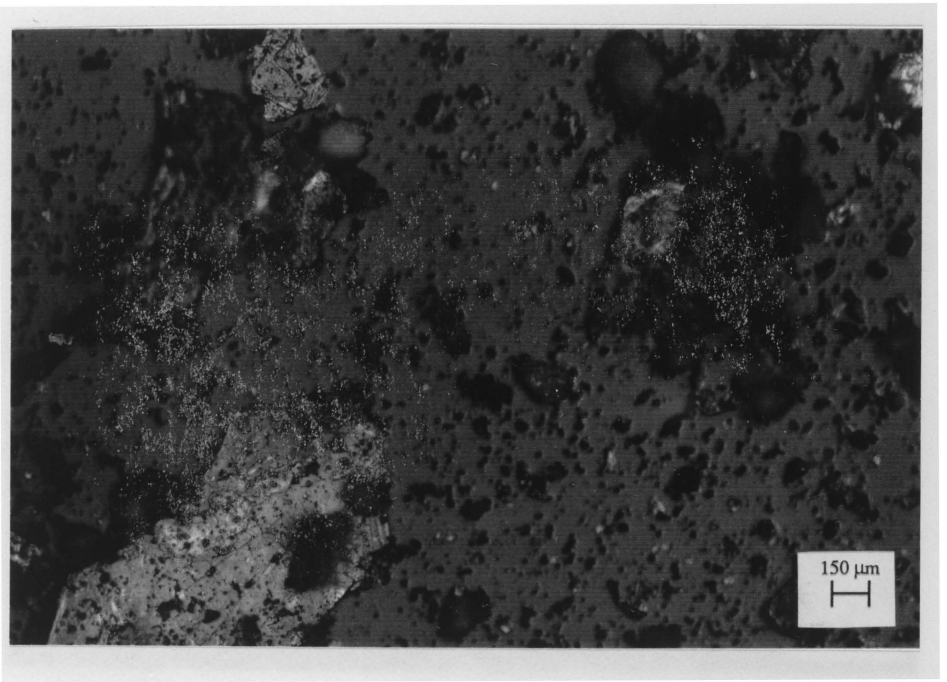

Figure A5. Micrograph of Torlon/suzorite powder mix.

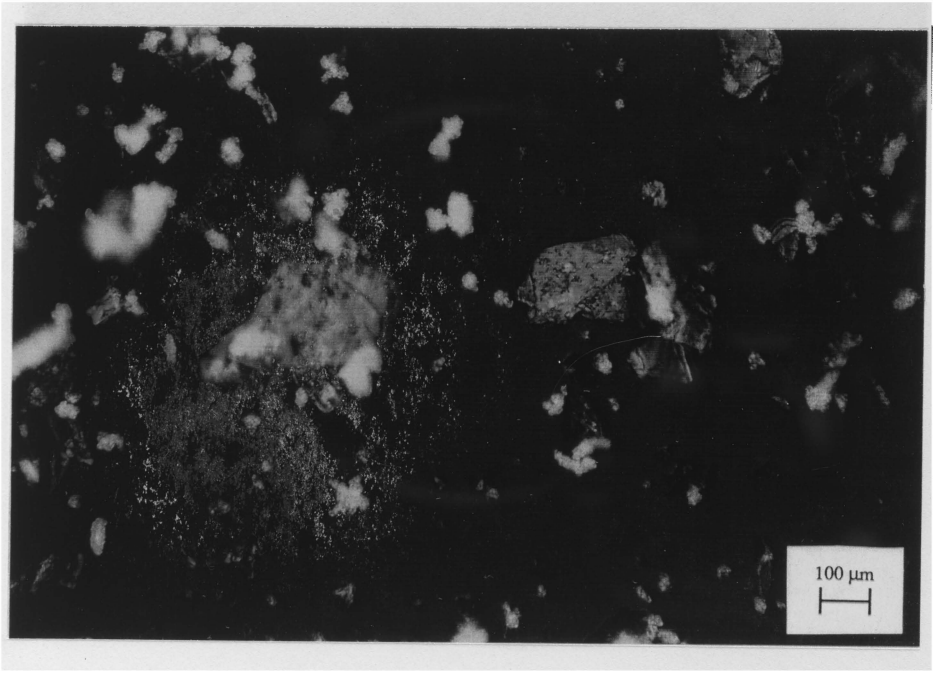

Figure A6. Micrograph of PEEK/suzorite powder mix.

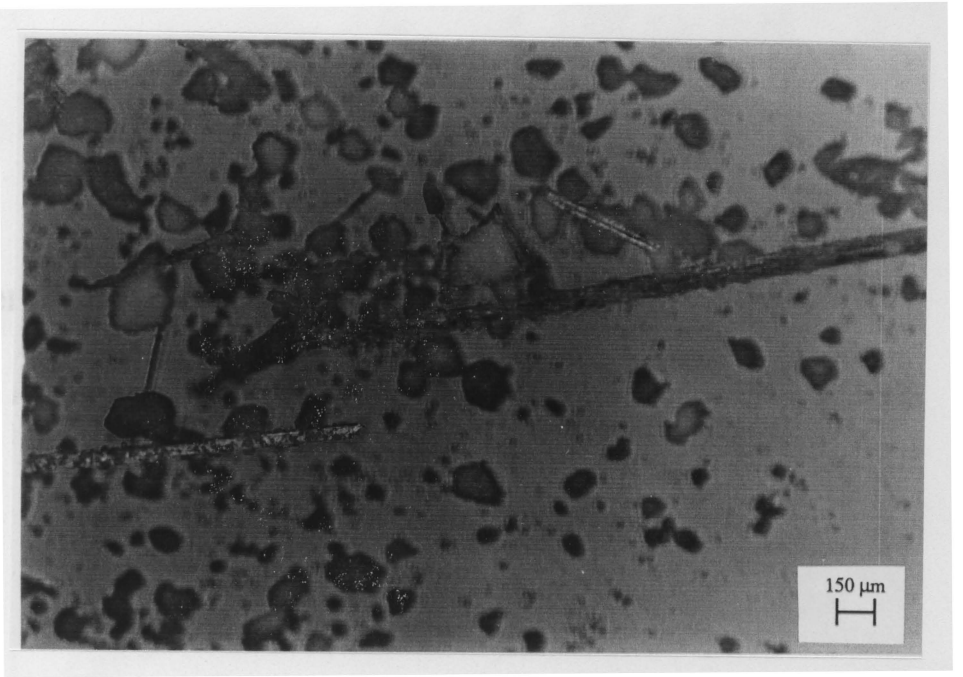

Figure A7. Micrograph of Torlon/wollastonite powder mix.

Appendix B Mechanical Behavior Graphs

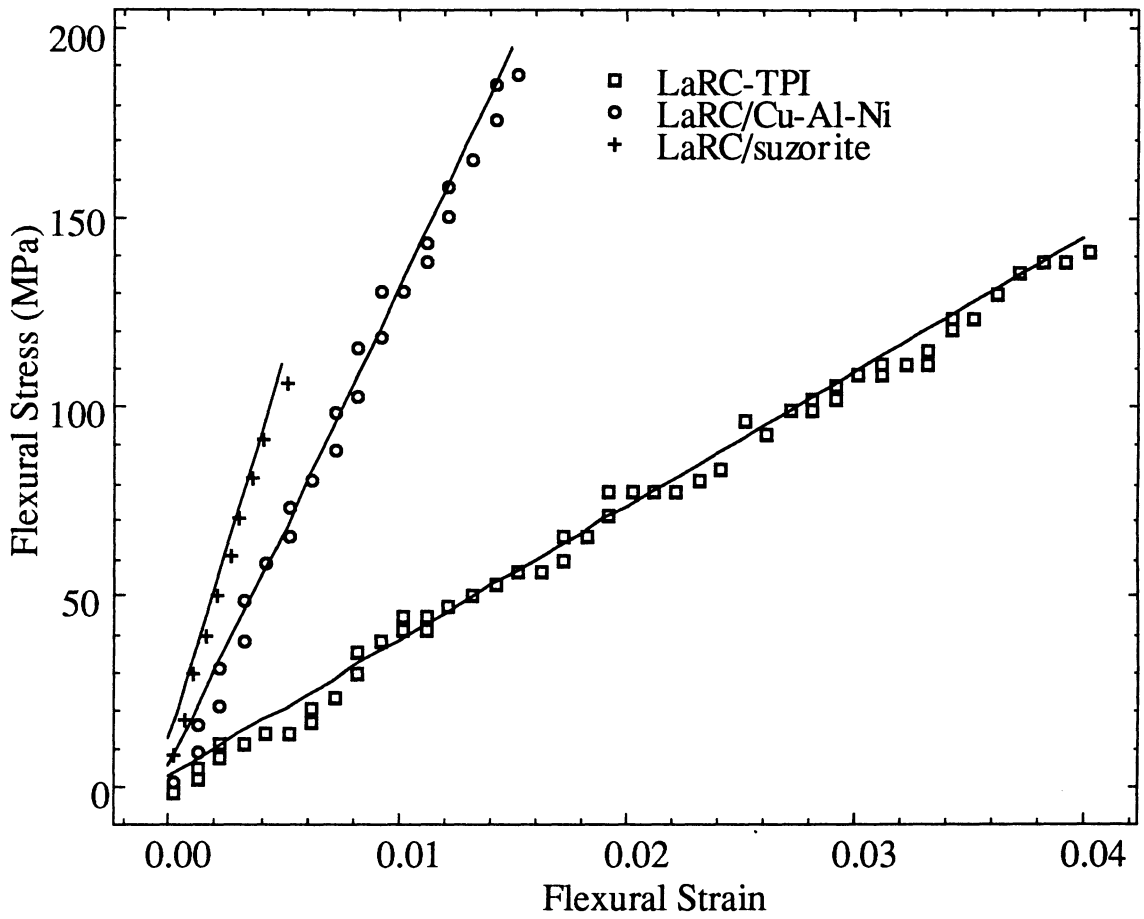

Figure B1. Mechanical behavior of LaRC-TPI and its composites.

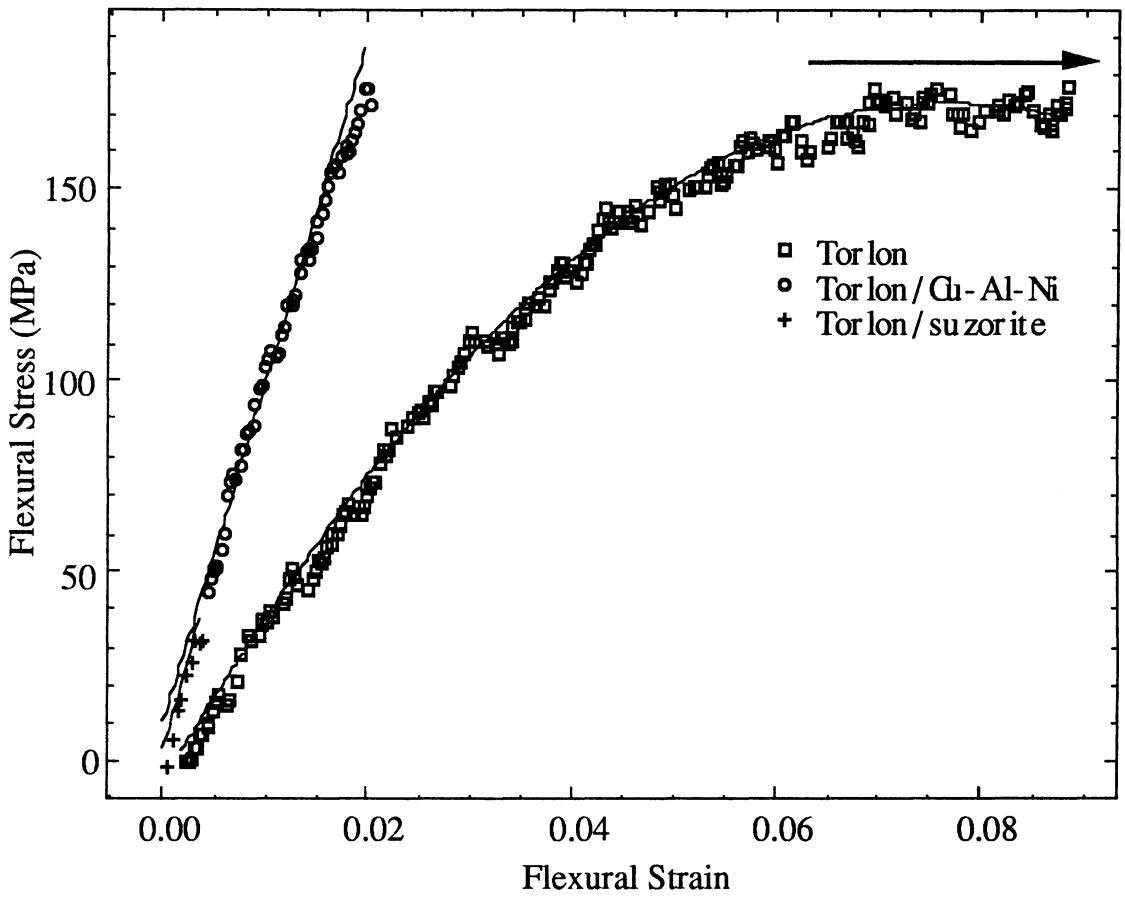

Figure B2. Mechanical behavior of Torlon and its composites. Data have been suppressed for clarity.

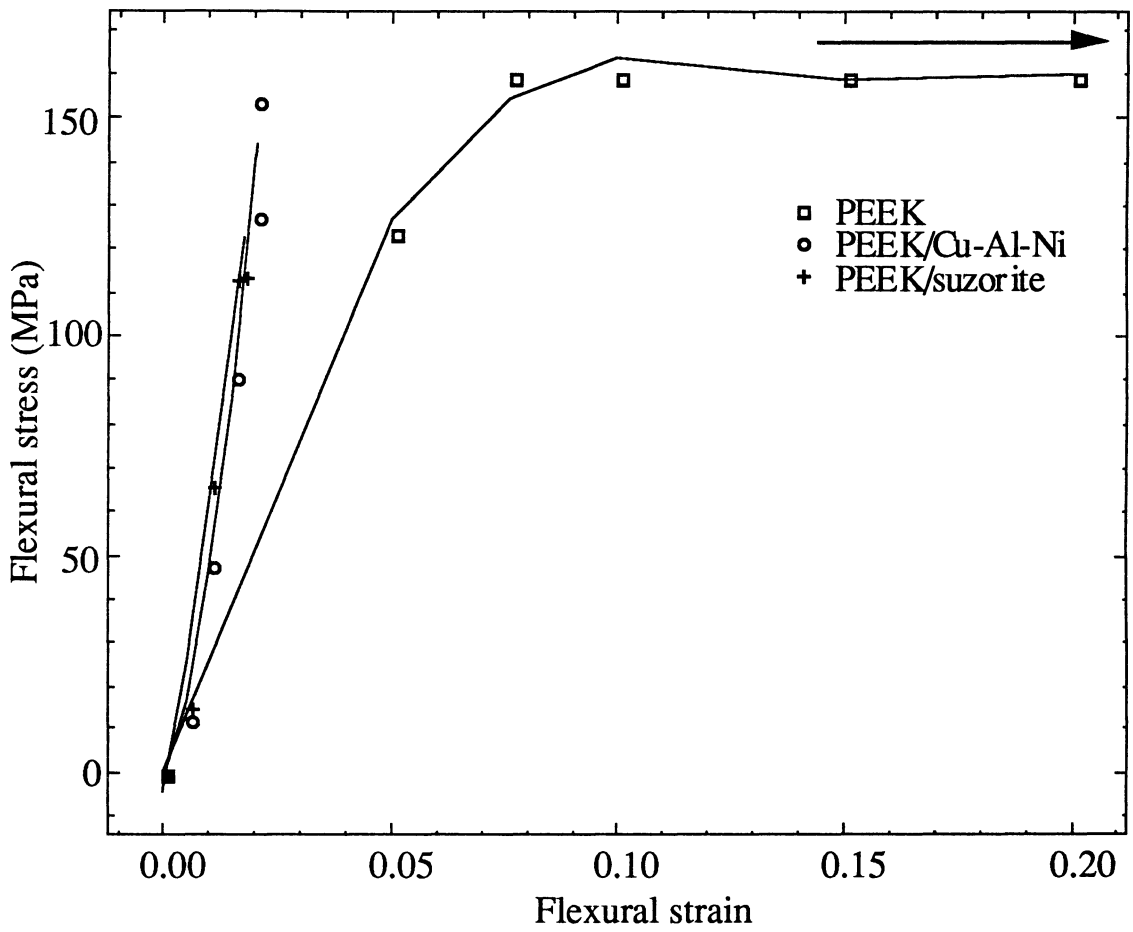

Figure B3. Mechanical behavior of PEEK and its composites.

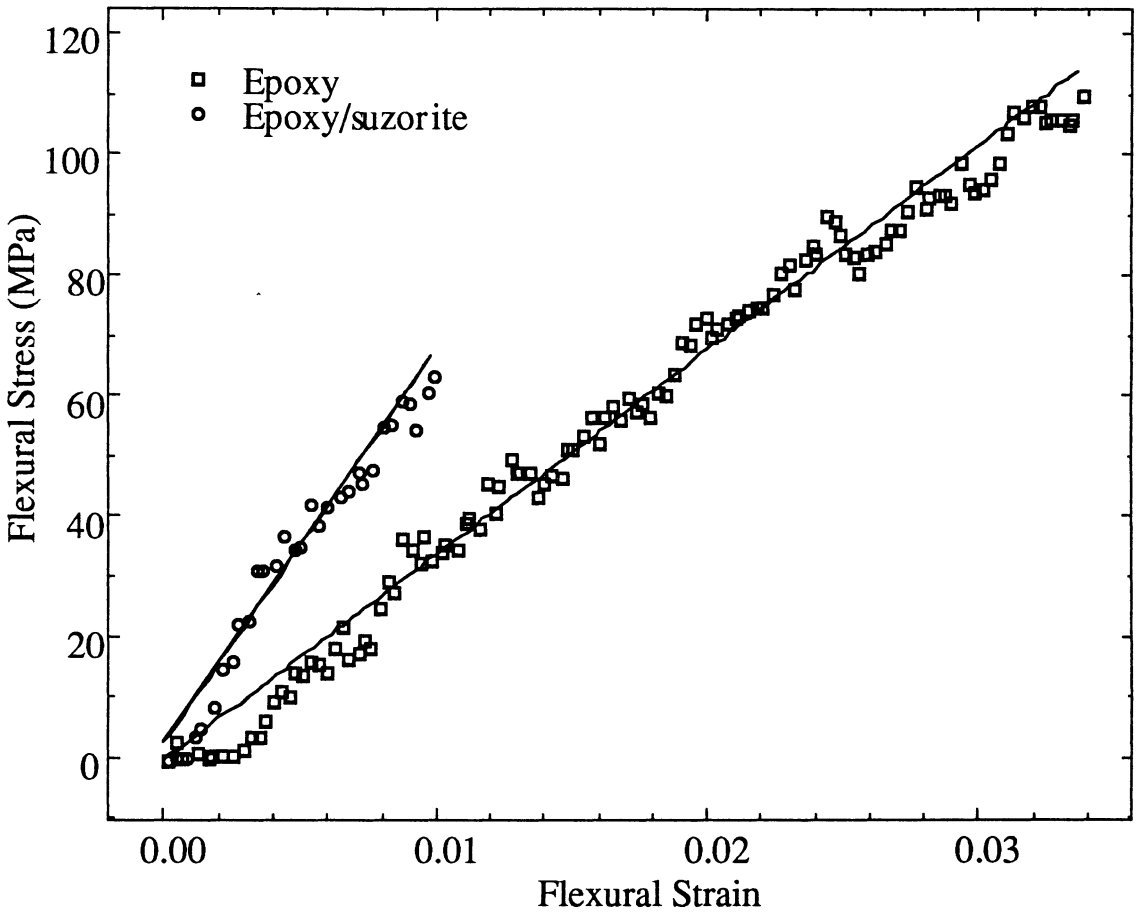

Figure B4. Mechanical behavior of MY721/DDS epoxy and its composite.

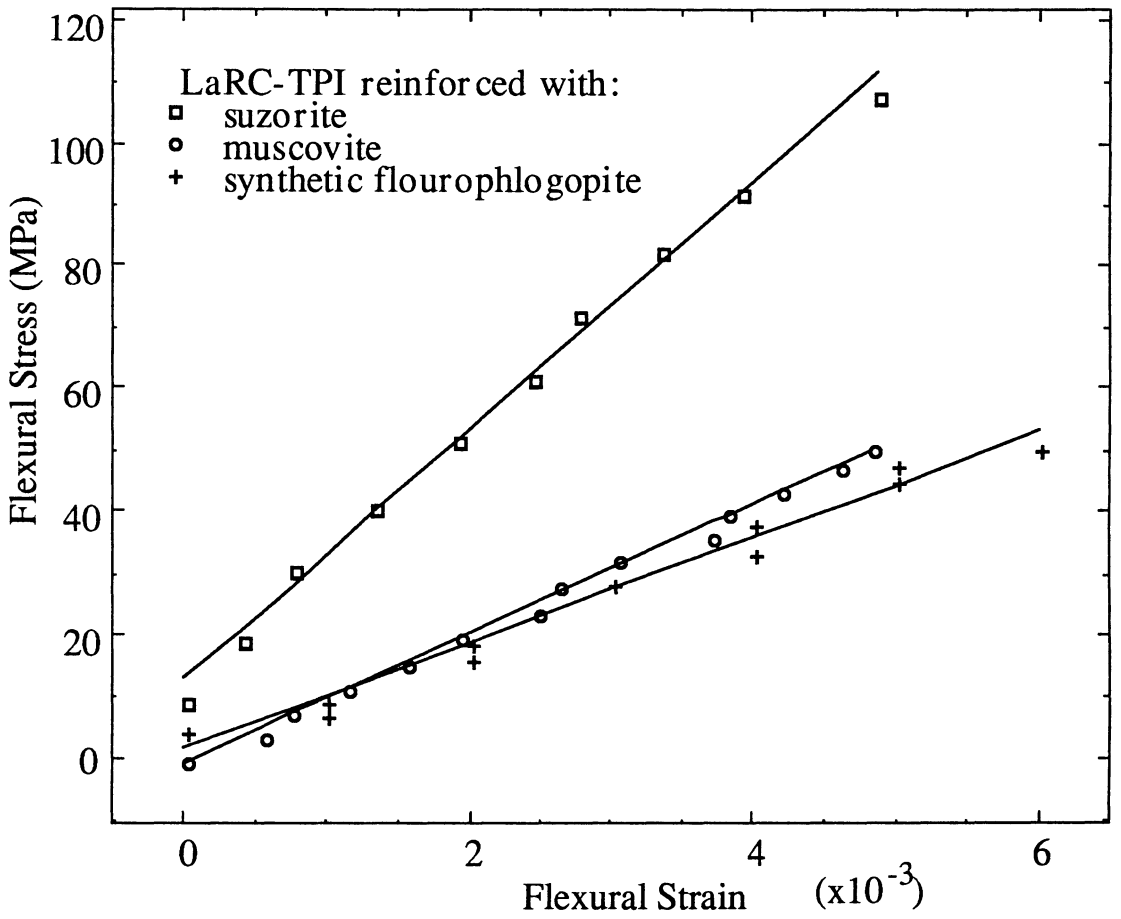

Figure B5. Mechanical behavior of LaRC-TPI/mica composites.

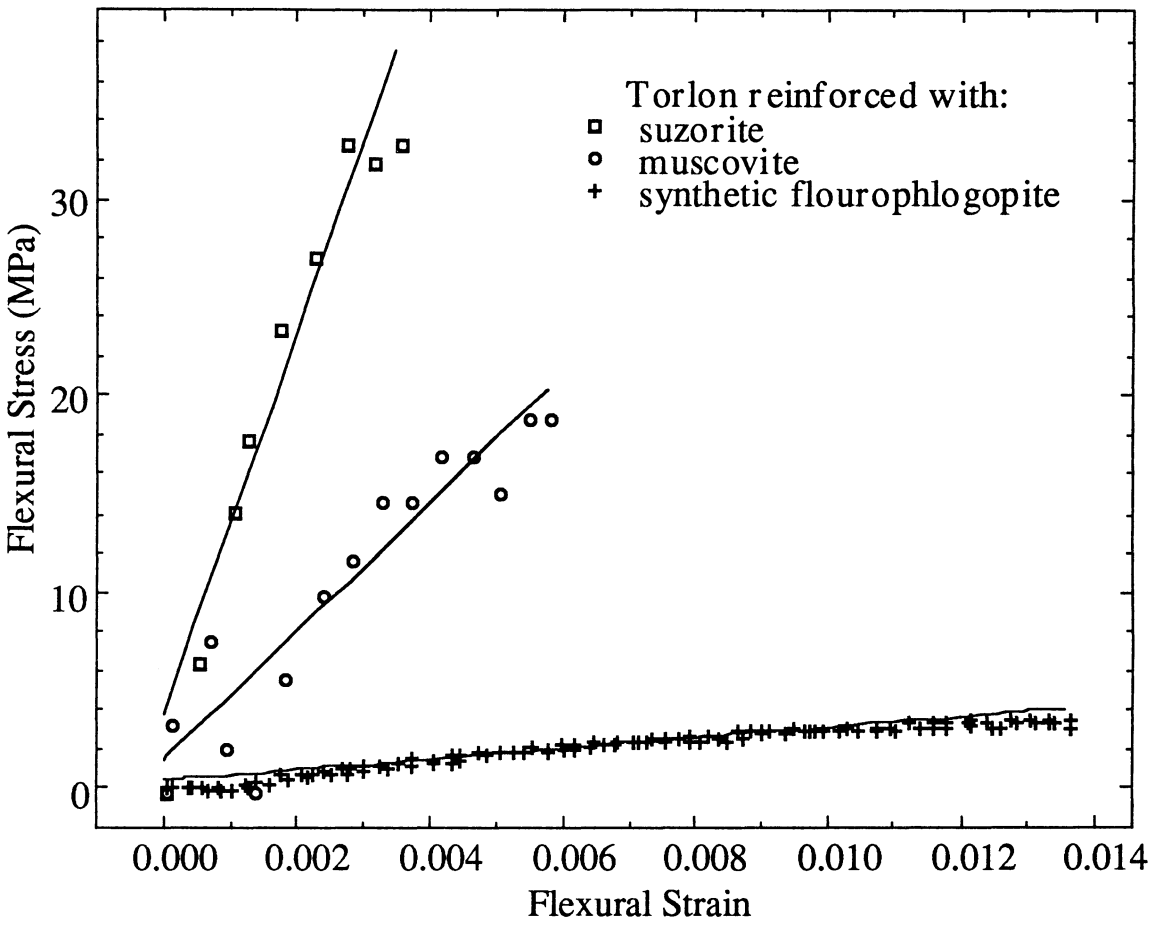

Figure B6. Mechancial behavior of Torlon/mica composites.

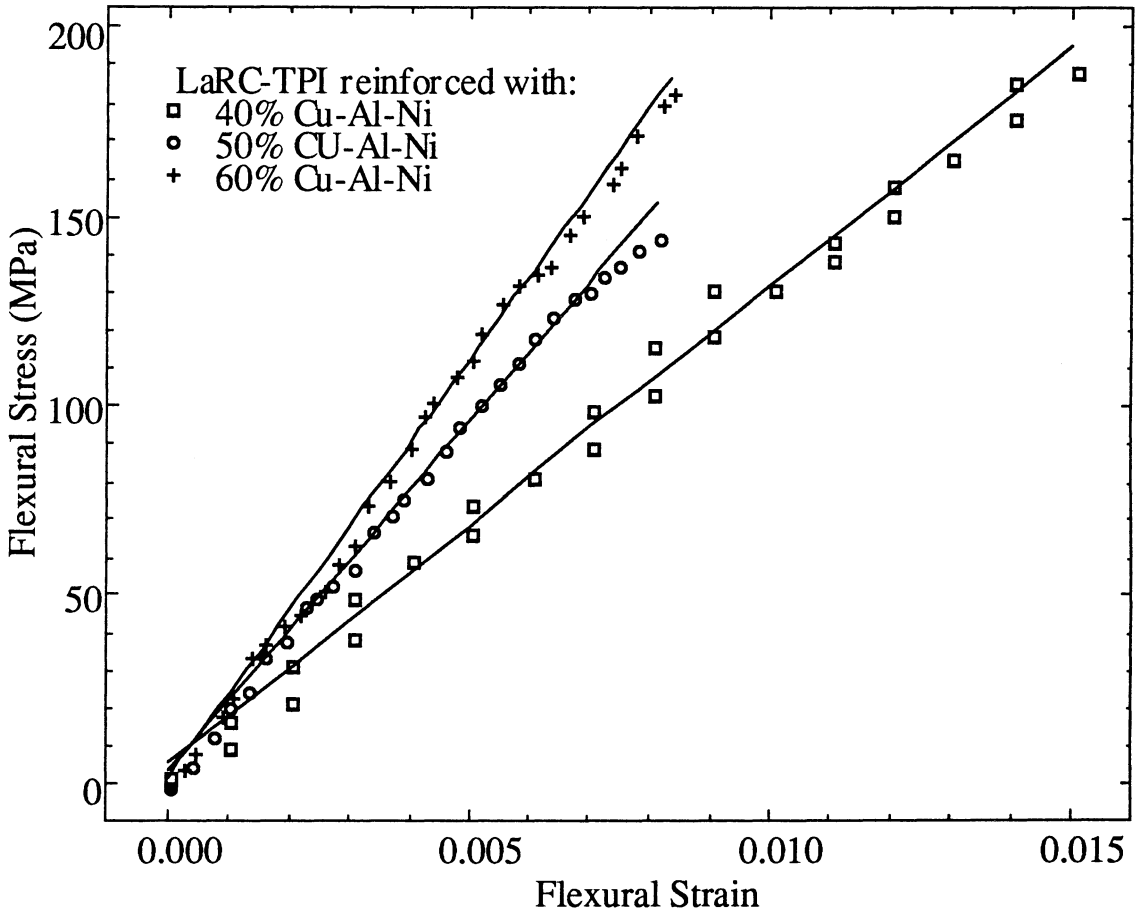

Figure B7. Mechanical behavior of LaRC-TPI/Cu-Al-Ni composites, showing the effect of reinforcement volume fraction.

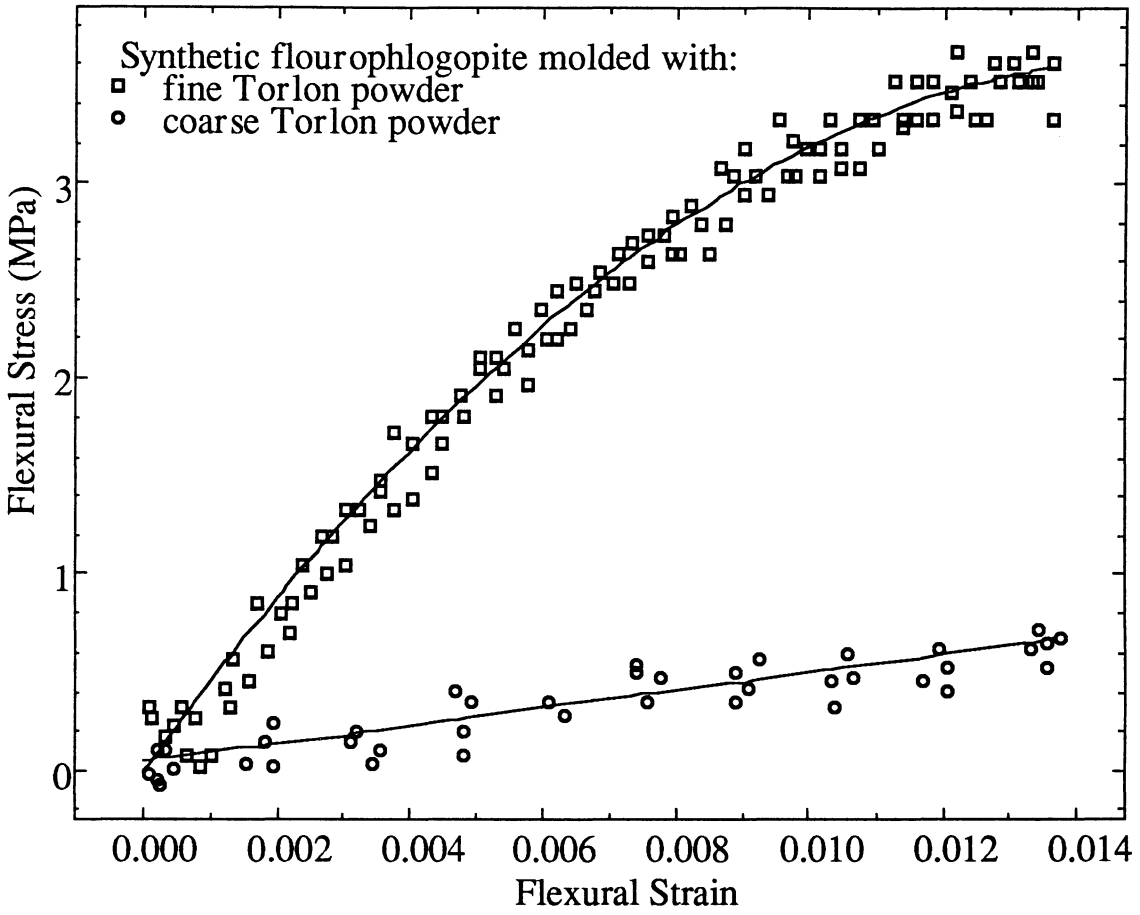

Figure B8. Mechanical behavior of Torlon/fluorophlogopite composites, showing the effect of particle size mismatch.

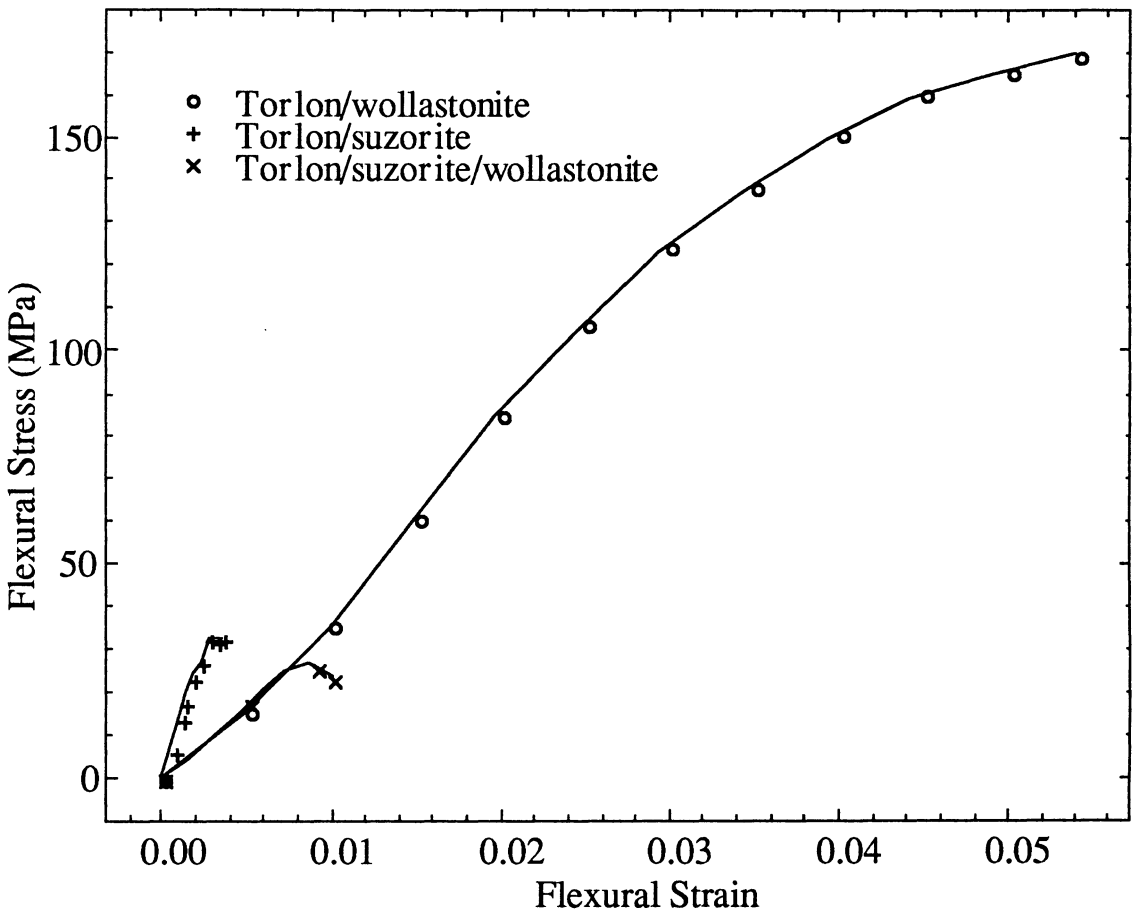

Figure B9. Mechanical behavior of wollastonite reinforced composites.

Appendix C Fracture Surface Scanning Electron Micrographs

Attention Patron: Page
104
is missing and is not
available via ILL

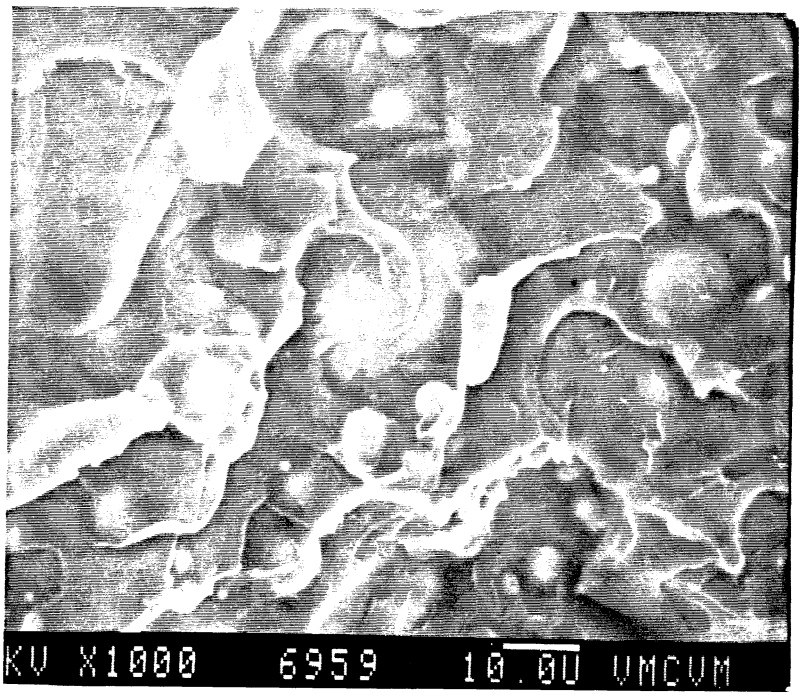

(a)

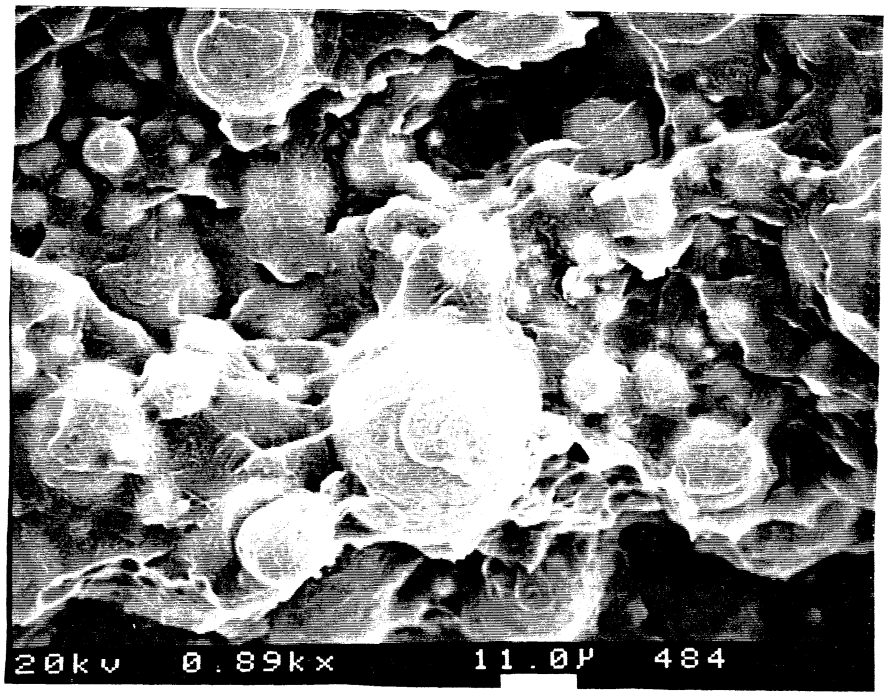

(b)

Figure C2. Fracture surface micrographs of LaRC-TPI/Cu-Al-Ni reinforced at (a) 40 volume percent and (b) 60 volume percent.

Figure C3. Fracture surface micrograph of LaRC-TPI/suzorite.

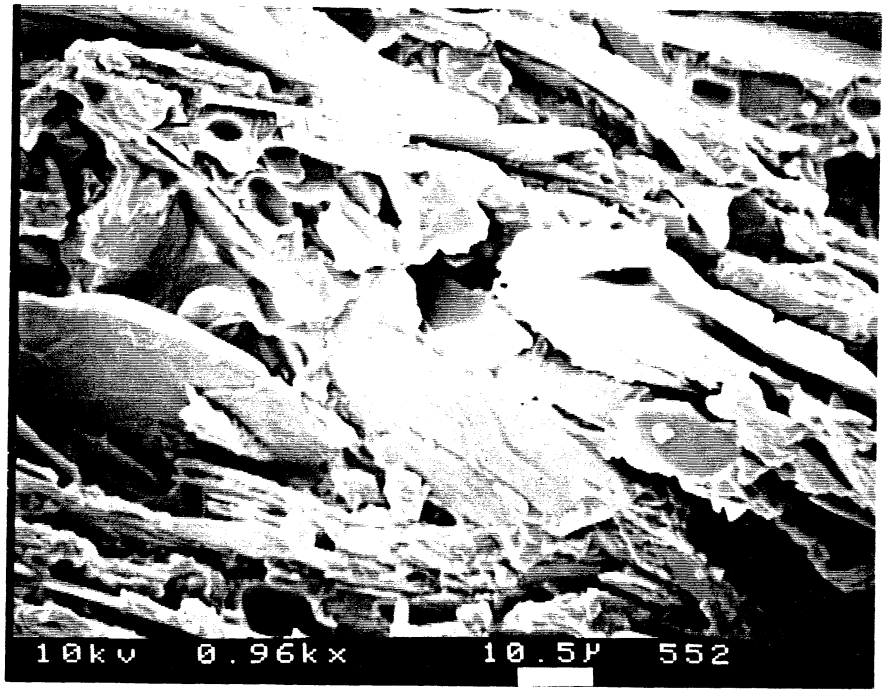

Figure C4 Fracture surface micrograph of LaRC-TPI/muscovite.

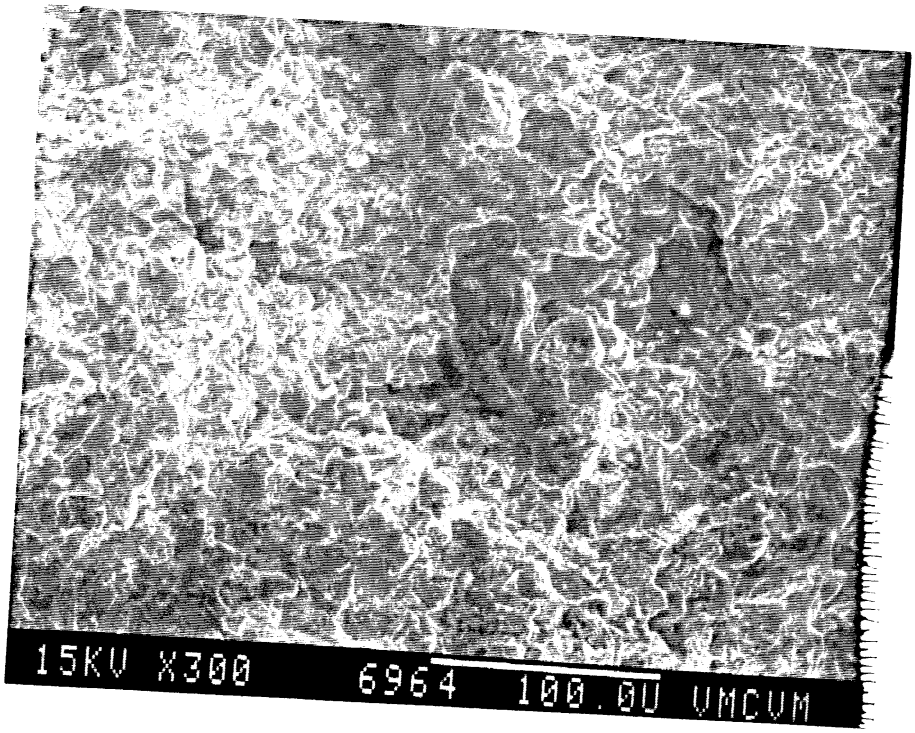

Figure C5. Fracture surface micrograph of LaRC-TPI/fluorophlogopite.

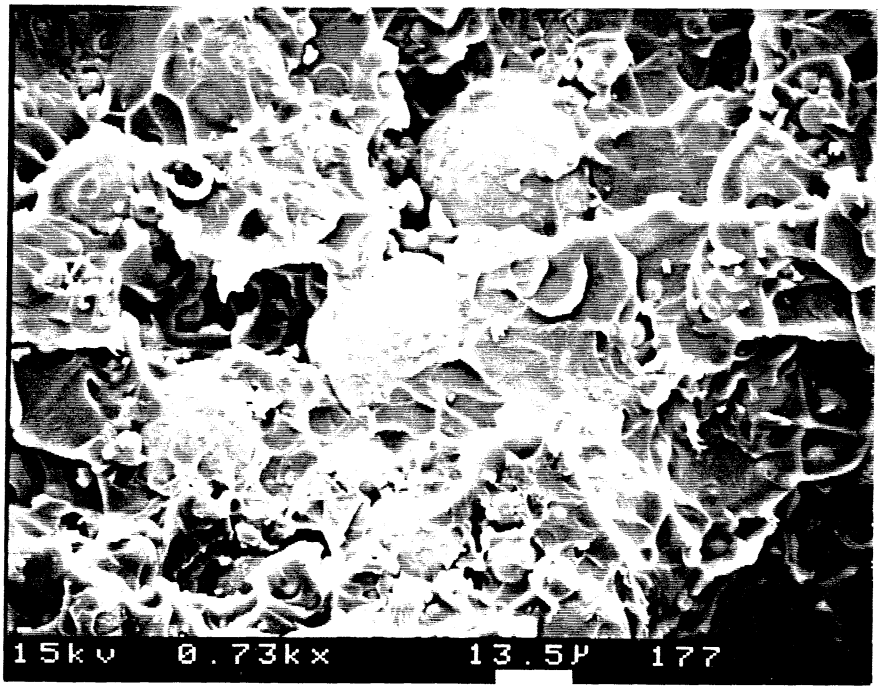

Figure C6. Fracture surface micrograph of Torlon/Cu-Al-Ni.

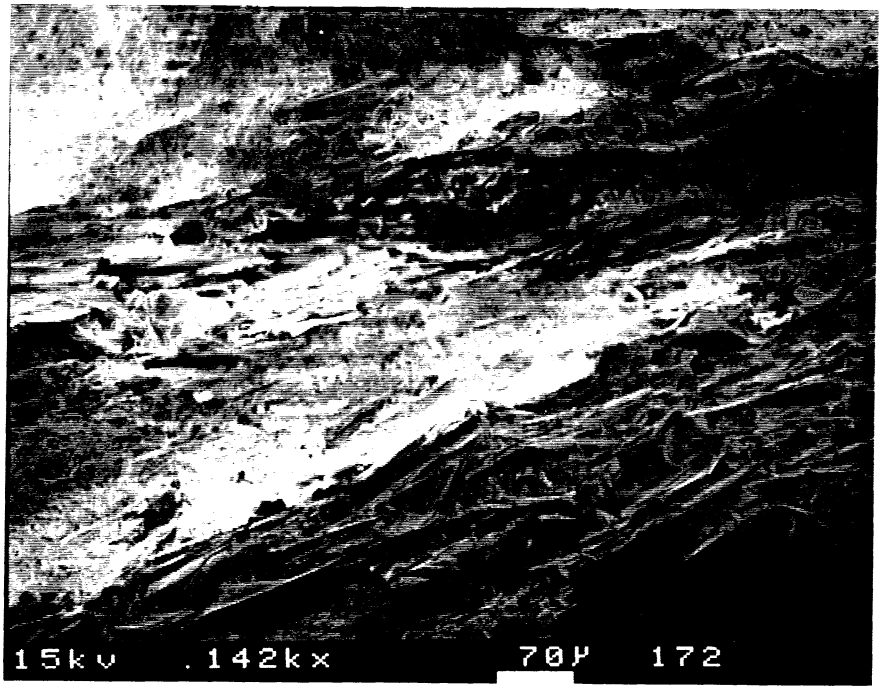

Figure C7. Fracture surface micrograph of Torlon/suzorite.

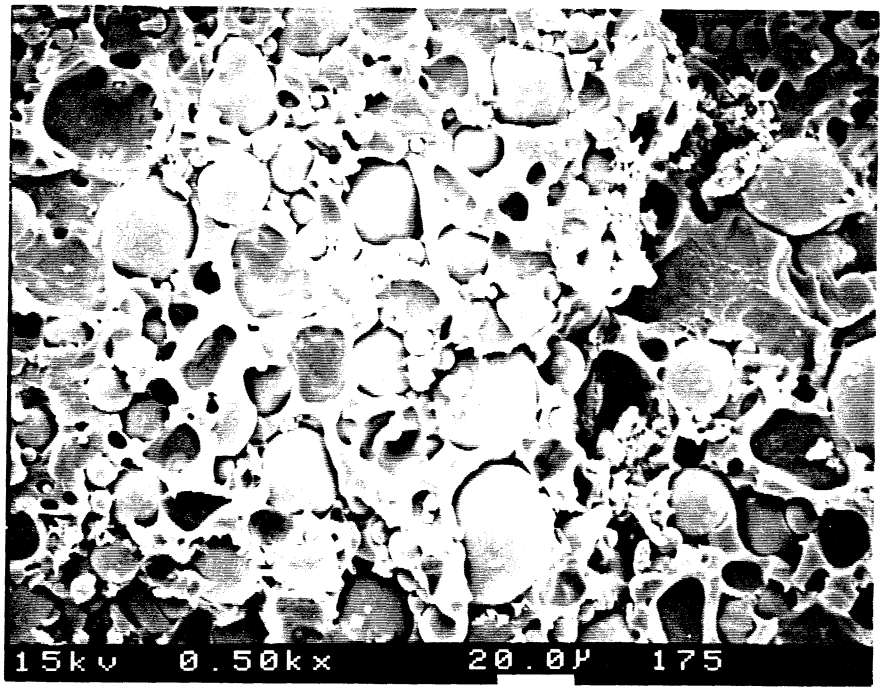

Figure C8. Fracture surface micrograph of PEEK/Cu-Al-Ni.

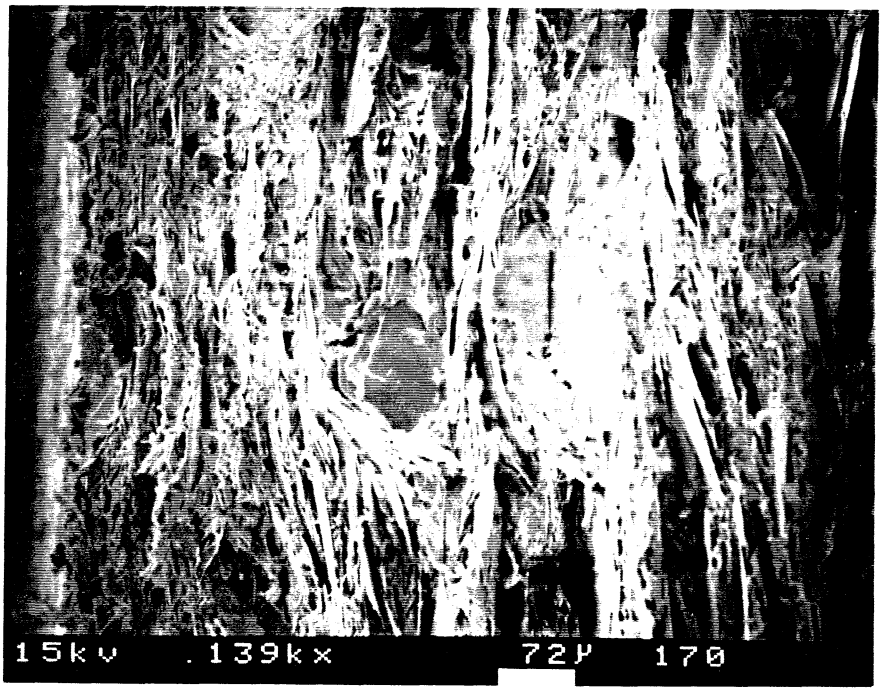

Figure C9. Fracture surface micrograph of PEEK/suzorite.

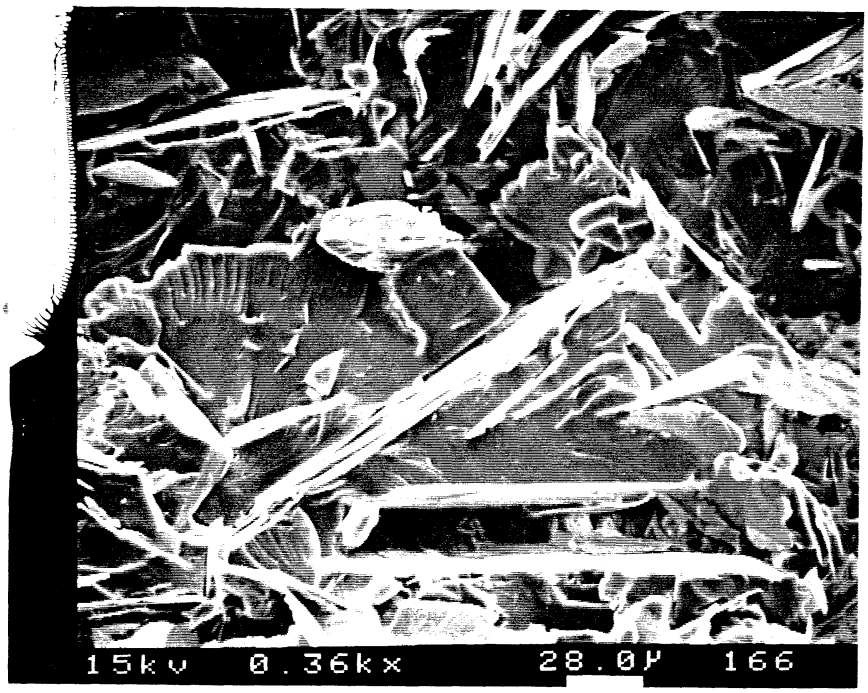

Figure C10. Fracture surface micrograph of epoxy/suzorite.

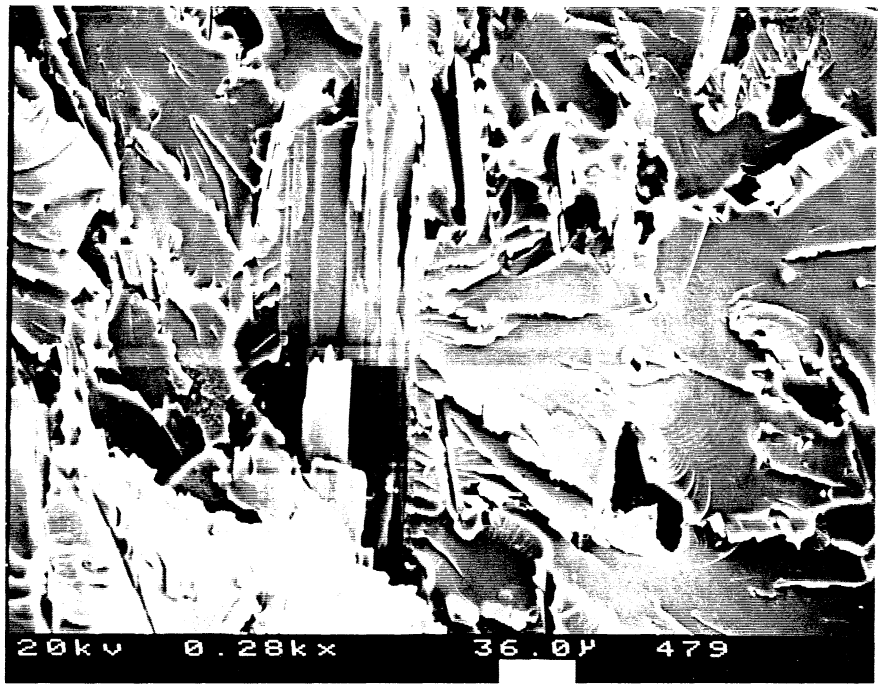

Figure C11. Fracture surface micrograph of Torlon/wollastonite.

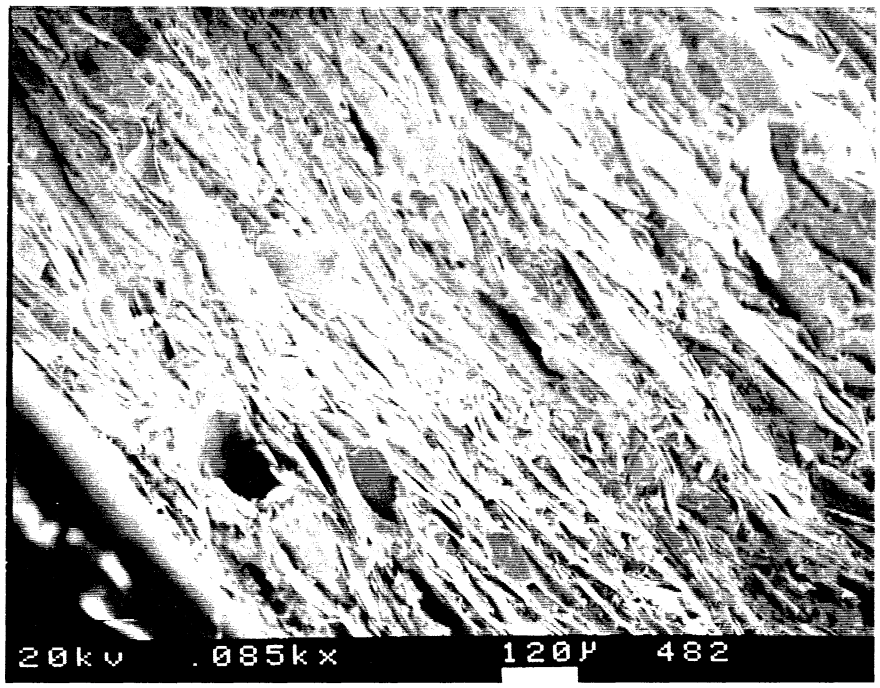

Figure C12. Fracture surface micrograph of Torlon/suzorite/wollastonite.

Appendix D Thermal Expansion Behavior Graphs

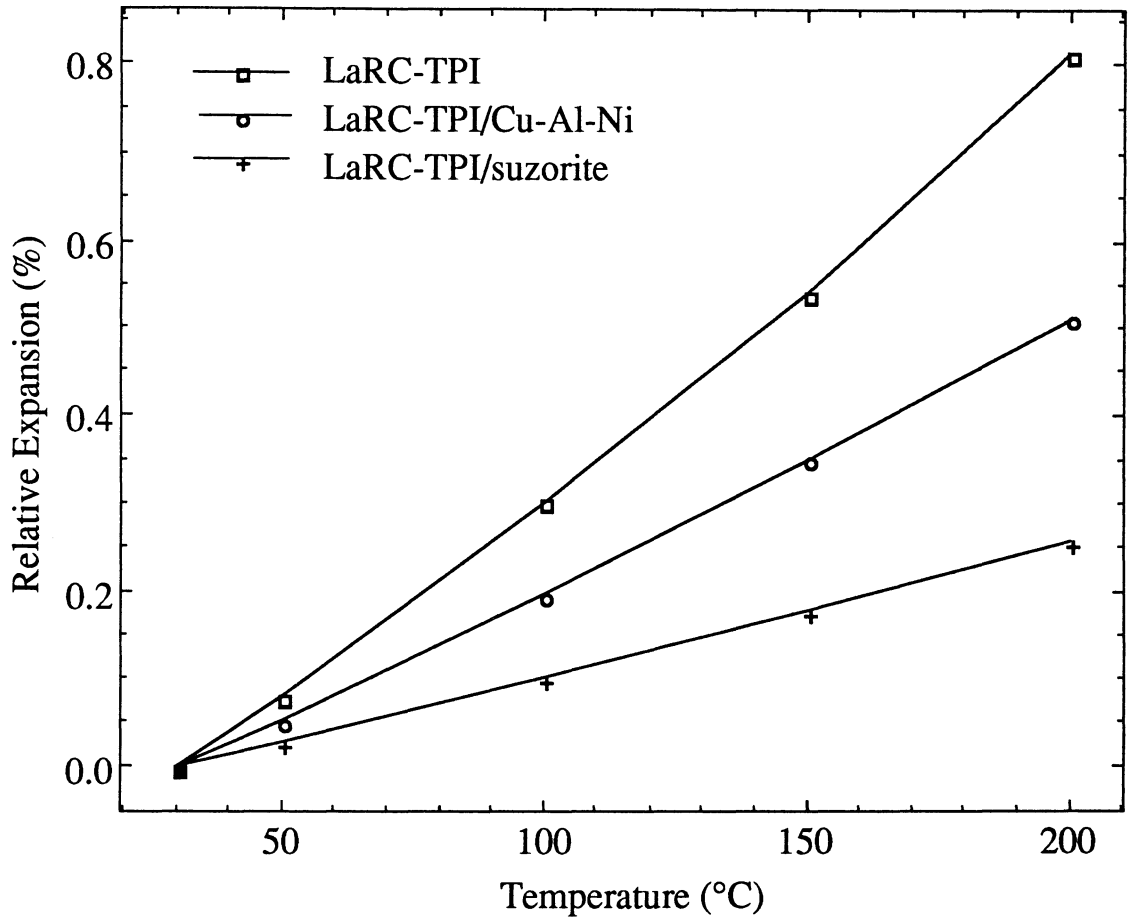

Figure D1. Thermal expansion behavior of LaRC-TPI and its composites.

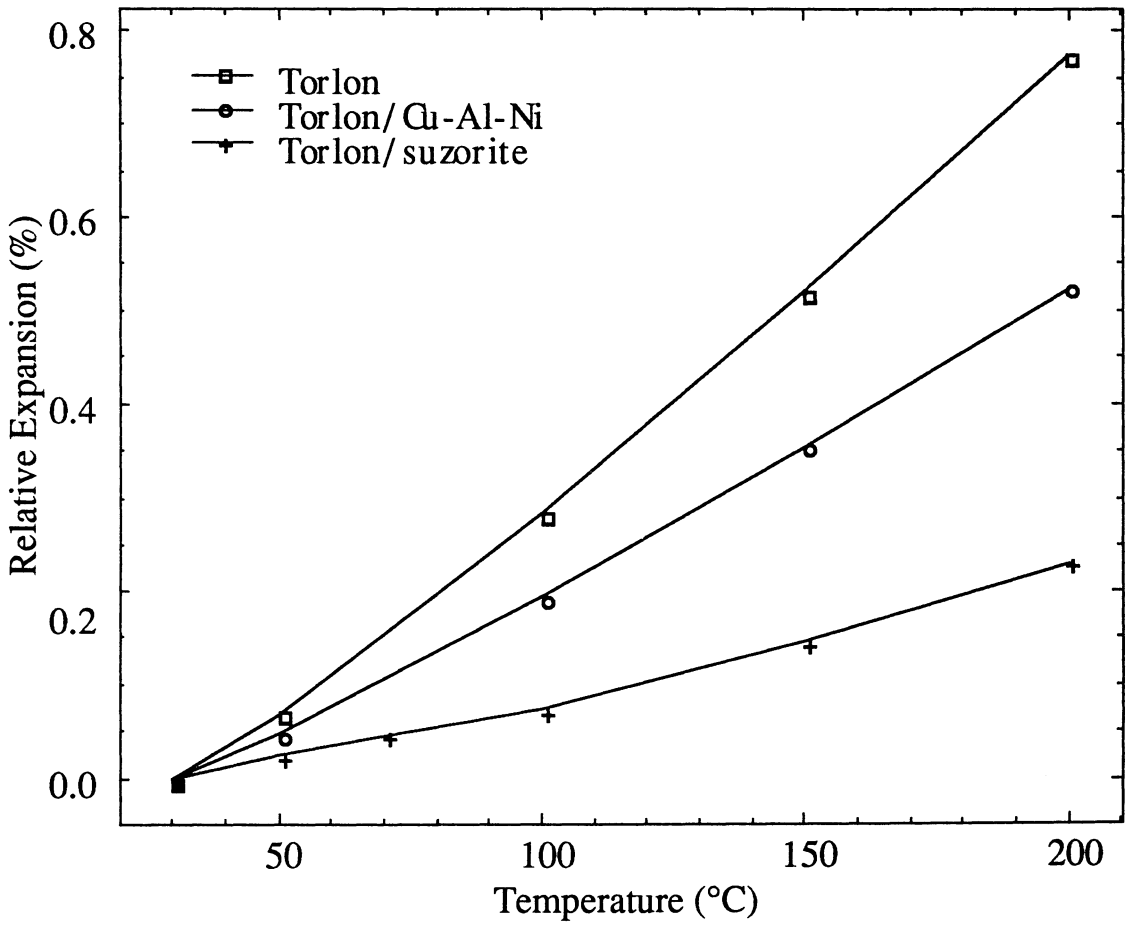

Figure D2. Thermal expansion behavior of Torlon and its composites.

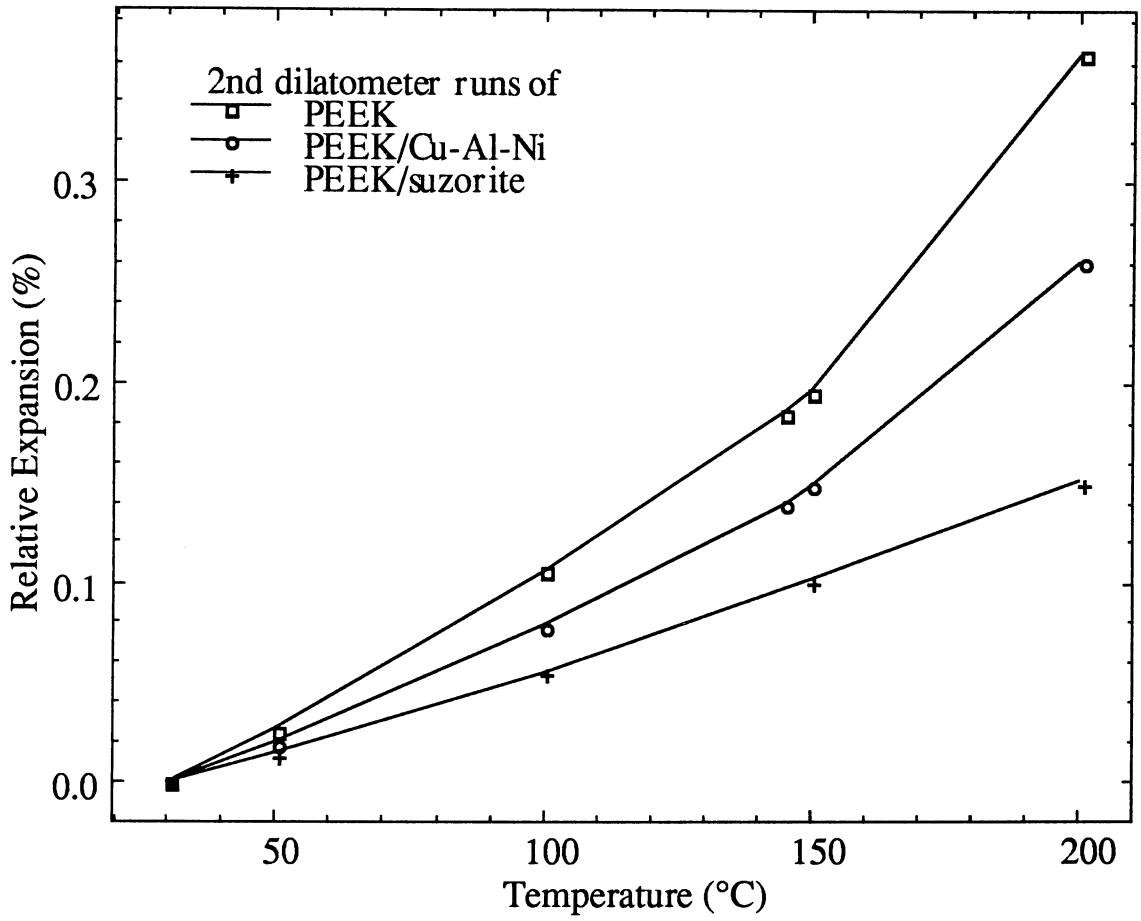

Figure D3. Thermal expansion behavior of PEEK and its composites.

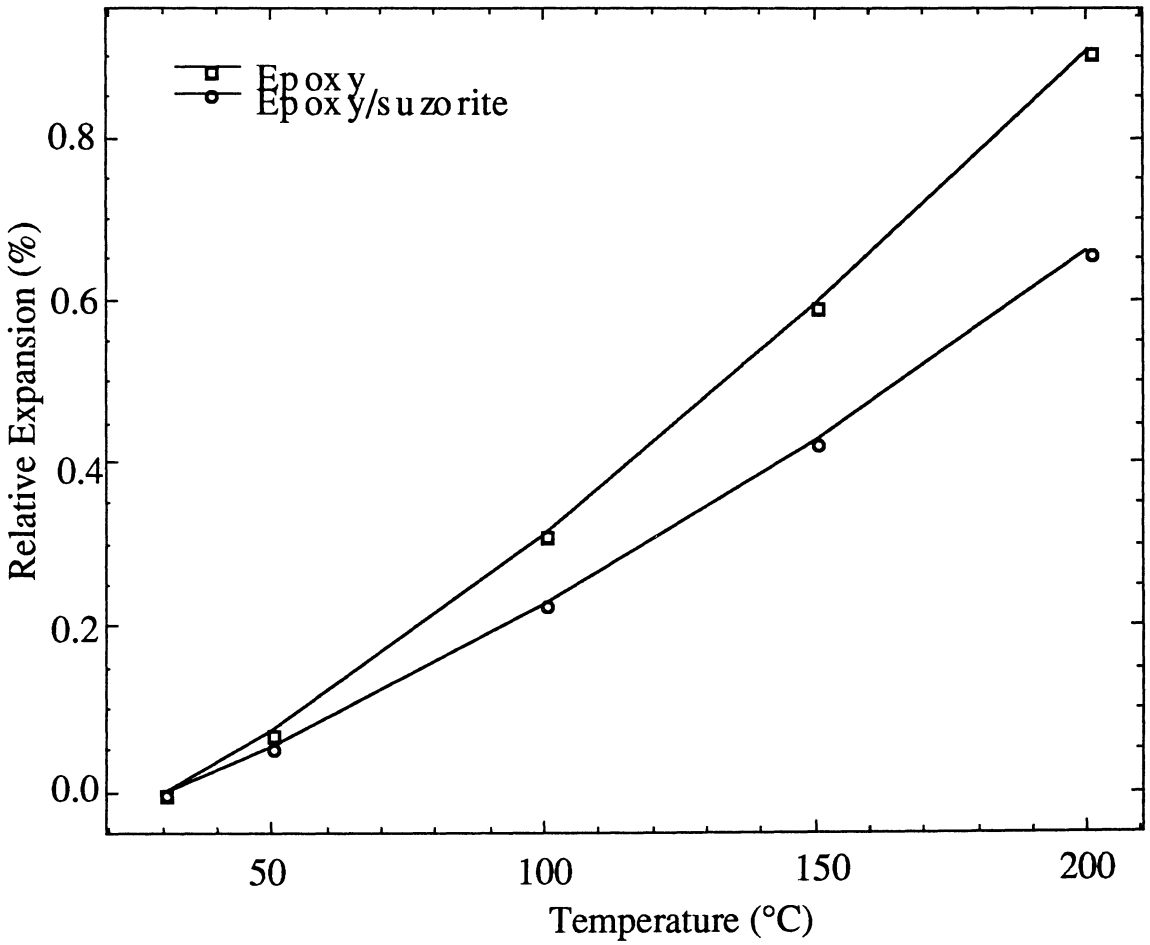

Figure D4. Thermal expansion behavior of MY721/DDS epoxy and its composite.

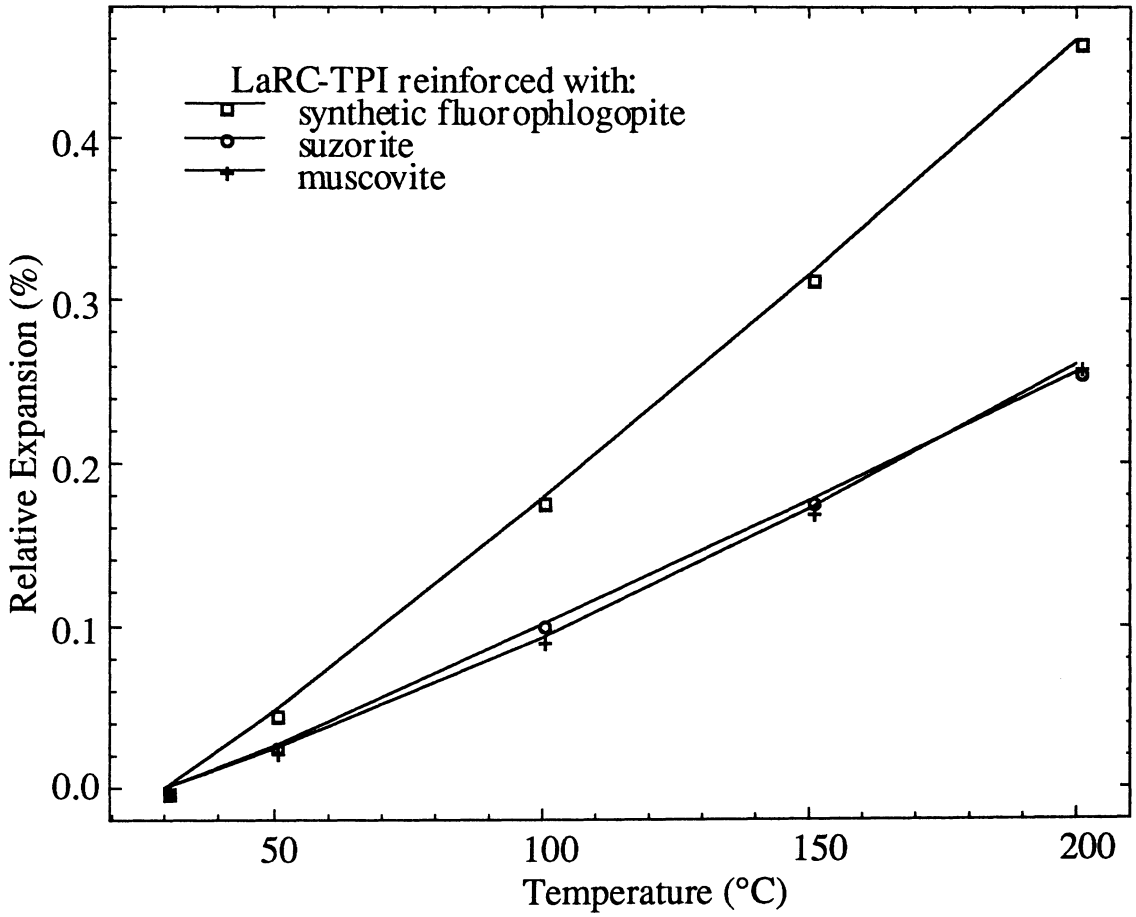

Figure D5. Thermal expansion behavior of LaRC-TPI/mica composites.

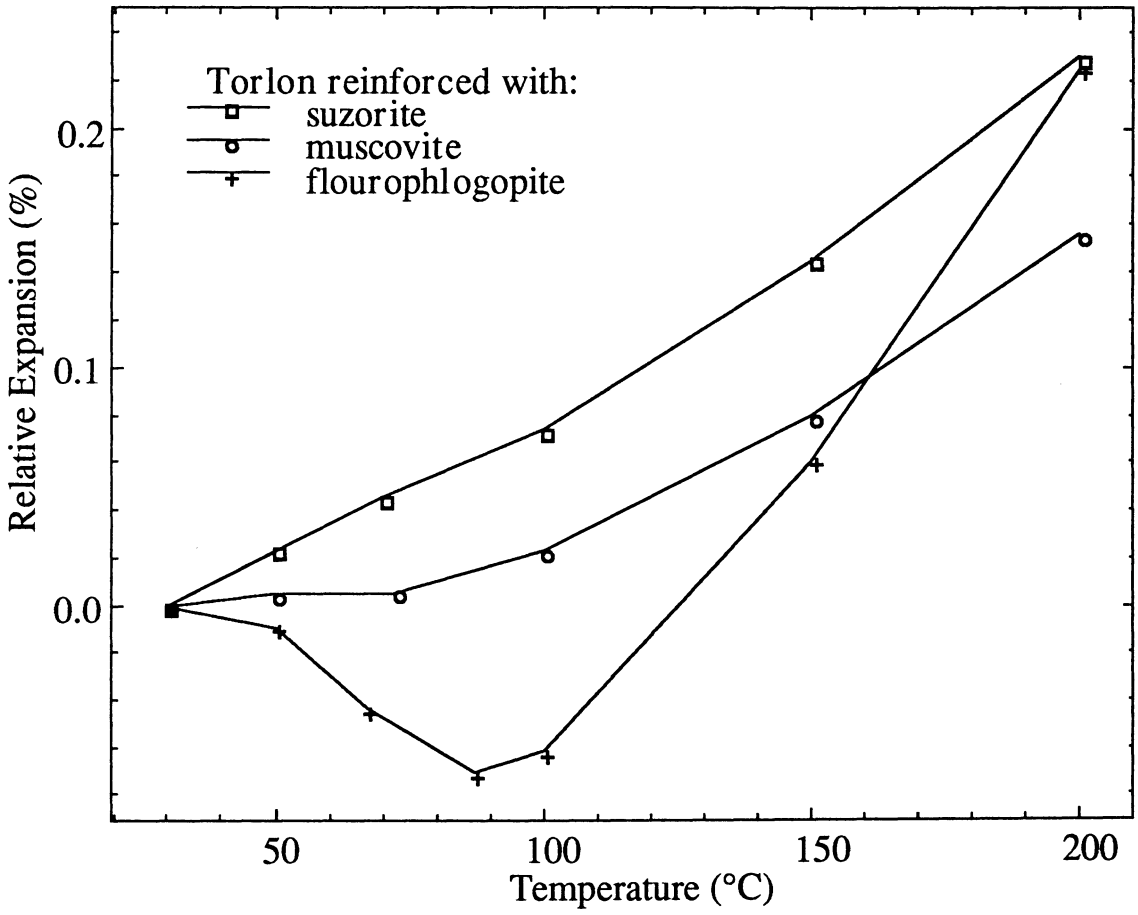

Figure D6. Thermal expansion behavior of Torlon/mica composites.

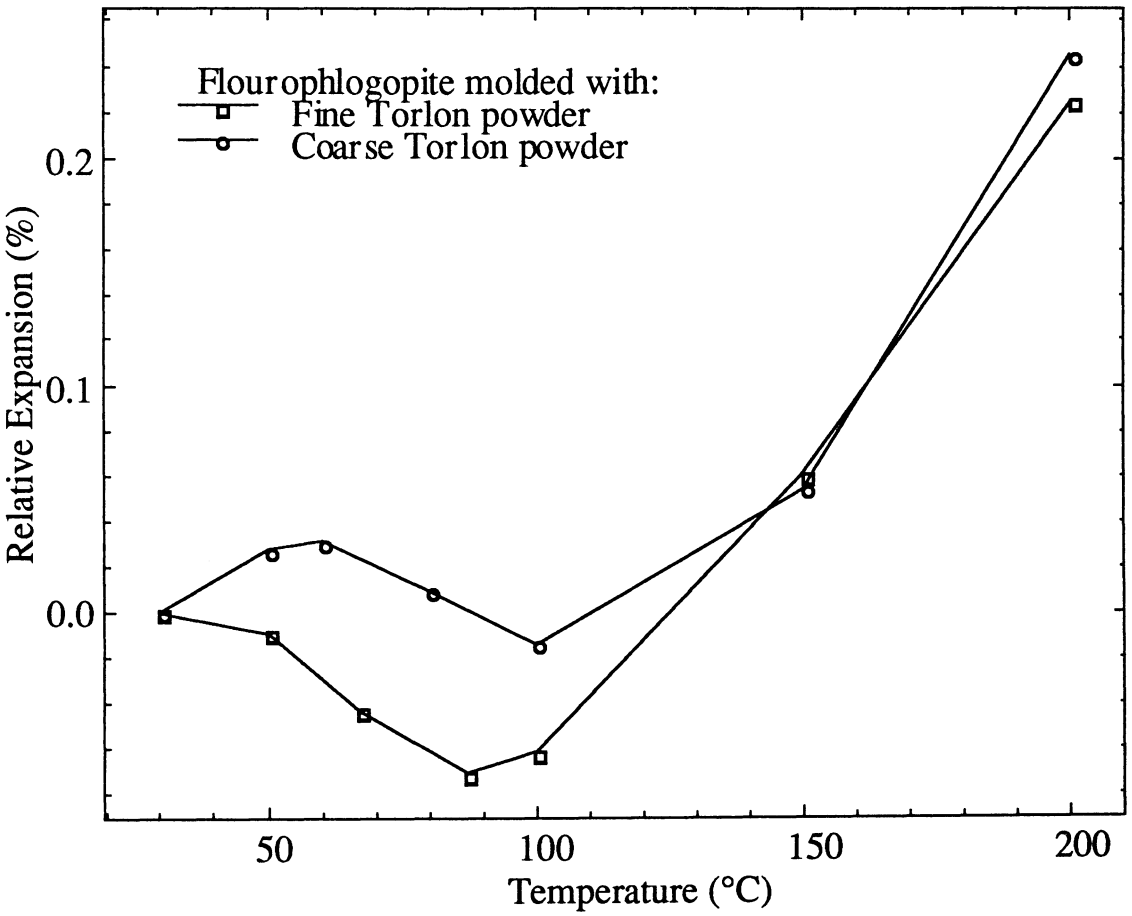

Figure D7. Thermal expansion behavior of Torlon/fluorophlogopite composites, showing the effect of particle size mismatch.

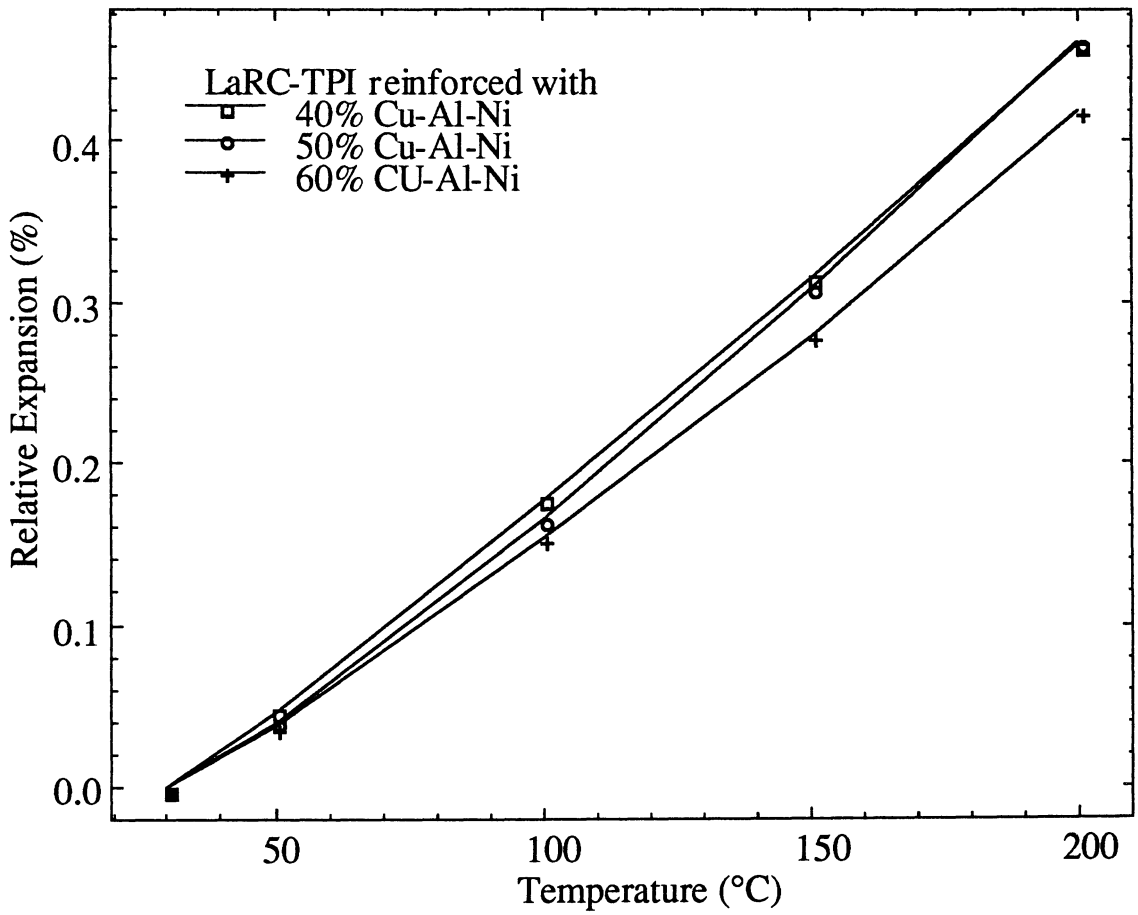

Figure D8. Thermal expansion behavior of LaRC-TPI/Cu-Al-Ni composites, showing the effect of reinforcement volume fraction.

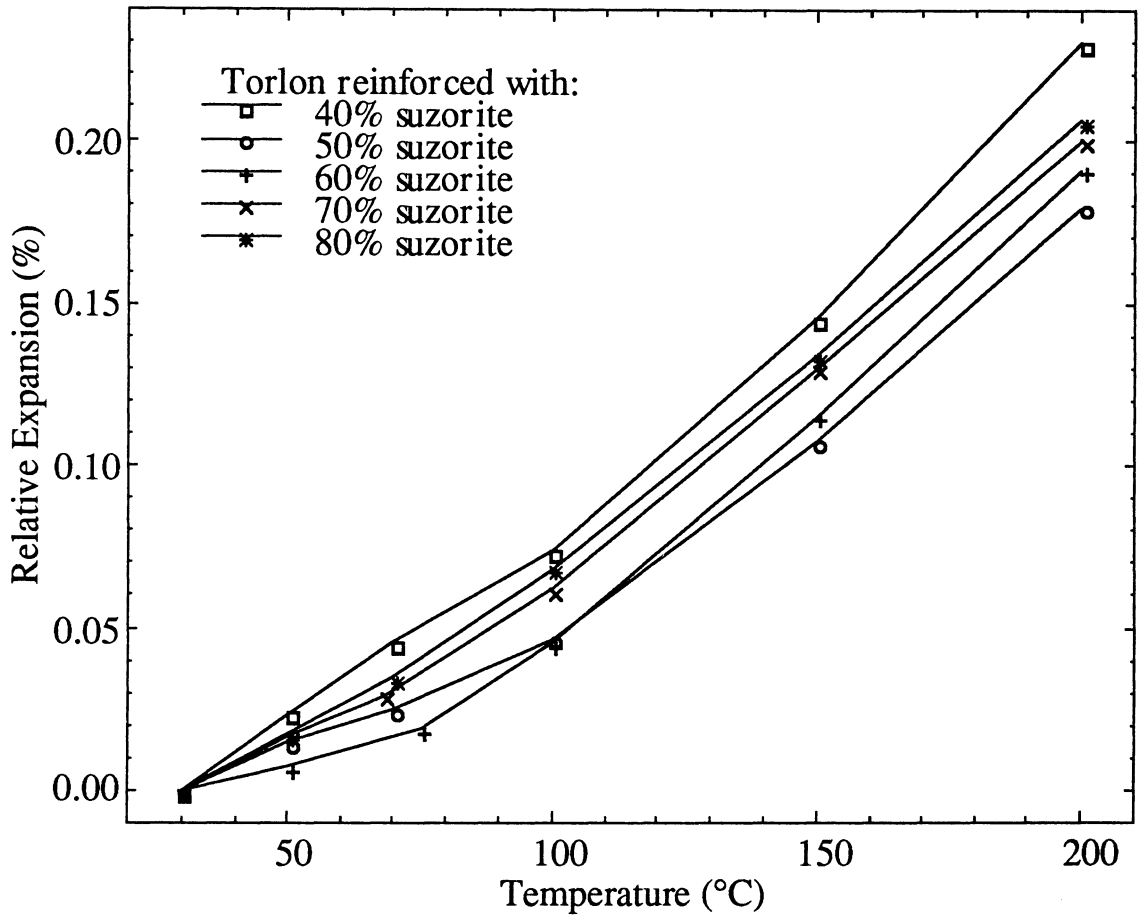

Figure D9. Thermal expansion behavior of Torlon/suzorite composites, showing the effect of reinforcement volume fraction.

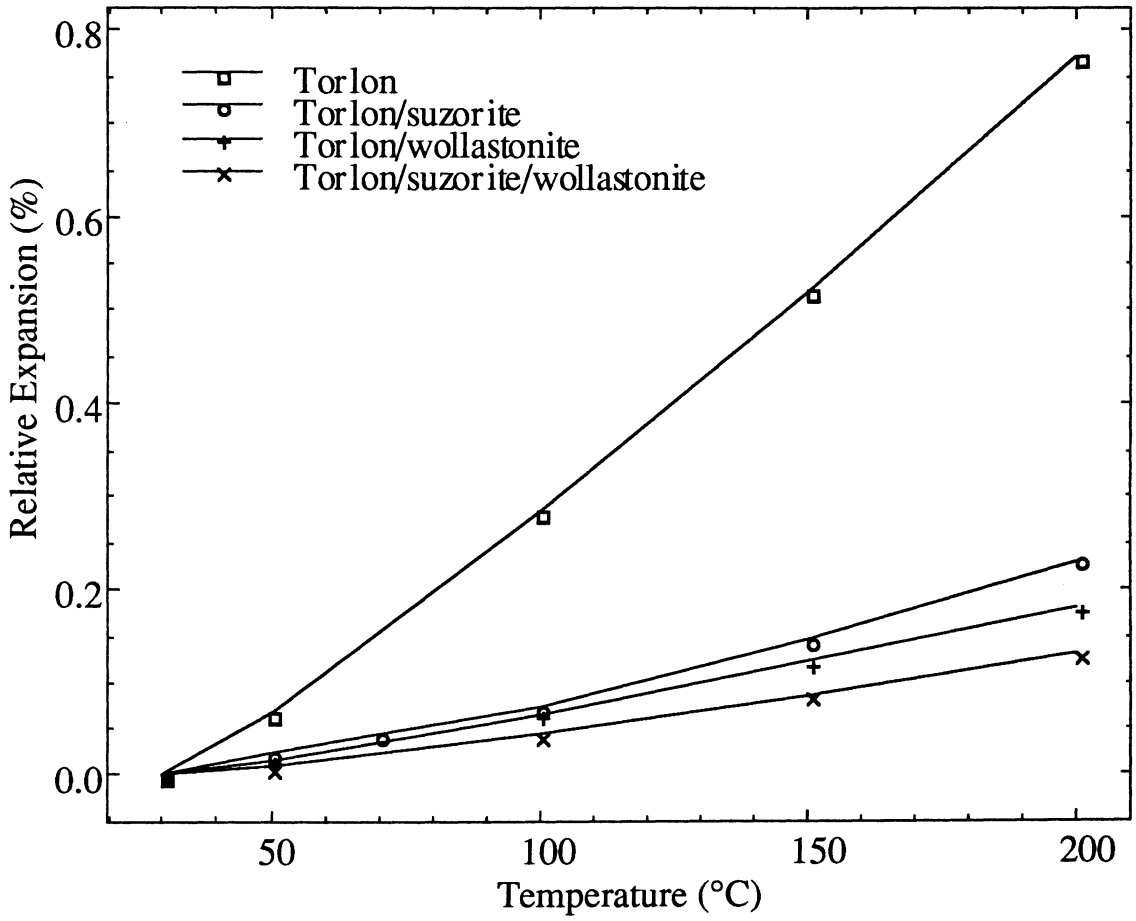

Figure D10. Thermal expansion behavior of wollastonite reinforced composites.

References

1. Ayers, J. D., *Fine Particles*, Proceedings of The Elliot Symposium, Iron and Steel Society,1990, pp. 236-262.

2. McGrath, J. E., Riffle, J. S. and Davis, R. M., Virginia Tech, Blacksburg, Virginia, *personal communications*, 1991.

3. Ashby, M. F., *On the Engineering Properties of Materials*, Acta metall., Vol. 37, No. 5,1989, pp.1273-1293.

4. Woodhams, R. T. and Xanthos, M., *Polyester Resins Reinforced with HAR Mica*, 29th Annual Technical Conference, Reinforced Plastics/Composites Institute, The Society of the Plastics Industry, Inc., 1974, Sect. 4-E.

5. Maine, F. W., Shepherd, P. D., Golemba, F. G., Moskal, E. A., and Osborne, A. D., *A New Family of Reinforced Thermoplastics*, 28th Annual Technical Conference, Reinforced Plastics/Composites Institute, The Society of the Plastics Industry, Inc., 1973, Sect 5-A.

6. Maine, F. W., and Shepherd, P. D., *Mica Reinforced Plastics: A Review*, Composites, Vol. 5, 1974, pp. 193-200.

7. Lusis, J., Woodhams, R. T., and Xanthos, M., *The Effect of Flake Aspect Ratio on the Flexural Properties of Mica Reinforced Plastics*, Polymer Engineering and Science, Vol. 13, 1973, pp. 139-145.

8. Schwartz, M. M., *Composite Materials Handbook*, McGraw-Hill, New York, 1984.

9. Bowles, D. E., and Tenney, D. R., *Composite Tubes for the Space Station Truss Structure*, SAMPE Journal, May/June, 1987, pp. 49-57.

10. Slemp, W. S., Santos-Mason, B., Sykes, G. F. Jr, and Witte, W. G. Jr., *Effects of STS-8 Atomic Oxygen Exposure on Composites, Polymeric Films, and Coatings*, Atomic Oxygen Effects Measurements for Shuttle Missions STS-8 and 41-G, Vol. I, Sect. 5, NASA Technical Memorandum 100459, 1988, pp. 1-15.

11. Banks, B. A., Rutledge, S. K., Brady, J. A., and Merrow, J. E., *Atomic Oxygen Effects on Materials*, NASA Conference Publication 3035, Part I, Section 1, Session 3, 1988, pp. 197-239.

12. Leger, L. J., and Visentine, J. T., *A Consideration of Atomic Oxygen Interactions with the Space Station*, J. Spacecraft, Vol. 23, No. 5, 1986, pp. 505-511.

13. Rutledge, S., Banks, B., DiFilippo, F., Brady, J., Dever, T., and Hotes, D., *An Evaluation of Candidate Oxidation Resistant Materials for Space Application in LEO*, NASA Technical Memorandum 100122, 1986.

14. Regola, M., Baer, E., and Hiltner, A., *Atomic Oxygen Effects on the Prefailure Damage Process in Highly Filled Glass/Mica Epoxy Composites*, J. Appl. Polym. Sci., Vol. 42, No. 9, 1991, pp. 2563-2577.

15. Klar, E., ed., *Metals Handbook, Ninth Edition, Vol. 7, Powder Metallurgy*, American Society for Metals, Metals Park, Ohio, 1984.

16. St. Clair, A. K., and St Clair, T. L., *A Multi-Purpose Thermoplastic Polyimide*, SAMPE Quarterly, Vol. 13, No. 1, 1981, pp. 20-25.

17. *Torlon Engineering Polymers/Design Manual*, Amoco Performance Products, Inc., Ridgefield CT.

18. *Araldite® MY721 Product Data*, Ciba-Geigy Corporation, Hawthorne, New York.

19. Locke, S. R., Lindsay, R., and Fenton, M., *The Properties of Suzorite Mica Flake as a Reinforcement in Plastic Composites*, 30th Anniversary Technical Conference, Reinforced

Plastics/Composites Institute, The Society of the Plastics Industry, Inc., 1975, Sect. 4-D.

20. Katz, H. S., and Milewski, J. V., eds., *Handbook of Fillers and Reinforcements for Plastics*, Van Nostrand Reinhold Co., New York, 1978.

21. Kauffman, S. H., Leidner, J., Woodhams, R. T. and Xanthos, M., *The Preparation and Classification of High Aspect Ratio Mica Flakes for Use in Polymer Reinforcement*, Powder Technology, Vol. 9, 1974, pp. 125-133.

22. *Goodfellow 1990/91 Catalog*, Malvern, PA.

23. *AESAR 1992-1993 Catalog*, Johnson Matthey, Ward Hill, MA.

24. Funakubo, H., ed., Kennedy, J. B., trans., *Shape Memory Alloys*, Gordon and Breach Science Publishers, New York, 1987.

25. Copeland, J. R., and Rush, O. W., *Wollastonite: Short-Fiber Filler/Reinforcement*, Plastics Compounding, Nov/Dec, 1978.

26. Boot, R. J., *Wollastonite Substitution for Glass Fiber in BMC*, Plastics Compounding, Jul/Aug, 1982.

27. Steve Liptak, Virginia Tech, Blacksburg, Va, *personal communication*, 1991.

28. DiMarzio, E. A., *Validity of the Ehrenfest Relation of a System with More Than One Order Parameter*, J. Appl. Phys., Vol. 45, No. 10, 1974, pp. 4143-4145.

29. Goldstein, M., *Validity of the Ehrenfest Relation of a System with More Than One Order Parameter: Critique of a Paper by DiMarzio*, J. Appl. Phys., Vol. 45, No. 10, 1974, pp. 4153-4156.

30. Nielsen, L. E., *Mechanical Properties of Polymers and Composites*, Vol. 2, Marcel Dekker, inc., New York, 1974.

31. Nielsen, L. E., *Simple Theory of Stress-Strain Properties of Filled Polymers*, J. Appl. Polym. Sci., Vol. 10, 1966, pp. 97-103.

32. Chawla, K. K., *Composite Materials: Science and Engineering*, Springer-Verlag, New York, 1987.

33. Nguyen, H. X., and Ishida, H., *Poly(Aryl-Ether-Ether-Ketone) and Its Advanced Composites: A Review*, Polymer Composites, Vol. 8, No. 27, 1978, pp. 57-73.

34. Simmons, G., and Wang, H., *Single Crystal Elastic Constants and Calculated Properties: A HANDBOOK*, The M. I. T. Press, Cambridge, Massachusetts.

35. Dean, J. A., ed., *Lange's Handbook of Chemistry, 11th edition*, McGraw-Hill, New York, 1973.

36. Namboodri, S. L., *Processing of Ceramic Superconductor/Polymer Composites*, Ceramic News, Vol. II, No. 4, Center for Advanced Ceramic Materials, Blacksburg, Va, 1991, pp. 4-6, and *personal communication*, 1991.

37. Iyer, V., and Kander, R., *Midterm Project Report*, submitted to ABEX, 1991.

The vita has been removed from the scanned document